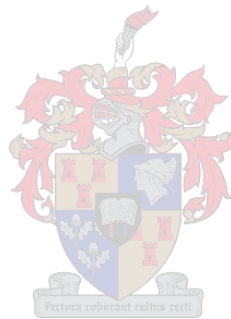


# **LANDSLIDE SUSCEPTIBILITY MAPPING: REMOTE SENSING AND GIS APPROACH**

by  
Zipho Tyoda



Thesis presented in fulfilment of the requirements for the degree of Masters in Geography and Environmental Studies, in the faculty of Science at Stellenbosch University

Supervisor: Dr Jaco Kemp  
Co-Supervisor: Ms Jeanine Engelbrecht

March 2013

## **Declaration**

By submitting this thesis electronically, I declare that the entirety of the work contained therein is my own, original work, that I am the sole author thereof (save to the extent explicitly otherwise stated), that reproduction and publication thereof by Stellenbosch University will not infringe any third party rights and that I have not previously in its entirety or in part submitted it for obtaining any qualification.

March 2013

## ABSTRACT

*Landslide susceptibility maps are important for development planning and disaster management. The current synthesis of landslide susceptibility maps largely applies GIS and remote sensing techniques. One of the most critical stages on landslide susceptibility mapping is the selection of landslide causative factors and weighting of the selected causative factors, in accordance to their influence to slope instability. GIS is ideal when deriving static factors i.e. slope and aspect and most importantly in the synthesis of landslide susceptibility maps. The integration of landslide causative thematic maps requires the selection of the weighting method; in order to weight the causative thematic maps in accordance to their influence to slope instability. Landslide susceptibility mapping is based on the assumption that future landslides will occur under similar circumstances as historic landslides. The weight of evidence method is ideal for landslide susceptibility mapping, as it calculates the weights of the causative thematic maps using known landslides points. This method was applied in an area within the Western Cape province of South Africa, the area is known to be highly susceptible to landslide occurrences. A prediction rate of 80.37% was achieved. The map combination approach was also applied and achieved a prediction rate of 50.98%.*

*Satellite remote sensing techniques can be used to derive the thematic information needed to synthesize landslide susceptibility maps and to monitor the variable parameters influencing landslide susceptibility. Satellite remote sensing techniques can contribute to landslide investigation at three distinct phases namely: (1) detection and classification of landslides (2) monitoring landslide movement and identification of conditions leading up to an event (3) analysis and prediction of slope failures. Various sources of remote sensing data can contribute to these phases. Although the detection and classification of landslides through the remote sensing techniques is important to define landslide controlling parameters, the ideal is to use remote sensing data for monitoring of areas susceptible to landslide occurrence in an effort to provide an early warning. In this regard, optical remote sensing data was used successfully to monitor the variable conditions (vegetation health and productivity) that make an area susceptible to landslide occurrence.*

## CONTENTS

Landslide susceptibility mapping: Remote sensing and GIS approach .....	i
Abstract .....	ii
Contents .....	iii
Figures.....	vi
<i>Tables</i> .....	xiv
ACKNOWLEDGEMENTS .....	xvi
Chapter 1 Background to the study .....	1
1.1 Introduction to Landslides and landslide susceptibility .....	1
1.2 Project aims and goals.....	2
1.3 The research questions and objectives .....	3
1.4 Landslides in South Africa and Description of the study area .....	5
Chapter 2 Literature review and theory .....	9
2.1 Landslide Classification .....	9
2.2 Landslide controlling parameters .....	11
2.2.1 Static factors.....	13
2.2.2 Variable factors .....	15
2.2.3 Triggering mechanisms.....	17
2.3 Remote sensing and GIS for Landslide susceptibility mapping .....	17
2.4 GIS modelling for landslide susceptibility mapping.....	18
2.4.1 Remote sensing on landslide susceptibility mapping .....	22
2.5 Final remarks.....	25

Chapter 3	GIS-Based landslide susceptibility mapping: Materials, results and accuracy assessment	26
3.1	Input data.....	26
3.1.1	Geology.....	26
3.1.2	Geomorphology.....	30
3.1.3	Landcover.....	33
	Description.....	39
3.1.4	Anthropogenic influences.....	41
3.2	Landslide susceptibility mapping – the weights of evidence APPROACH.....	42
3.2.1	Weight of evidence landslide susceptibility map.....	44
3.2.2	Accuracy Assessment for the Weight of Evidence method.....	49
3.3	Landslide susceptibility mapping – the Map combination Approach.....	53
3.3.1	Accuracy Assessment for the Map Combination approach.....	59
Chapter 4	Remote monitoring of variable conditions and identification of triggering mechanisms.	62
4.1	Extraction of NDVI and NDWI – MODIS data.....	65
4.2	Extraction of NDVI and NDWI and phenology data – Landsat data.....	73
4.2.1	Image pre-processing.....	74
4.2.2	Derivation of information on vegetation health and productivity and moisture conditions	
		77
4.3	Triggering mechanisms.....	82
Chapter 5	Discussion, recommendations and conclusions.....	87
5.1	Discussion.....	87
5.2	Intergration of landslide susceptibility mapping and development planning.....	90

5.3	Recommendations .....	91
5.4	Conclusions .....	91
	References .....	92
	Special references .....	103

## LIST OF ACRONYMS

ARC	Agricultural Research Council
ANN	Artificial Neural Network
CSIR	Council for Scientific and Industrial Research
DST	Department of Science and Technology
DEM	Digital Elevation Model
DTM	Digital Terrane Model
DN	Digital Numbers
GCP	Ground Control Points
LSI	Landslide Susceptibility Index
LIDAR	Light Detection And Ranging
GIS	Geographic Information system
MODIS	Moderate Resolution Imaging Spectroradiometer
NGO	Non-governmental organization
NDVI	Normalized Difference Vegetation Index
NDWI	Normalized Difference Water Index
NIR	Near-infra-red
NGI	National Geo-spatial Information
NIR	Near-Infrared
RMSE	Root Mean Square Error
SWIR	Short-Wave-Infrared
SAR	Synthetic Aperture Radar
SANSA	South African National Space Agency

## FIGURES

<i>Figure 1: The schematic diagram illustrating the standard procedure that is used when modelling landslide susceptibility maps.</i> .....	4
<i>Figure 2: The extent of the study area in the Western Cape Province of South Africa and a selection of field-verified historical landslide positions.</i> .....	6
<i>Figure 3: Geological map of the study area.</i> .....	8
<i>Figure 4: A classification of mass movement processes on slope (Carson &amp; Kirby 1972).</i> .....	11
<i>Figure 5: Effect of water content on cohesive strength of clay (Zhou 2006).The x-axis shows the water content and the y-axis it shows the cohesive strength.</i> .....	16
<i>Figure 6: The taxonomy of the different weighting approaches when conducting landslide susceptibility modelling (Source: Kanungo et al. 2009 pp 11).</i> .....	19
<i>Figure 7: The spectral reflectance curve of green and dry vegetation and soil along with the spectral wavelength (Clarck et al.1999).</i> .....	24
<i>Figure 8: The geological parameter of the study area, the lithological units are shown on the legend. This geological layer was one of the causative thematic layers used to modell a landslide susceptibility map of the study are using the weight of evidence method.</i> .....	27

*Figure 9: The 250 meter buffered lithological contacts and faults layer for the study area. This thematic layer was one of the causative thematic layers used to model a landslide susceptibility map of the study area. The localities for the landslides are also shown. 28*

*Figure 10: The graph shows the number of landslides per lithology. On the y-axis is the stratigraphic units and on the x-axis is the number of landslides. The alluvium deposits recorded the highest number of landslides and the Skurweberg, Rietvlei and Peninsula stratigraphic units recorded the second highest, and the third highest number of landslides, in decreasing order.29*

*Figure 11: Slope layer of the study area. The classes that were used in the weight of evidence method are also shown on the legend. ....30*

*Figure 12: The number of landslides per slope class. Roughly 90 % of the landslides fall on the 0-20° and 20-40° class. 31*

*Figure 13: The aspect layer for the study area. The classes are shown in the legend. The aspect thematic layer was one of the causative layers used to model a landslide susceptibility map of the study area, using the weight of evidence method. The black dots on the map are the localities for the known historic landslides within the study area. ....32*

*Figure 14: The number of landslides per aspect class. The south facing slope recorded the highest number of landslides and the east facing slopes recorded the least number of landslides. ....33*

*Figure 15: The land cover layer used when modelling the landslide susceptibility map of the study area. The landcover classes are shown in the legend. ....34*

*Figure 16: The number of landslides per landcover class. A large number of landslides fall on the Shrubland and low fynbos class. The other landcover classes recorded a very low number of landslides. ....35*

*Figure 17: The soil depth layer of the study areas. The depth classes are also shown on the legend. This thematic layer was one of the causative parameters used to model a landslide susceptibility map of the study area. ....36*

*Figure 18: The number of landslides per soil depth class. More than 90 % of the landslides fall on the soil depth less 300 mm, 300-600mm and 600-900 mm; in decreasing order. Soil depth less than 300mm recorded the highest number of landslides and the soil depth between 900-1200mm recorded the least number of landslides. ....37*

*Figure 19: The soil type layer for the study area, which was used to model the landslide susceptibility map using the weight of evidence method. The description for the codes used in the legend is shown on the Table 3. ....38*

*Figure 20: The number of landslides per soil type class. Class Lb (Rock outcrops comprise >60% of land type) recorded the highest number of landslides and class Gb (Podzols occur (comprise >10% of land type); dominantly shallow) recorded the least number of landslides. ....41*

*Figure 21: The layer containing the roads and rails within the study area. A buffer of 50 meter was used. The localities of known historic landslides are represented by the black dots on the map. ....42*

*Figure 22: Classification of the landslide susceptibility map using the natural break method. ....45*

*Figure 23: The unclassified weight of evidence landslide susceptibility map. The legend shows the increasing susceptibility of the map, with the higher values representing higher susceptibility and lower values representing lower susceptibility. 46*

*Figure 24: The landslide susceptibility map of the study area based on the weight of evidence model. The classes are shown on the legend. The red and orange areas are very high and high susceptibility, the yellow areas are moderately susceptible areas and the green areas are the very low and low susceptible areas. ....47*

*Figure 25: The number of landslides per susceptibility class. These landslides points were used to run the weight of evidence model. A large number of landslides fall on the very high and high class (96.8 %). .....48*

*Figure 26: The number of landslides per susceptibility class. These landslide points were not used when the susceptibility map was modelled; they were only used to test the efficiency of the model. A large number of landslides fall on the high and very high class (90 %). .....49*

*Figure 27: Classification of the landslide susceptibility map using equal interval method. ....50*

*Figure 28: The success (blue) and prediction (red) rate curves for the weight of evidence susceptibility model. 51*

*Figure 29: The overall success percentage for the weight of evidence method, the blue highlighted area is the overall percentage for the training data set. ....52*

*Figure 30: The overall success percentage for the weight of evidence method, the red highlighted area is the overall percentage for the reference data set .....53*

*Figure 31: The landslide susceptibility map of the study area. The map was modelled using a map combination approach. The susceptibility values are shown in the legend, the higher the values, the higher the susceptibility and the lower the value the lower the susceptibility. ....56*

*Figure 32: The landslide susceptibility map modelled using the map combination approach. The susceptibility classes are shown on the legend. The red and orange areas represent very high and high susceptibility areas, the yellow areas depict moderate susceptibility areas and the green areas are low susceptible areas. ....57*

*Figure 33: The graph shows the number of landslides per susceptibility class. ....58*

*Figure 34: The graph shows the number of landslides per susceptibility class. These landslide localities were attained from the Council for Geosciences. ....59*

*Figure 35: The success rate curve for the map combination approach. The red line is the success rate curve for the reference data set and the blue trend is the success rate curve for the training data set. ....60*

*Figure 36: The cumulative success percentage for the map combination approach. The blue highlighted area is the success percentage for the training data. ....60*

*Figure 37: The cumulative success percentage for the map combination approach. The red highlighted area is the success percentage for the reference data. ....61*

*Figure 38: The geographic location of the 2005, 2007 and 2008 landslide events. The landslides are located on the far north western and south western part of the study area. ....63*

*Figure 39: The geographic location of several landslide events. The landslides are located close to the towns of Stanford and Hermanus. The landslide localities are represented by black dots on the map. ....64*

*Figure 40: Google Earth images indicating the landscape before landslide occurrence (29-09-2004) and the landscape after landslide occurrence (02-11-2006). ....64*

*Figure 41: The NDVI time-series profile, of the selected area which is known to have landslide occurrence. The profile is from the year 2003 to the year 2006. The red line indicates the period at which the landslide is thought to have occurred. The plot shows that the minimum NDVI values for the year at which the landslides occurred are lower than the previous years. 66*

*Figure 42: The NDVI time-series profile of the area known to have landslide occurrence. The plot is from the year 2006 to the year 2009. The red line indicates the period at which the landslide is thought to have occurred. The plot shows relatively low minimum NDVI values for the year prior to landslide occurrence. ....68*

*Figure 43: The NDVI time series profile for the year 2003 to 2008. The red line on the graph indicates the period at which the landslide is thought to have occurred. The minimum NDVI values are slightly lower for the year prior to the occurrences of landslide event. ....69*

*Figure 44: The NDVI time-series profile of an area with numerous landslide scars. The area is close to the town of Hermanus and Stanford. The landslides are estimated to have occurred between the year 2004 and 2006. The red line on the graph indicates the time at which the landslide could have occurred, based on the previous observations that landslide in the study area are associated with low minimum NDVI values for the year prior to landslide occurrence. ....71*

*Figure 45: The NDVI time-series profile for the area known to have landslide occurrence. The red line on the graph indicates the period at which the landslide is thought to have occurred. The minimum NDVI values are lower for the year prior to landslide occurrence (2006). ....72*

*Figure 46: The NDVI time-series profile for the year 2005 to 2009. The red line on the graph indicates the period at which the landslide is thought to have occurred. The minimum NDVI values are slightly lower for the year prior to landslide occurrence. 73*

*Figure 47: Steps followed when performing atmospheric corrections. ....77*

*Figure 48: The 2005-02-27 scene for the area close to the town of Stanford and Hermanus. There are no visible landslide scars on this image, except one feature close the small round water body. ....78*

*Figure 49: The 2005-09-27 scene for the area close to the town of Stanford and Hermanus. The image shows several landslide scars (the bright feature on the south facing slope on the mountain. ....79*

*Figure 50: NDVI change detection computed from the landsat scenes between 2004-09-20 and 2005-02-27. The light red areas on the map are areas where there has been a decrease in NDVI and the strong red areas are those that had more than 15 % NDVI decrease. The light green and bright green areas depict those areas that experienced some NDVI increase and greater than 15 % NDVI increase, respectively. The localities of the landslides are represented by the black stars on the map. 80*

*Figure 51: NDVI change detection computed from the images taken from 2005-09-07 and 2006-04-19. The light red areas on the map are areas where there has been a decrease in NDVI and the strong red areas are those that had more than 15 % NDVI decrease. The light green and strong green areas depict those areas that experienced some NDVI increase and greater than 15 % NDVI increase, respectively. The exact localities of the landslides are represented by the black stars on the map. ....81*

*Figure 52: NDVI change detection computed from the images taken from 2006-08-09 to 2007-02-17. The light red areas on the map are areas where there has been a decrease in NDVI and the strong red areas are those that had more 15 % NDVI decrease. The light green and strong green areas depict those areas the experienced some NDVI increase and greater than 15 % NDVI increase, respectively. The exact localities of the landslides scars are represented by the black stars on the map.82*

*Figure 53: Annual rainfall for the year 2004, 2005 and 2006. The year of 2005 recorded the highest annual rainfall, slightly higher than 800 mm.....84*

*Figure 54: The plot for the monthly rainfall for the year 2005. The months of April and June show monthly rainfall greater than 100 mm, with the month of April recording close to 250mm.....86*

## ***TABLES***

<i>Table 1: The schematic landslide classification system adapted from Varnes (1978).</i> .....	10
<i>Table 2: The comprehensive review of the different GIS techniques that have been used for landslide susceptibility modelling.</i> .....	19
<i>Table 3: The description for the soil type classes (source: ARC institute for Soil, Climate and Water).</i> .....	39
<i>Table 4: The weights and ranks for the causative thematic layers used to model an expert based landslide susceptibility map.</i> .....	54
<i>Table 5: Shows the number of landslides and the date of occurrence for each area.</i> .....	62
<i>Table 6: The annual average, minimum and maximum values of NDVI. The values are calculated from the beginning of the year to the end of the year.</i> .....	67
<i>Table 7: The yearly average, minimum and maximum values of NDVI. The values are calculated from the beginning of the year, to the end of the year.</i> .....	70
<i>Table 8: Landsat scenes that will be used in this study.</i> .....	74
<i>Table 9: Table representing the scene date RMS error and the number of GCP's collected when geometric correction was performed.</i> .....	75
<i>Table 10: The annual rainfall for the weather station in Hermanus (-34.417: 19.237). The monthly average and the total annual rainfall are also indicated. The rainfall is in millimetres (mm).</i> .....	83
<i>Table 11: The annual rainfall data (in millimeters) for the weather station close to the town of Hermanus. The blank areas in the table indicate that no rain fell on that day, *** indicates that the data is missing or not yet available in the current month, C next to</i>	

*the value indicates that the rainfall was accumulated over a number of days, = indicates that the total for the month is unreliable due to missing daily values, and A or B indicates that any rainfall that did occur is included in the accumulation. .... 85*



## **CHAPTER 1 BACKGROUND TO THE STUDY**

### **1.1 INTRODUCTION TO LANDSLIDES AND LANDSLIDE SUSCEPTIBILITY**

Landslides are defined as mass movement processes that involve down-slope movement of slope material along discrete shear surfaces under the influence of gravity (Cruden & Varnes 1996). Landslides play a significant role in the evolution of the hill-slope and long-term landscape evolution. The abrupt nature and the catastrophic forces of the process can have undesirable socio-economic impacts. The hazardous nature of landslides can result in substantial economic losses, fatalities, geomorphologic disturbances, ecosystem disturbances and infrastructure disturbances. Landslides can be triggered by earthquakes/seismicity, human activities (i.e. road-cuts and vegetation removal) but in mountainous landscapes, landslides are more frequently triggered by heavy rainfalls (Brunetti, Peruccacci, Rossi, Luciani, Valigi & Guzzetti 2010). Landslide susceptibility mapping is a vital tool for disaster management and planning development activities in mountainous terrains of tropical and subtropical environments (Dahal, Hasegawa, Nonomura, Yamanaka, Masuda & Nishino 2007).

Steep terrain, considerable topographic variation, high relief, diverse geology, humid climate and seismicity make some parts of South Africa susceptible to landslide activity. Landslides are often associated with severe, high intensity rainfall events (Singh 2009). In 1989 the estimated annual costs of landslide associated expenses in Southern Africa, were estimated at approximately US\$ 20 million (Paige-Green 1989). Based on an annual standard inflation rate of 10%, the current suggested amount means that annual landslide associated expenses would cost Southern Africa ~US\$ 163 million (Singh, Forbes, Diop, Musekiwa & Claasen 2011).

Landslide susceptibility mapping has had little improvements in principle and the difficulty in landslide prediction is the result of different factors controlling landslide occurrences (Kanungo, Arora, Sarkar & Gupta. 2009). Nevertheless the evolution of remote sensing, GIS and field work techniques has produced reliable landslide susceptibility maps, which has been successfully used during development planning by governments and NGOs in different regions around the world (e.g. Sarkar & Kanungo 2004, Hung, Batelaan, San & Van 2005). Landslide prediction methodologies are based on the assumption that future landslides will occur under circumstances similar to the ones of past landslides (Chung & Shaw 2000). Consequently, previous research has devoted significant amount of time on developing techniques for studying the spatial distribution of the landslide controlling parameters. Historically, landslide susceptibility assessment and mapping were considered to be laborious and time consuming. However, significant developments in remote sensing, computer application and

geographic information systems have facilitated the process significantly (Dahal et al. 2007) and played a significant role in landslide forecasting and modelling (Temesgen , Mohammed & Korme, 2001; Sarkar & Kanungo 2004; Hung et al 2005, Singh 2009).

The research presented here aimed to synthesize a landslide susceptibility map of a selected area in the Western Cape Province of South Africa. Additionally, standard techniques and methodologies for landslide susceptibility modelling were introduced that can be used for landslide susceptibility and early warning investigations in South Africa.

## **1.2 PROJECT AIMS AND GOALS**

The likelihood that an area will be affected by landslides is dependent on several factors. These factors are static factors (such as the slope of the terrain and the underlying geology) as well as variable factors (such as the health and productivity of vegetation in the area and the soil water content). If a critical combination of static and variable conditions is met, the area would have a high likelihood to be affected by a landslide event. The presence of a triggering mechanism (such as a high intensity rainfall event or an earthquake) would then lead to slope failure and landslide occurrence.

This study aims to synthesize a landslide susceptibility map by considering the static variables and how they influence landslide susceptibility. Secondly, the variable factors influencing landslide occurrence will be investigated using satellite remote sensing techniques and a selection of historical landslide events that affected parts of the Western Cape Province. Finally, the triggering mechanisms that lead to the landslide occurrence will be investigated.

The combination of these activities will lead to techniques that can be used for landslide early warning systems by identifying priority areas and monitoring conditions that can lead up to a landslide event if a triggering event takes place.

### **1.3 THE RESEARCH QUESTIONS AND OBJECTIVES**

The research project aimed to address the following research questions:

1. Can a combination of remote sensing and ancillary data be used to identify conditions leading up to historical landslide events and their triggering mechanisms?
2. Can a combined GIS and remote sensing approach be used to create a landslide susceptibility map for selected regions of the Western Cape?

Since investigations on landslide occurrence are based on the assumption that future landslides will occur under similar conditions as historical landslides (Chung & Shaw 2000) the ultimate objective of the research is to identify the static and variable conditions leading to historical landslides. This will include the identification of the triggering mechanisms of those landslides. The results of this phase of the research will then be incorporated with GIS modelling to create a landslide susceptibility map for the area of interest. The approach that will be used when deriving landslide susceptibility maps is presented in Figure 1. Information on the landslide controlling parameters is derived from a combination of existing maps, information derived from remote sensing data as well as field-based measurements. These maps define thematic data layers which are used as input for modeling landslide susceptibility maps. The data processing phases consists of using either expert knowledge or computer algorithms or both to weight the relative importance of each of the controlling factors to landslide occurrence.

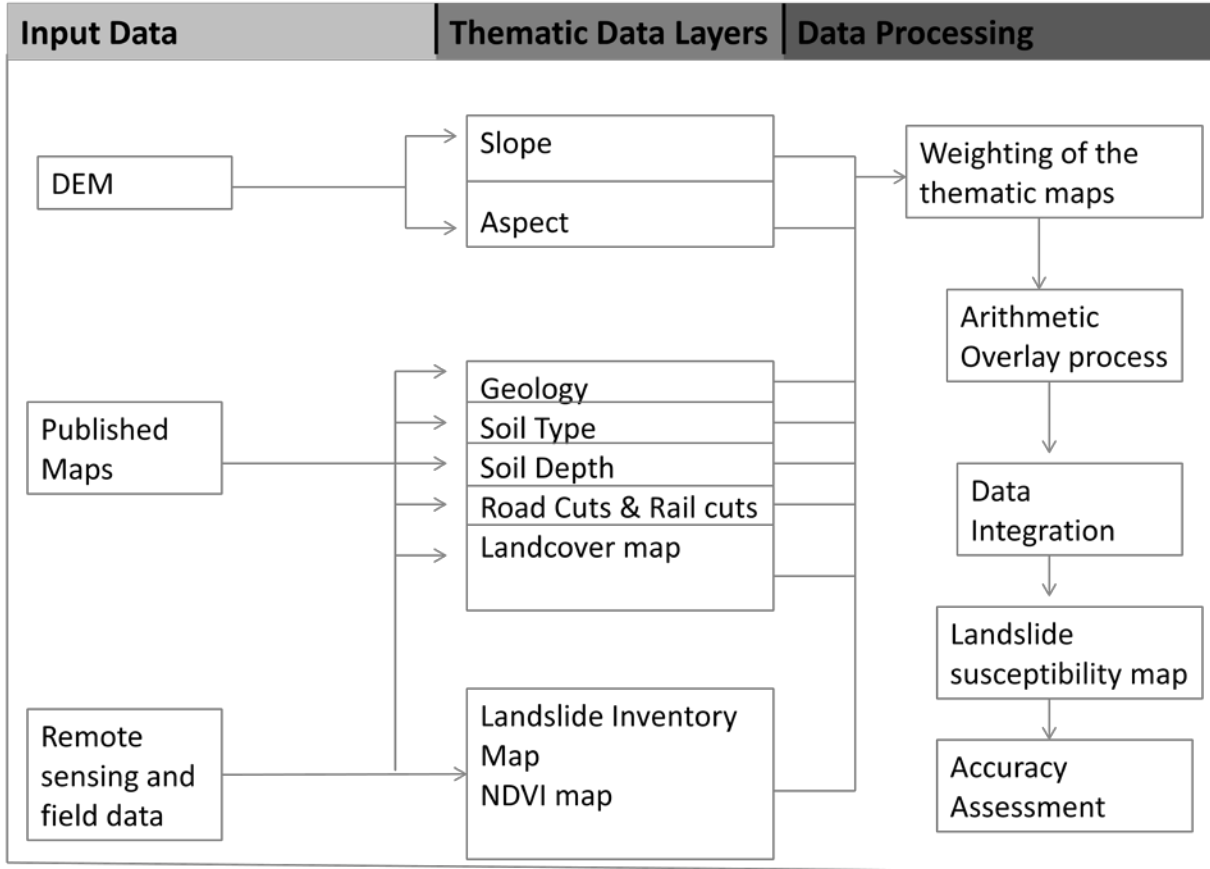


Figure 1: The schematic diagram illustrating the standard procedure that is used when modelling landslide susceptibility maps.

The specific objectives for the research are:

- I. Identify landslide causative factors and further investigate their individual influence to slope instability in the study areas.
- II. Apply the weight of evidence method on landslide susceptibility mapping.
- III. Apply the map combination approach on landslide susceptibility mapping, in order to compare the success rate of these two models.
- IV. Investigate the applicability of remote sensing as a monitoring system
- V. Investigate the triggering mechanism for the landslides within the study area.

#### 1.4 LANDSLIDES IN SOUTH AFRICA AND DESCRIPTION OF THE STUDY AREA

South African landslides tend to occur in mountainous regions experiencing high rainfall frequency (Singh et al. 2011). Areas that are highly susceptible to landslides are the Western Cape Mountains, eastern coastal regions and the mountainous areas of the KwaZulu Natal Drakensberg (Paige-Green 1989). Several studies have examined the occurrence of landslides in Southern Africa (e.g. Paige-Green 1989; Garland & Olivier 1993). Durban frequently suffers from landslides and it has been found that housing developments and construction work have contributed towards most slope failures (Garland & Olivier 1993). In South Africa debris flow occurs in the KwaZulu Natal Drakensberg and in the Eastern Cape and Western Cape mountains (Lewis 1996, Boelhouwers, Duiker, van Duffelen 1998). A debris flow deposit has been described by Hanvey, Lewis & Lewis (1986) near Rhodes in the Eastern Cape and it was suggested that this debris deposit was related to the existence of a former snow body and occurred under the Quaternary periglacial conditions. In the Eastern Cape debris flow are extensive even at low altitudes (Lewis 1996). The large section of a road that slide away on the N2 between Port Elizabeth and Grahamstown on the 21 October 2003 is another example. One example of a large paleo-landslide is Lake Fududzi in the Limpopo province. This 2km long lake is located in the Soutpansberg Range, and is an inland freshwater lake formed by a huge palaeo-landslide which blocked the course of the Mutale River (Janisch 1931). The area most known for rockfalls in the Western Cape is the Chapman's Peak drive along the Cape Peninsula Atlantic coastline, prompting extensive structural improvements and removal of loose rocks from the steep slopes (Singh 2009). Boelhouwers et al. (1998) investigated the morphology and sedimentology of recent debris flow in the Western Cape Mountains. A debris flow deposit in the Cederberg Mountain of the Western Cape has also been described by Boelhouwers et al. (1998). Further work from the Cape Province describes debris flow studied in the Bushmans River Valley, which have been attributed to the heavy rainfall events under contemporary climatic conditions (Lewis & Illgner 1998). Landslide distributions have been observed in Du Toit's Kloof area in the Western Cape, with 78 % of landslides investigated occurring in the south-facing slopes, which is attributed to slope asymmetry by Boelhouwers et al. (1998).

To test the accuracy of landslide susceptibility modelling and the possibility to define a methodology for landslide early warning systems, a study area in the Western Cape Province of South Africa was selected. The area in question was known to be the subject of historical landslide events and the landslide locations and dates of occurrence have been verified by field observations (Stapelberg pers com. 2011). The location of the study area and some of the known landslide locations are presented in Figure 2.

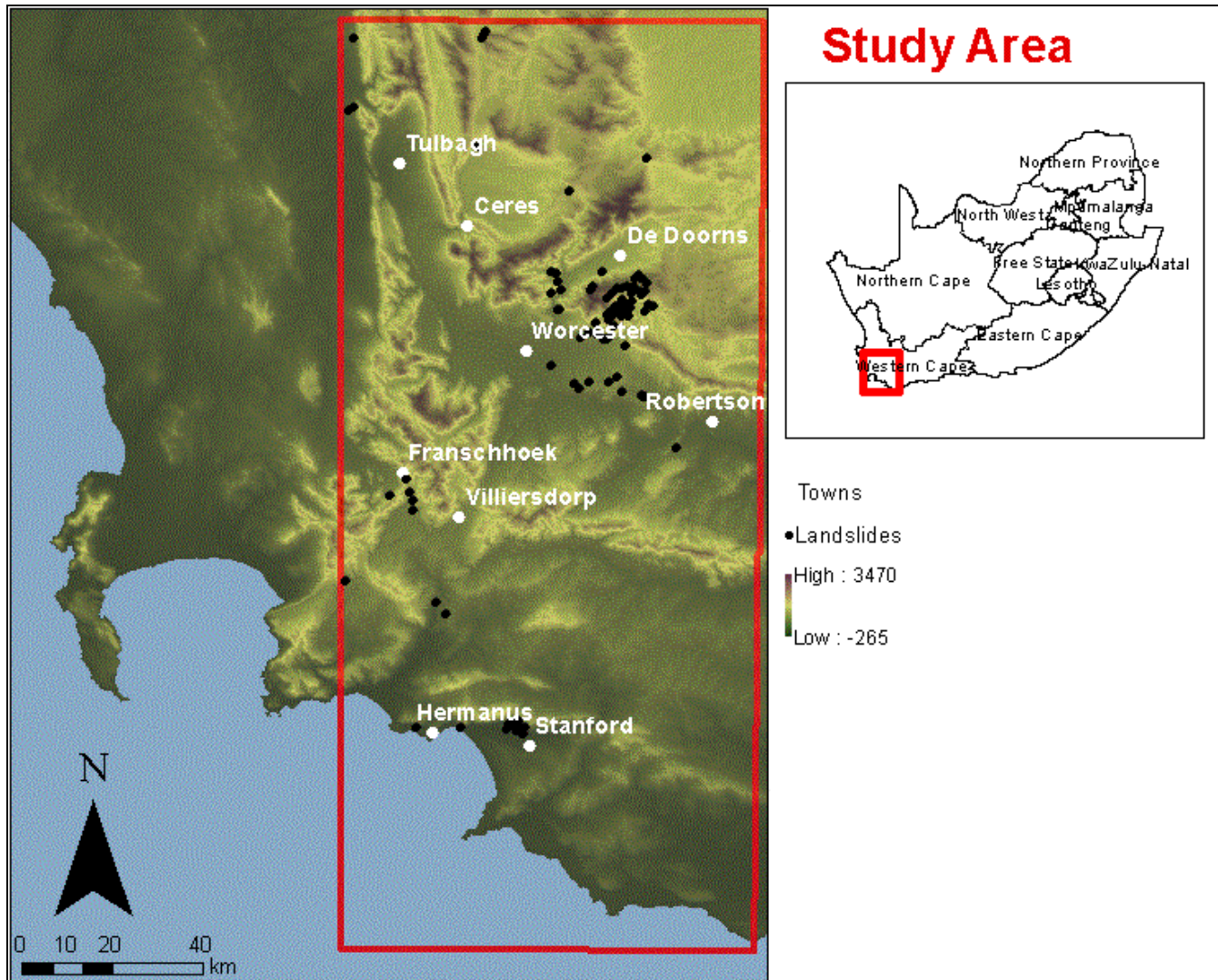


Figure 2: The extent of the study area in the Western Cape Province of South Africa and a selection of field-verified historical landslide positions.

The area of interest extends from 0 meters to 2298 meters above sea level with slopes ranging between 0 and 88°. The area receives a total annual rainfall in excess of  $\pm 822$ mm (2005 annual rainfall for the weather station in Hermanus, South African Weather Services) with the majority of precipitation occurring during winter to spring (May to September). Geologically the study area is situated in the Cape Fold belt which consists of the Cape Supergroup, Karoo Supergroup and younger tertiary sediments capping the basement of pegmatites and granitic intrusions of the Namaqua Natal belt. The predominant structural features are the large and small scale folds, and faulting events associated with the Cape Fold Belt orogeny. Lithologically the Cape Supergroup consists of the sandstone and shale sequence of the Table Mountain Group, the marine shales and sandstones of the Bokkeveld Group and the sequence of sandstones and shales of the Witterberg Group. The Karoo Super

Group consists of the glacial deposit of the Dwyka Formation, the fluvial sandstones and mudstones of the Beaufort Formation and the sequence of marine turbidites and shales of the Ecca Group (Johnson, Annhauser & Thomas 2006). The different lithologies, the location of the lithological boundaries, dolerite contact zones and the presence of faults and other structural features could have a significant impact on landslide susceptibility. The impact of the various lithologies and structural features will be discussed in Section 2.2. The geological map of the study area is presented in Figure 3. The sedimentary successions in the area support mostly Fynbos vegetation types, which experience their growing season in spring and summer months.



## CHAPTER 2 LITERATURE REVIEW AND THEORY

### 2.1 LANDSLIDE CLASSIFICATION

The term "landslide" is a part of a broad spectrum of mass movements involving the movement of surface materials down a slope (Cruden & Varnes 1978). Standard classification schemes for different kinds of mass movement do not exist although various researchers have suggested classification schemes based on different criteria (Terzaghi 1950; Carson & Kirkby 1972, Varnes, 1978, Cruden & Varnes in 1996).

For several years, the type of classification system used was primarily based on the type of movement (e.g. Varnes 1978 & 1984). The most accepted landslide classification systems are based on different factors such as:

- The material being transported (the terms rock, earth and debris are the terms generally used to distinguish the materials involved in the landslide process. If less than 20% of the material is greater than 2 millimetres in size, the material will be defined as earth. (Otherwise it will be termed debris),
- The type of movement ( the main movement types are falls, slides and flows but usually lateral spread, topples and complex movement are added to these),
- Movement velocity and
- Its current activity (this system is good particularly when evaluating future landslides and currently active landslide).

Table 1 shows the schematic landslide classification system adapted from Varnes (1978) and modified by Cruden & Varnes, in 1996.

Table 1: The schematic landslide classification system adapted from Varnes (1978).

Type of movement			Type of material		
			Bedrock	Engineering soils	
				Predominantly fine	Predominantly coarse
Falls			Rock fall	Earth fall	Debris fall
Topples			Rock topple	Earth topple	Debris topple
Slides	Rotational		Rock slump	Earth slump	Debris slump
	Translational	Few units	Rock block slide	Earth block slide	Debris block slide
Many units		Rock slide	Earth slide	Debris slide	
Literal spread			Rock spread	Earth spread	Debris spread
Flows			Rock flow	Earth flow	Debris flow
			Rock avalanche		Debris avalanche
			Deep creep	Soil creep	
Complex and compound			Combination in and/or in space of two or more principle types of movement		

Another classification scheme is based on the speed at which the material is transported in addition to the moisture content of the material and the type of material being transported (Carson & Kirkby 1972).

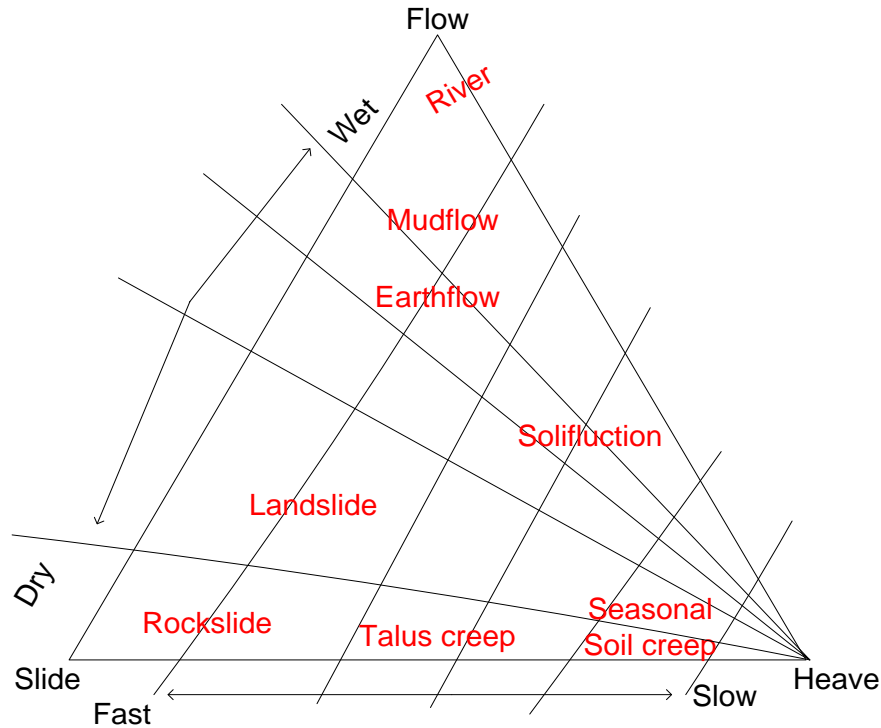


Figure 4: A classification of mass movement processes on slope (Carson & Kirby 1972).

Irrespective of classification scheme used, the probability of having downslope movement of surface materials are affected by specific controlling parameters. These parameters or factors are related to the physical characteristics of the surface in question. The following sections aim to identify specific landslide controlling parameters for the purpose of highlighting those parameters that will lead to an area being susceptible to landslide occurrence.

## 2.2 LANDSLIDE CONTROLLING PARAMETERS

The identification of historic landslides and the analysis of the conditions leading to those landslide events is critical when attempting to identify landslides controlling parameters (Campbell 1975; Clerici, Perego, Tellini, Vescovi 2002; Morton, Alvarez, Glade 2005). The parameters affecting landslide occurrences can be broadly grouped into two categories (1) preparatory factors, which make the area susceptible to slope failure and (2) triggering factors, which sets off the movement (Crozier & Michael 1986). The parameters that affect an area's susceptibility to landslide include (1) geology, (2) geomorphology (3) human activities (4) and landcover (Pearce & O'Loughlin 1995; Wu & Siddle 1995; Atkinson & Massari 1998, Sidle, Dai, Lee, Li & Xu 1991, Sarkar & Kanungo 2004, Dahal et al. 2007,

Singh 2009). Hence, in landslide hazard assessment practice, the term “landslide susceptibility mapping” is addressed without considering the variable factors in determining the probability of occurrence of a landslide event (Dai et al. 2001). The investigation of triggering mechanisms such as earthquakes and rainfall are critical but determining the magnitude and temporal behaviour of these parameters and how it relates to landslide susceptibility has proved to be challenging (Sarkar & Kanungo 2004). The following sections describe some of the controlling parameters affecting landslide development. These factors have been subdivided into three categories, each contributing to a separate category of landslide causative factors (preparatory parameter or triggering mechanism). They are:

1. Static factors – These factors are those that are unlikely to change within a short period of time like geology, the geomorphology, the soil type and depth and the vegetation type – these define the landslide preparatory factors.
2. Variable factors – These are the highly variable factors that can vary seasonally to daily including vegetation health and productivity and soil water contents – these contribute to both preparatory factors and triggering mechanisms.
3. Triggering mechanisms – These are the mechanisms that, when both static and variable conditions are favourable for landslide occurrence, will cause a landslide. Potential triggering mechanisms include high intensity rainfall events and/or seismic activity.

The premise behind the subdivision lies in the fact that the static factors will define the area's susceptibility to landslide occurrence (Dahal et al. 2007). For instance, at specific geomorphology and landcover classes, a specific area may be highly susceptible to landslide occurrence. The variable factors will then define the likelihood of a landslide occurring in the near future. For instance, a dry spell may cause the health and productivity of vegetation in a susceptible area to decline rapidly, increasing the likelihood of landslide occurrence. This then creates a scenario where a triggering event will cause a landslide to occur.

The following sections investigate the static and variable factors affecting landslide occurrence and describes the potential triggering mechanisms associated with landslide activity.

## 2.2.1 Static factors

### 2.2.1.1 *Geology*

The geology of an area is a critical parameter controlling the occurrence of landslides and various studies have used geology as a parameter when modeling landslide susceptibility maps (e.g. Dahal et al. 2007, Singh 2009, Chauhan, Sharma, Arora, Gupta 2010; Temesgen et al. 2010; Singh et al. 2011). Different lithologies have different chemical and physical properties leading to different susceptibility to mass movement. For example, different rock types have different hydrological properties i.e. transmissivity, hydraulic conductivity and permeability (Varnes 1984). These properties play a significant role on slope instabilities during rainfall events. Hence shales and siltstones are considered to be more susceptible to slope instability, while sandstones and conglomerates are regarded to have moderate to low susceptibilities to landslide occurrence (Stapelberg pers com. 2011). Singh et al. (2011) has emphasized the influence of a dip of the strata, abrupt changes in lithological characteristics, geological structure and bedding planes, on slope instability. The sequence of the stratigraphy can also determine the stability of the area. One such example is a sequence that consists of an impermeable layer on the bottom, which is overlain by a permeable layer. Such a sequence would have higher potential to saturate with water during rainfall events, resulting in a higher susceptibility to landslide occurrence. Additionally, the presence of dykes and sills are of importance since they could have weakening effects on the lithologies (Singh 2009). The structural features on the area of interest may also influence landslide occurrence. In this regard, properties including the dip of the strata and the presence of faults and lithological boundaries may signify zones of weakness along which slope failures may occur (Dahal et al. 2007). The combination of rock types and structures in an area will dictate the resistance to weathering and erosion processes and ultimately, landslide susceptibility (Singh et al. 2011).

### 2.2.1.2 *Geomorphology*

The geomorphology of the area has been found to be the most important controlling parameter by several authors (Sarkar & Kanungo 2004). Information on the geomorphology, including slope, aspect and profiles can be derived from digital elevation models of the area of interest using GIS techniques. Slope is the most substantial parameter influencing landslide development. On a slope of uniform isotropic material, increased slope correlates positively with increased likelihood of failure (Chauhan et al. 2010). In order to assess the contribution of various slope gradients to the development of landslides, it is necessary to know the spatial distribution of the slope categories, which can be obtained from a DEM (Dai & Lee 2002). The other important geomorphologic parameter is relative relief. Landslides generally

occur in high relative relief areas. The relief of the area is defined as the difference between maximum and minimum elevation values within the area. This parameter can be computed using DEM (Chauhan et al. 2010). Aspect is one of the most important parameter as it directly and indirectly influences the area's susceptibility to slope failure. South facing slopes are generally less vegetated in Southern Africa, as there is limited amount of sunlight reaching the south facing slopes. It is well known that sunlight is vital for vegetation health, and slopes with healthy vegetation are generally less susceptible to slope failure (detailed explanation in 2.2.2.1). Secondly South facing slopes receive limited amount of sunlight in the Southern hemisphere, therefore they are wetter, and more susceptible to landslide occurrence (Stapelberg pers com. 2011). ). Landslide distribution has been observed in Du Toit's Kloof area in the Western Cape, with 78 % of landslides investigated occurring in the south-facing slopes (Boelhouwers et al. 1998), which signifies the importance of aspect on landslide investigations in South Africa.

### 2.2.1.3 *Landcover*

While landcover is not strictly "static" it is regarded to be relatively stable over the course of few months. It does not change daily just like rainfall and vegetation. Landcover can be defined as the observed physical and biological cover on the earth's surface. Glade (2002) concurs that vegetation cover is an important factor influencing the rate of surface runoff, which enhance chances of landslide occurrence. For instance barren slopes are more likely to have landslide occurrence. In contrast vegetative areas tend to reduce the action of rainfall thereby preventing the erosion due to the anchorage provided by the tree roots (Gray & Leiser 1982; Greenway 1987, Styczen & Morgan 1995). In general, sparsely vegetated areas are associated with higher runoff during rainy seasons when compared to densely vegetated areas. Similarly, the type of vegetation would have an impact on slope stability (i.e. forested areas are expected to be more stable than grassland).

Different soil types have different properties such as grain size, porosity, transmissivity and hydrolic conductivity, therefore different soils have diverse influence on susceptibility to slope failure. Clay rich deep soils are considered to be more susceptible to landslide, in comparison with sandy shallow soils (Stapelberg pers com. 2011). An increase in absorbed moisture is a major factor in the decrease in strength of cohesive soils (Zhou 2006). Dahal et al. (2007) have also emphasized the importance of soil type as a parameter when modeling landslide susceptibility maps using the weight of evidence method. It has also been noticed that soil depth between 0.5-2 meters have maximum susceptibility to landslide (Dahal et al. 2007). It is therefore important to input soil depth as a static parameter when modeling a landslide susceptibility map.

#### *2.2.1.4 Anthropogenic influences*

Human-induced changes can affect an area's susceptibility to landslides and must be understood when assessing landslide potential of an area. Examples of such activities are road-cuts, deforestation, mining artificial vibrations, and cutting of slope toe during construction. One of the controlling factors for the stability of slopes is road construction activity (Dahal et al. 2007). Road cuts in mountainous areas can make the area susceptible to slope instability. One such example is the Chapman's Peaks drive in the Western Cape Province. Unsuitable construction on mountainous areas can also cause slope failures - it has been documented in Durban, KwaZulu Natal, that urban construction has caused some areas to be susceptible to slope failure (Garland & Olivier 1993). The increase in moisture content in the soil or changing the form of a slope can increase the area's susceptibility to landslide (Garland & Olivier 1993). Development activities such as cutting and filling along roads and the removal of forest vegetation are also capable of greatly altering slope form and ground water conditions and therefore increasing the susceptibility to landslide occurrence (Swanson & Dyrness 1975). These altered conditions may significantly increase the degree of landslide hazard present (Sidle, Pearce & O'Loughlin 1985). Trees act as natural anchors during rainy seasons, and therefore reduce the effect of rainfall on erosion (Gray & Leiser 1982). Deforestations therefore can cause an area to be more susceptible to slope failure, during rainy seasons. The positive influences of vegetation on slope failure have been discussed on section 2.2.1.3. In South Africa, the positive influence of vegetation to slope failure has also been emphasized by Stapelberg (pers com, 2011).

### **2.2.2 Variable factors**

#### *2.2.2.1 Vegetation*

As mentioned previously, the vegetation in an area has a significant impact on slope instability and various studies have emphasized the significance of vegetation on slope failure (Gray & Leiser 1982; Greenway 1987, Styczen & Morgan 1995). However, it is not only the vegetation type that governs landslide susceptibility, but also the health and productivity of vegetation at a specific time. The effect of vegetation on slope stability appears to be complex in that, depending on local conditions of soil depth, soil type, slope and vegetation, a vegetation cover in some ways definitely promotes stability and in other ways it may not. In a review of behaviour of vegetation on slope stability, Prandini et al. (1977) makes the following points regarding the beneficial effects of forest cover: as a whole forest cover reduces the action of climatic agents on natural mass, in a manner favourable to slope stability by:

- (1) Intercepting and protecting the mass from the action of sunshine, winds and rains,

- (2) Retaining a considerable amount of rain water by wetting the large surface made up of leaves, branches, and trunks and eliminating the water as a vapour,
- (3) Eliminating, as a vapour, a large amount of water from the ground by means of evapotranspiration, and
- (4) Vegetal debris on the forest floor immobilizes a large amount of water and cuts down on runoff and erosion.

When identifying conditions leading up to landslide events, the identification of the vegetative conditions prior to landslide occurrence can be performed. In this regard, landslides may occur preferentially in areas with little vegetation or in areas where vegetation is stressed due to drought or disease.

#### 2.2.2.2 Soil water content

In addition to the vegetative conditions, the wetness of the soil as an indication of soil moisture is known to play a role on slope stability (Ray, Jacobs & de Alba 2009). Saturated soils are believed to be more prone to instabilities and would therefore have a higher probability of landslide occurrence. Certain clay minerals react to the presence of water and cause volume changes of the clay mass. The relationship between an increase in absorbed moisture and the decrease in the cohesive strength of soils is shown schematically in Figure 5. Water absorbed by clay minerals causes increased water contents that decrease the cohesion of clayey soils (Zhou 2006). These effects are augmented if the clay mineral happens to be expansive, e.g., montmorillonite (Zhou 2006). Groundwater and soil moisture therefore play a critical role in triggering slope failure (Ray et al. 2009).

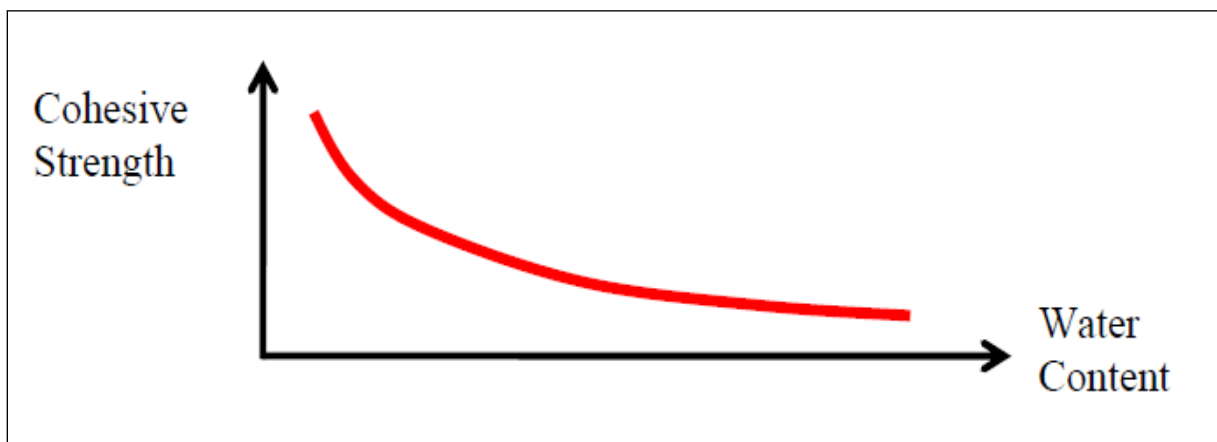


Figure 5: Effect of water content on cohesive strength of clay (Zhou 2006). The x-axis shows the water content and the y-axis it shows the cohesive strength.

### **2.2.3 Triggering mechanisms**

#### *2.2.3.1 Seismicity*

Natural and human-induced seismicity could trigger landslides and other mass-movement events (Borcherdt 1970, Harp 1991, Griggs 1998). Earth quakes can also trigger landslides in some areas (Spudich, Hellweg & Lee 1996). In this regard, a magnitude 6 earthquake that struck the town of Ceres in 1969 was associated with rock-falls and other mass movement events (Singh et al. 2011). Although seismically triggered landslides can be disastrous, South Africa is generally regarded to be seismically inactive (Singh et al. 2011). Earth tremors in South Africa are generally associated with either naturally occurring earthquakes or earth tremors associated with mining activities. Seismically triggered landslides are widespread phenomena within tectonically active mountain ranges.

#### *2.2.3.2 Rainfall*

Rainfall is a trigger for several landslides around the globe (Iverson 2000, Cardinali 2005) and in mountainous areas of South Africa (Singh et al. 2011). Water is recognized to be a factor almost important as gravity in slope instability (Varnes 1984). Landslides triggered by rainfall are caused by the buildup of water pressure into the ground (Cambell 1975; Wilson 1989). Iverson (2000) has also linked slope failure and landslide motion to groundwater pressure heads that change in response to rainfall. van Schlkwyk & Thomas (1991) have argued that prolonged precipitation events associated with high intensity rainfall are often the trigger for landslides in South Africa i.e. heavy rainfall of September 1987 and February 1988 occurring in KwaZulu Natal. High intensity and short rainfall duration can trigger mostly shallow landslides and debris flows in relatively high permeability soils (Corominas & Moya 1999; Corominas 2000). Whereas long rainfall periods characterized by low to moderate average rainfall intensity can initiate shallow and deep-seated landslides in low permeability soils and rocks (Cardinali, Galli, Guzzetti, Ardizzone, Reichenbach, Bartoccini 2005).

### **2.3 REMOTE SENSING AND GIS FOR LANDSLIDE SUSCEPTIBILITY MAPPING**

Techniques for landslide mapping have changed little, in principle, over the past few decades even when newer data sources become available (Sarkar & Kanungo 2004). Landslides are most often detected and mapped by a combination of interpretation of air photos or multispectral digital imagery and selected ground verification information (Roering & McKean 2004), and is often based on “professional judgment” (Wieckzorek 1984). There has been a drastic increase in magnitude and frequency of natural disasters around the globe but at the same time there has been improvements in the technical capabilities

to mitigate them. The increased efficiency of computers has created opportunities for detailed rapid analysis of natural hazards. The acquisition of information through remote sensing and spatial data analysis using GIS has improved the capabilities of geo-informatics in the field of disaster management (Dahal et al. 2007). The following section describes some of the GIS techniques and remote sensing tools that have been used for landslide susceptibility mapping and early warning.

## **2.4 GIS MODELLING FOR LANDSLIDE SUSCEPTIBILITY MAPPING**

Landslide hazard is normally depicted on maps which show spatial distribution of hazard classes. The development of these maps requires knowledge of the processes active in the area being studied (geological, hydrological, land-cover, and morphological factors), as well as triggering mechanisms leading to the occurrence of landslides (e.g. rainfall and seismicity) (Kanungo et al. 2009). Landslide hazard maps typically aims to predict where failures are likely to occur without any clear indication of when they are likely to occur. However, the focus on time-based modelling techniques have proved to be useful for providing landslide hazard information needed for planning and protection purposes (e.g. Brunettii et al. 2010 ).

Geographic information systems and the selection of parameters that are deemed to influence landslide occurrence in a certain area and the consequent preparation of corresponding thematic data layers are crucial components of models for landslide susceptibility mapping (Sarkar & Kanungo 2004). The parameters that are generally deemed to govern instabilities include geology, geomorphology, land use, climatic conditions, hydrology, vegetation and geohydrology (Dahal et al 2007). These factors can vary both locally and/or regionally. The derivation of landslide susceptibility maps involves the combination and integration of spatial information on these factors to provide an indication of the areas where the combination of factors is such that they create an environment conducive to landslide occurrence.

Different approaches have been used to weight landslide controlling parameters and to model landslide susceptibility maps. The choice of the appropriate technique strongly depends on the nature of the problem, the observation scale and data availability (Temesgen et al. 2001, Lee, Choi. & Min 2004, Sarkar & Kunongo 2004). Landslide susceptibility mapping approaches can be grouped into two broad categories; qualitative and quantitative (Glade & Crozier 2005). In the qualitative approach, a lot of subjectivity is introduced in preparation of various thematic data layers contributing for landslide occurrences, which are integrated in a GIS to create a landslide susceptibility map of the area (Kanungo et al. 2009). The quantitative approach focuses on developing the ways of quantifying the relative

importance of various causative factors (Kanungo et al. 2009). A classification of the different approaches for landslide susceptibility mapping is given in Figure 6 and a summary of different techniques is provided in Table 2.

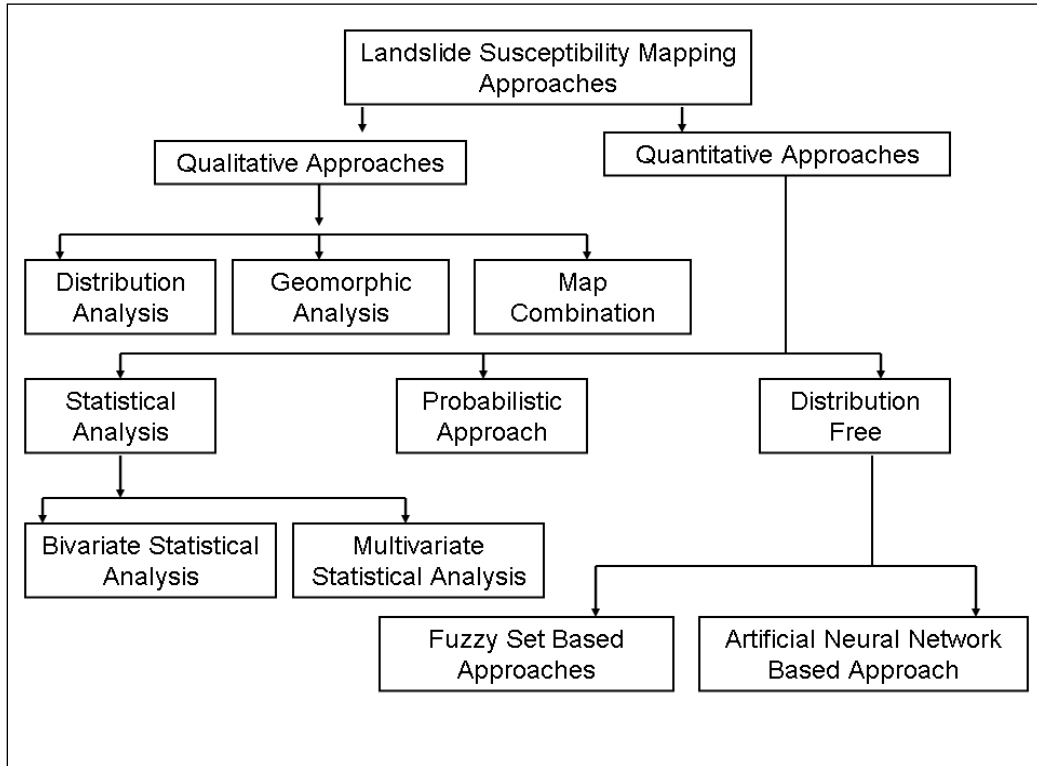


Figure 6: The taxonomy of the different weighting approaches when conducting landslide susceptibility modelling (Source: Kanungo et al. 2009 pp 11).

Table 2: The comprehensive review of the different GIS techniques that have been used for landslide susceptibility modelling.

Method	Description
<b>Qualitative Approach</b>	
<b>Distribution Analysis</b>	This method is also known as landslide inventory and provides a spatial distribution of existing landslides represented on a map either as the affected area (polygon) or as point events (Wieczoreck 1984 & 1987). <b>Disadvantage:</b> it does not relate landslides to their causative factors <b>Advantage:</b> it is economic and can cover a large area

<p><b>Map Combination</b></p>	<p>The map combination approach is a simple procedure that combines different thematic maps based on the knowledge of the expert. This approach involves The following steps (Soeters &amp; van Westen 1996):</p> <ol style="list-style-type: none"> <li>1. The Selection and mapping of landslide controlling parameters.</li> <li>2. Thematic data layer preparation with relevant categories of the parameters.</li> <li>3. Assignments of weights and rankings to parameters and their categories respectively.</li> <li>4. Integration of thematic data layers.</li> <li>5. Preparation of landslide susceptibility map showing different zones.</li> </ol> <p><b>Disadvantage:</b> It strongly depends on expert knowledge and therefore can inherit human error and bias judgment.</p> <p><b>Advantage:</b> It is simple as compared to the other methods, which normally use complex equations.</p>
<p><b>Quantitative Approach</b></p>	
<p><b>Probabilistic Approach</b></p>	<p>This approach compares the spatial distribution of landslides in relation to different causative factors. It is based on the Bayesian probability. Some models based on this approach include conditional probability model, Weight of evidence method, certainty factor method under favourability mapping model, etc.</p> <p><b>Disadvantages:</b> It requires known landslide points as an input data set and can over estimates if the number of known landslide points is too much. Therefore random selection of the landslide point that would be used is crucial.</p> <p><b>Advantages:</b> The fact that it uses known landslides points makes it the most suitable model for landslide susceptibility mapping, as landslide studies are based on the assumption that future landslides will occur under similar circumstances as historic landslide.</p>
<p><b>Artificial Neural Network Based Approach</b></p>	<p>Amongst others Gomez &amp; Kavzglu (2005) used Artificial Neural Networks (ANN) black box approach for landslide susceptibility mapping. In this process, multilayer perceptron with back propagation learning algorithm are used. The approach uses a wide range of causative factors and the existing landslide distribution layer derived from DEM, remote sensing imagery and field data for neural network training and</p>

	<p>testing. Afterwards, existing landslides are considered to validate the landslide susceptibility map. Recently Chauhan et al. (2010) modified the ANN by creating a rating system that depicts the influence of each category on a parameter, on landslide occurrence. Satisfactory results were obtained.</p> <p><b>Disadvantages:</b> There are no known disadvantages for this model as it has not been applied extensively on landslide susceptibility mapping.</p> <p><b>Advantages:</b> It uses both known landslide localities and areas known not to have landslide occurrences, therefore it is less likely to over predict.</p>
<p><b>Fuzzy Set Based Approach</b></p>	<p>This model was proposed by Elias &amp; Bandis (2000) for landslide susceptibility mapping. Fuzzy linguistic rules are used to assign fuzzy membership values to different categories of thematic data layers. The fuzzy membership values are used to provide data to the input neurons for neural network model. A single output neuron with values from 0 to 1 is considered to represent the degree of landslide susceptibility based on actual landslide data. The back error propagation neural network is used for training and a landslide susceptibility map is prepared.</p>
<p><b>Bivariate Statistical analysis</b></p>	<p>In bivariate statistical analysis, each individual thematic data layer is compared to the existing landslide distribution layer. The weighting value of each category of the controlling parameter is assigned based on landslide density. It is based on this equation:</p> $LSI = \sum \log_e \left( \frac{\rho Landslides / parameterclass}{\rho Landslide} \right) \quad \{1\}$ <p><b>Advantage:</b> it provides a good combination between expert-derived parameter choices and quantitative spatial analysis-It renders quantitative and objective measure on landslide susceptibility.</p> <p><b>Disadvantage:</b> it assumes complete independence of input parameter.</p>
<p><b>Multivariate Statistical Analysis</b></p>	<p>Multivariate approaches consider relative contribution of each of the thematic data layer to the total susceptibility within a defined area. The procedure involves several important steps ( Aleotti &amp; Chowdhury 1999):</p> <ol style="list-style-type: none"> <li>1) Identification of percentage of landslide affected areas in each pixel and their classification into stable and unstable zones.</li> </ol>

	<p>2) Preparation of an absent/present matrix of given category of a given thematic layer.</p> <p>3) Multivariate statistical analysis and reclassification of the area based on the results and their classification into susceptibility classes.</p>
--	--

### 2.4.1 Remote sensing on landslide susceptibility mapping

Satellite remote sensing techniques can be used to derive the thematic information needed to synthesize landslide susceptibility maps and to monitor the variable parameter influencing landslide susceptibility (e.g. Lee, Choi & Min 2004b). The advancements in digital image processing has provided additional tools such as data fusion or data merging, enhancement, classification and accuracy assessment techniques. To put these technical advancements into good use the interpretation of remote sensing data should focus on extracting information related to the following features:

- Distinctive features associated with slope movement
- Morphological expression of landslides
- Landslide characteristics including size, shape and contrast to surrounding areas

In this regard, the interpretability of remote sensing data is strongly influenced by the contrast that results from the spectral differences between landslides and its surroundings.

Satellite remote sensing techniques can contribute to landslide investigations at three distinct phases namely: **(a)** detection and classification of landslides **(b)** monitoring landslide movement and identification of conditions leading up to an event, and **(c)** analysis and prediction of slope failures (Morton et al. 2003). Various sources of remote sensing data can contribute to these phases including medium and high resolution optical data, synthetic aperture radar (SAR) data and LiDAR data (Joyce, Samsonov, Levick 2011).

Synthetic Aperture Radar (SAR) data can be employed for the detection and classification of landslides through the analysis of radar backscatter or as early warning by detecting slow-moving landslides through differential interferometry techniques (Joyce et al. 2011). LiDAR data through the derivation of very high resolution digital terrain models (DTMs) is useful for the delineation of landslide morphological features (Joyce et al. 2011). Furthermore, the high resolution DTM data will provide high quality geomorphological information for landslide susceptibility mapping. In addition to SAR and LiDAR data, high resolution optical data including aerial photographs have been commonly used for the detection and classification of landslides (Mantovani, Soeters & van Western 2000). After detection of landslides, the

movement of the landslide can be monitored. This involves a comparison of conditions associated with landslides over time including the aerial extent of the landslide, the speed of movement and the changes in surface topography. Here optical, SAR and LiDAR data can be used in combination with several change detection algorithms (Joyce et al. 2011).

Although the detection and classification of landslides through the techniques described above is important to define landslide controlling parameters, the ideal is to use remote sensing data for monitoring of areas susceptible to landslide occurrence in an effort to provide an early warning. In this regard, optical remote sensing data can be used to monitor the variable condition (vegetation health and productivity and soil water content) that makes an area susceptible to landslide occurrence.

To monitor the health and productivity of the vegetation in an area, optical remote sensing data have frequently been used. Using remote sensing data through normalized difference vegetation indices (NDVIs) and tasseled cap greenness components, the vegetative conditions prior to landslide occurrence can be identified. In addition to the vegetative conditions, the wetness of the soil as an indication of soil moisture is known to play a role on slope stability. Saturated soils are believed to be more prone to instabilities and would therefore have a higher probability of landslide occurrence. In this regard, satellite remote sensing data could assist with the identification of the moisture content of soils through tasseled cap analysis and consequent analysis of the derived wetness component. Although not perfect yet, research is ongoing on the use of SAR backscatter for soil moisture retrieval (Wagner & Pathe 2008)

#### *2.4.1.1 Normalized difference vegetation index (NDVI)*

The Normalized Difference Vegetation index (NDVI) is the simple equation that has been used for several years to calculate vegetation health. It is an index of plant greenness or photosynthetic activity, and is one of the most commonly used vegetation indices (Anderson, Hanson, Haas 1993.). The Normalized Difference Vegetation Index (NDVI) is related to the proportion of photosynthetically absorbed radiation. Many natural surfaces are about equally as bright in the visible red and near-infrared part of the spectrum with the notable exception of green vegetation. Red light is strongly absorbed by photosynthetic pigments (such as chlorophyll) found in green leaves, while near-infrared light either passes through or is reflected by live leaf tissues, regardless of their colour (Stoner & Baumgardner 1980). This means that areas of bare soil having little or no green plant material will appear similar in both the red and near-infrared wavelengths, while areas with much green vegetation will be very bright in the near-infrared and very dark in the red part of the spectrum. Put another way, for healthy living

vegetation, this ratio will be high due to the inverse relationship between vegetation brightness in the red and infrared regions of the spectrum (Paruelo, Epstein, Lauenroth & Burke 1997). The Normalized Difference Vegetation Index (NDVI) is a simple numerical indicator that has been used to analyse remote sensing measurements, typically but not necessarily from a space platform (Perry & Laulenschlager, McFeeters 1996, Pats & Charez 1996). This technique can also be used to gather information about the land cover of the study area (Xiao, Zhang, Yan, Wu, Biradar, 2009, McCloy 2010). The NDVI algorithm subtracts the red reflectance values from the near-infrared and divides it by the sum of near-infrared and red bands.

$$\text{NDVI} = (\text{NIR} - \text{RED}) / (\text{NIR} + \text{RED}) \quad \{2\}$$

The spectral reflectance curve of green and dry vegetation and soil is presented on Figure 7.

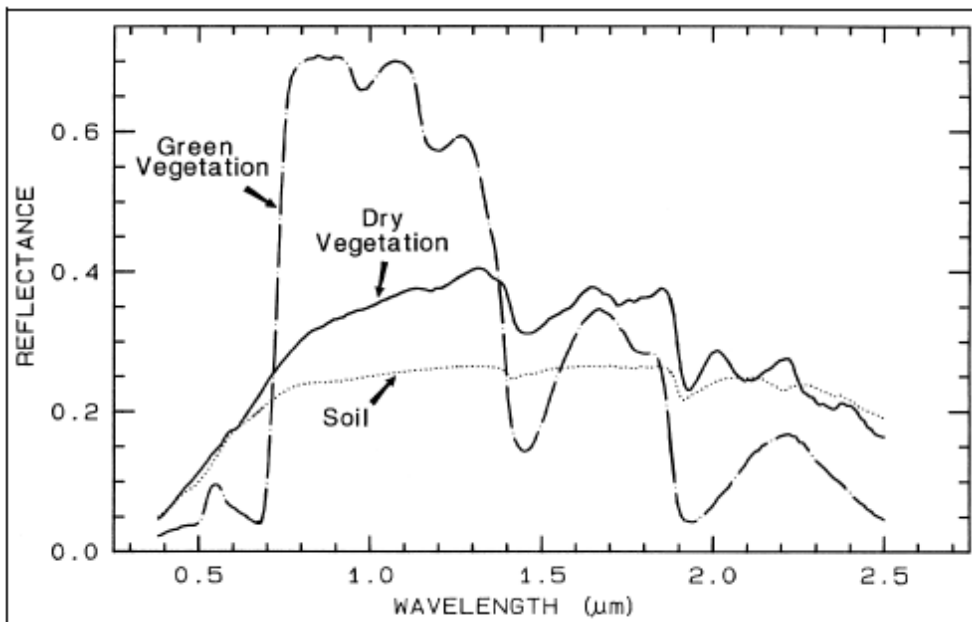


Figure 7: The spectral reflectance curve of green and dry vegetation and soil along with the spectral wavelength (Clarck et al.1999).

#### 2.4.1.2 Normalise difference water index

The normalised difference water index (NDWI) is derived using similar principles to the Normalised Difference Vegetation Index (NDVI). In an NDVI (the comparison of differences of two bands, red and near-infra-red (NIR), the presence of terrestrial vegetation and soil features is enhanced while the

presence of open water features is suppressed because of the different ways in which these features reflect these wavelengths (McFeeters 1996). The NDWI is derived from the Near-Infrared (NIR) and Short Wave Infrared (SWIR). The SWIR reflectance reflects changes in both the vegetation water content and the spongy mesophyll structure in vegetation canopies, while the NIR reflectance is affected by leaf internal structure and leaf dry matter content but not by water content (Rahman 2011). The combination of the NIR with the SWIR removes variations induced by leaf internal structure and leaf dry matter content, improving the accuracy in retrieving the vegetation water content. The NDWI is calculated according to the following equation (Gao 1996):

$$\text{NDWI} = (\text{SWIR} - \text{NIR}) / (\text{SWIR} + \text{NIR}) \quad \{3\}$$

## 2.5 FINAL REMARKS

Landslides have been extensively studied, dating back to 1970s. There have been only minor changes in the principles of landslide susceptibility mapping over the years but the evolution of remote sensing and GIS has contributed significantly to the efficiency and accuracy of landslide susceptibility maps. Landslide susceptibility mapping strongly depends on the identification of landslide causative factors and weighting of the causative factors in accordance with their significance to slope instability. The landslide causative factors can be categorized into three classes (1) static factors (i.e. slope, aspect, geology, infrastructure, landcover, soil type, and soil depth), (2) variable factors (i.e. vegetation and soil moisture) and (3) triggering factors (i.e. rainfall, seismicity and human causes). The static factors are the only parameter used to model a landslide susceptibility map and the variable factors can be used to monitor the changes that make an area susceptible to landslide and can therefore be used as an early warning system.

## **CHAPTER 3 GIS-BASED LANDSLIDE SUSCEPTIBILITY MAPPING: MATERIALS, RESULTS AND ACCURACY ASSESSMENT**

Landslide susceptibility mapping is the technique that is used to zone those areas that are likely to have landslides, using different data sets. GIS and remote sensing have been used extensively when deriving landslide causative thematic maps. A geographic information system is a major tool that is used to integrate different landslide causative thematic maps when modeling landslide susceptibility maps. The landslide causative factors that are used when modeling a landslide susceptibility map are discussed on Section 2.2. Landslide susceptibility mapping methodologies are based on the assumption that future landslides will occur under similar conditions as historic landslides. For this reason the weight of evidence method was used to model a landslide susceptibility map of the study area. Moreover, the weight of evidence method was chosen because of its proven success in landslide susceptibility mapping (Athanasopoulos, Pelekis, Leonidou 1995). The map combination approach is also evaluated in this study, mainly because it does not use landslide inventory data as one of the inputs when modeling a landslide susceptibility map, unlike the weight of evidence. The following section describes the input data available for susceptibility mapping by considering the static controlling parameters discussed in Section 2.2 of Chapter 2. This is followed by the description of the landslide susceptibility mapping techniques employed and presents the results and accuracy of the landslide susceptibility maps.

### **3.1 INPUT DATA**

The two models require a variety of input data set. The Cape datum was used. These inputs are discussed below.

#### **3.1.1 Geology**

The 1:250 000 geological map was attained from the Council for Geoscience. The main lithological types that were encountered within the study area were: shales, sandstone, siltstone, conglomerate, glacial deposits (Dwyka) and unconsolidated alluvium deposits. The granites of the Cape Granites suit were also prominent. The geological layer is presented in Figure 8. The structural features such as faults, dykes, lineaments and lithological contacts will affect the area's susceptibility to landslides, as discussed in Section 2.2.1.1. Since geological mapping took place at 1: 250 000 scale, a 250 m buffer was applied to the faults and lithological contacts data.

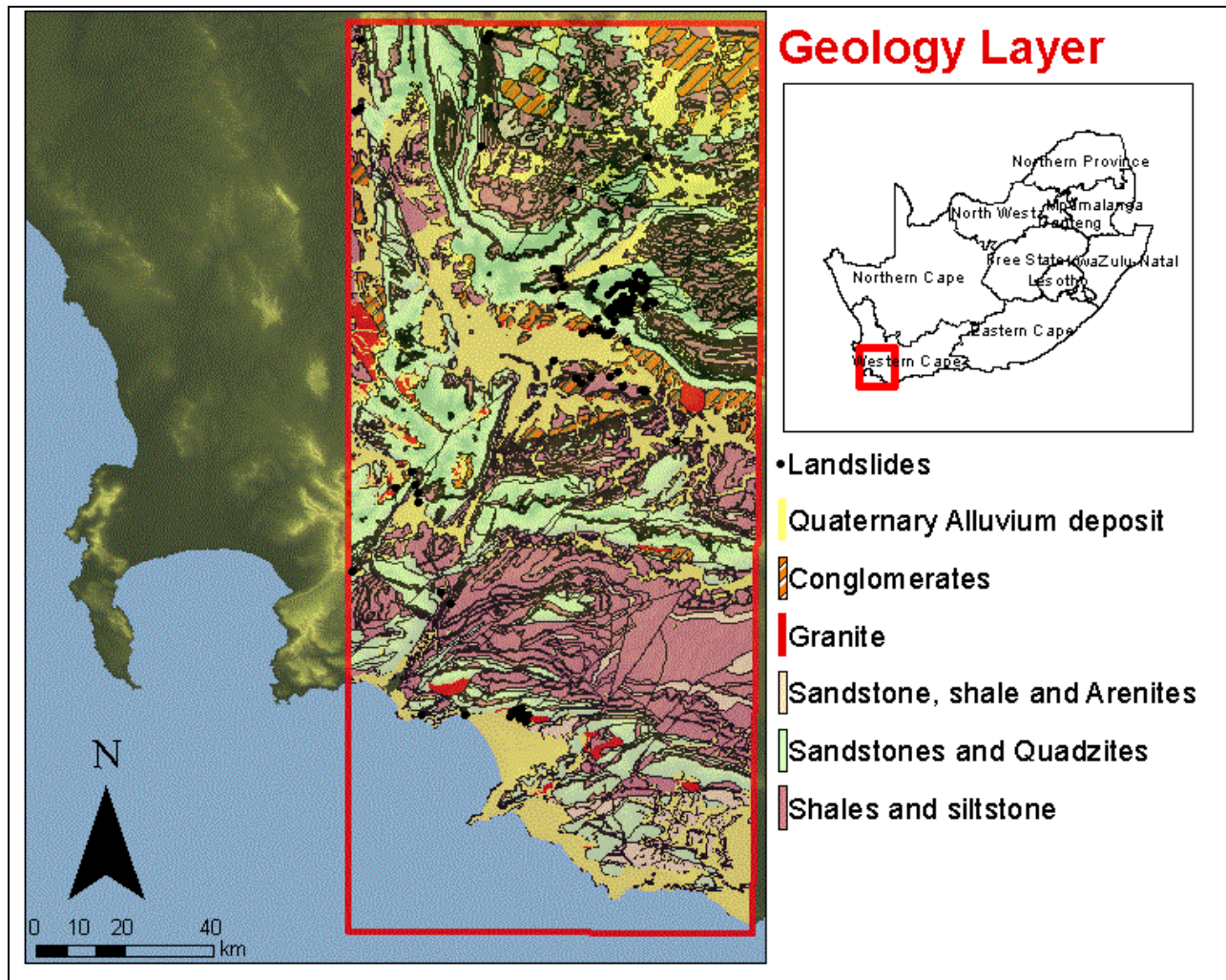


Figure 8: The geological parameter of the study area, the lithological units are shown on the legend. This geological layer was one of the causative thematic layers used to model a landslide susceptibility map of the study area using the weight of evidence method.

The faults and lithological contacts layer is presented on Figure 9, where a buffer of 250 metre was applied.

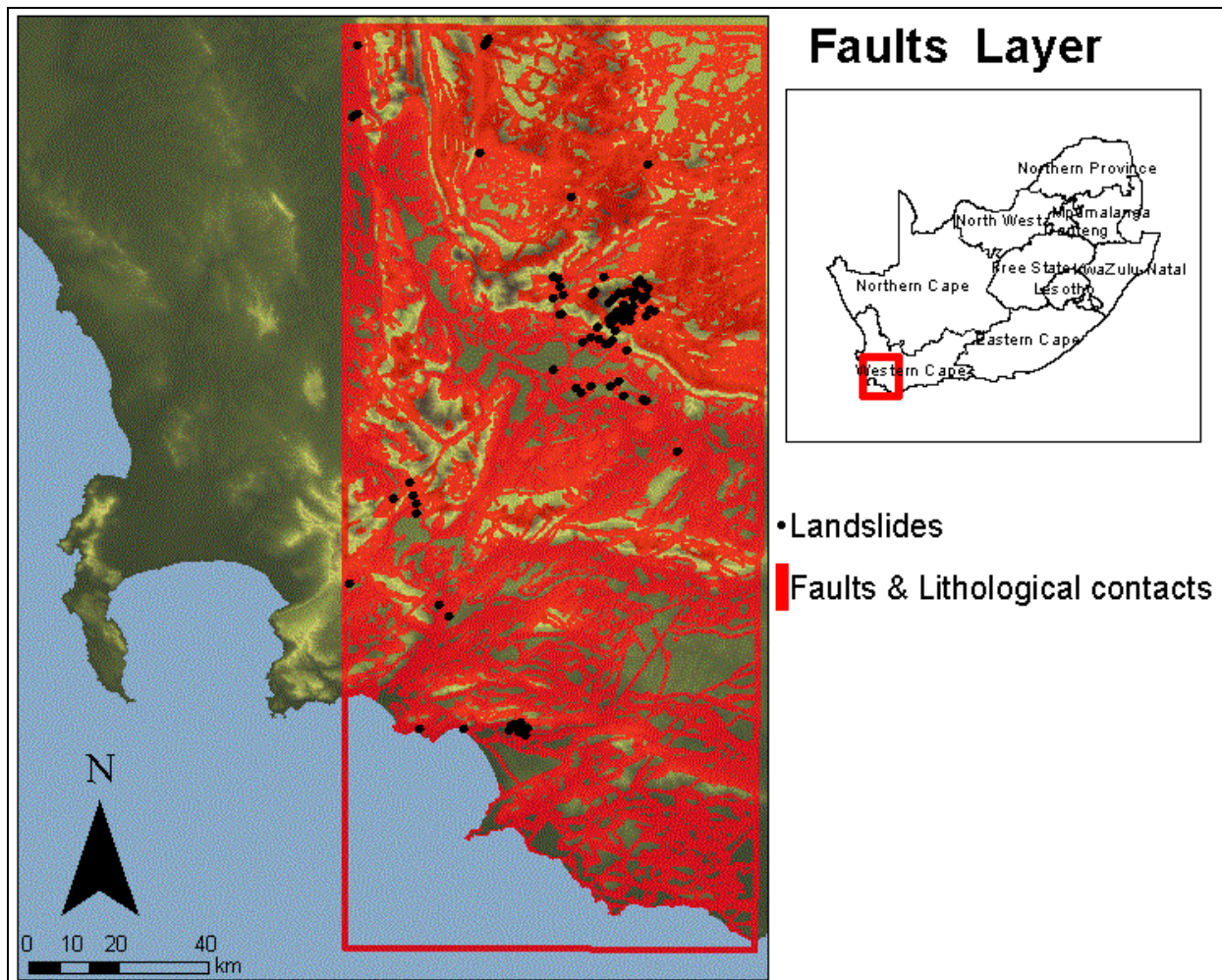


Figure 9: The 250 meter buffered lithological contacts and faults layer for the study area. This thematic layer was one of the causative thematic layers used to model a landslide susceptibility map of the study area. The localities for the landslides are also shown.

The numbers of landslides per stratigraphic unit is presented on Figure 10, a large number of landslides fall on the Quaternary Alluvium deposits, Skurweberg, Rietvlei and Peninsula stratigraphic units, in decreasing order. It is observed that a large number of landslides fall on the unconsolidated alluvium deposits. The Peninsula, Rietvlei and Skurweberg stratigraphic units are dominated by sandstones and quartzites lithologies, which are generally considered to be moderately susceptible to landslide occurrences. These stratigraphic units recorded a large number of landslides. It is also observed that 53 landslides out of 93 landslide localities used to run the weight of evidence method fall within the 250 meter faults and lithological contacts buffer. This indicates that areas with faults and lithological contacts are generally more susceptible to landslide occurrence.

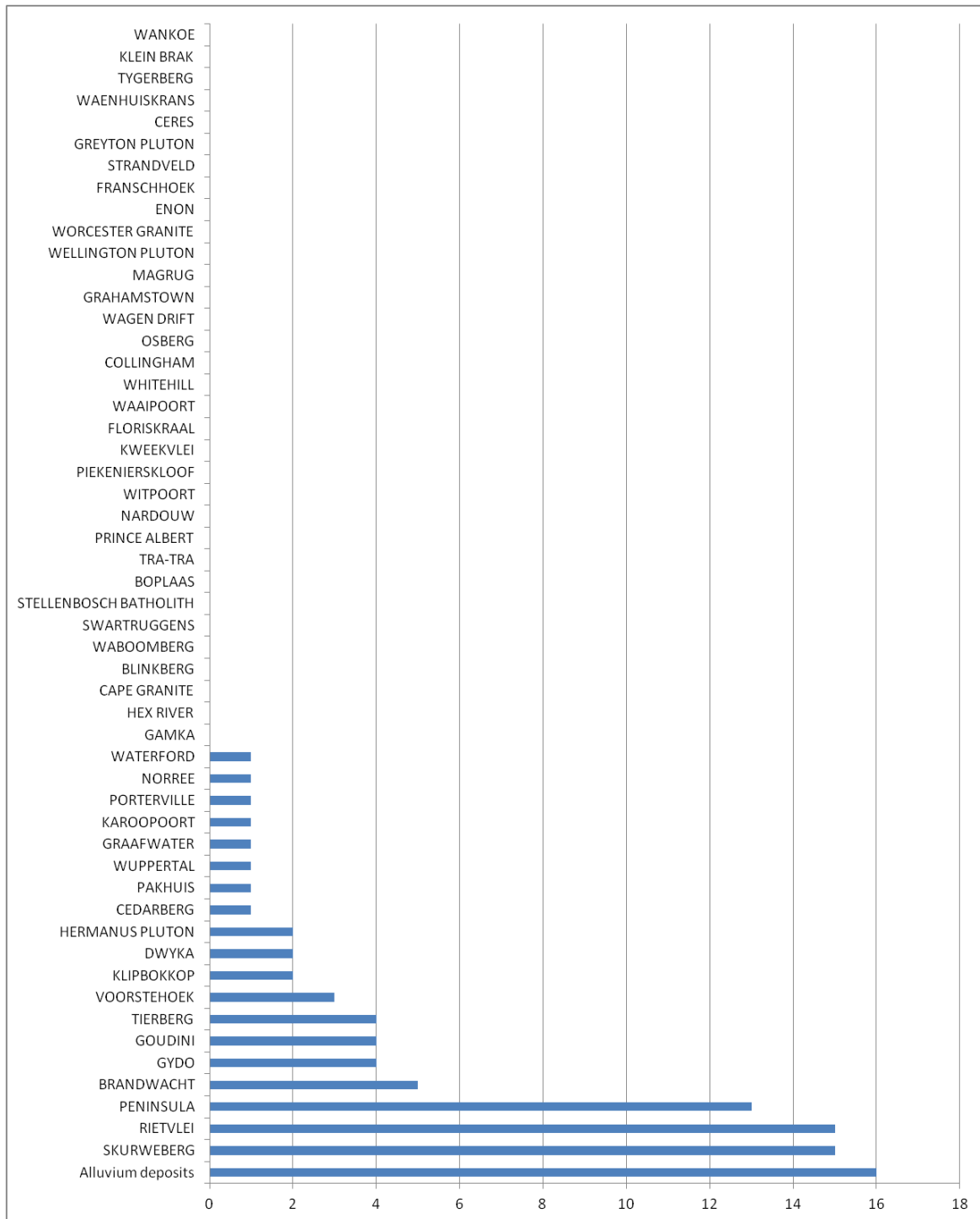


Figure 10: The graph shows the number of landslides per lithology. On the y-axis is the stratigraphic units and on the x-axis is the number of landslides. The alluvium deposits recorded the highest number of landslides and the Skurweberg, Rietvlei and Peninsula stratigraphic units recorded the second highest, and the third highest number of landslides, in decreasing order.

### 3.1.2 Geomorphology

The geomorphological factors affecting landslide susceptibility (including slope and aspect) were derived from the 20 meter resolution digital elevation model (DEM). The digital elevation model was interpolated from a 20 meter contour map, attained from National Geo-spatial Information (NGI). The slope and aspect layers are presented on Figure 11 and Figure 13, respectively; the known landslide localities are also shown on these layers.

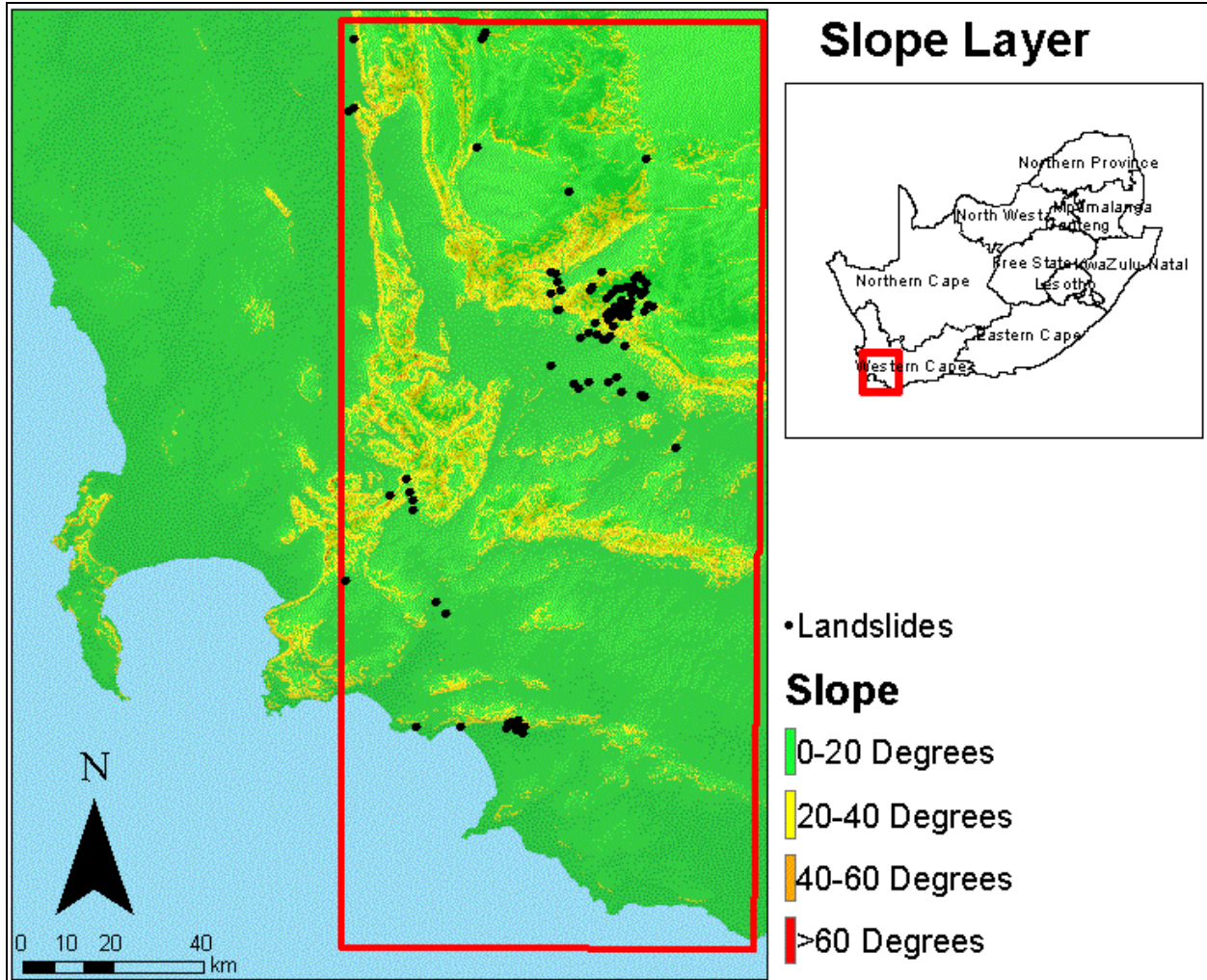


Figure 11: Slope layer of the study area. The classes that were used in the weight of evidence method are also shown on the legend.

Figure 12 shows the number of landslides per slope class. Approximately 90 percent of the landslides fall on the 0-20° and 20-40° classes. This is no surprise as slopes greater than 18° in South Africa are considered to be susceptible to landslide occurrence. There is only one landslide on slopes greater than

40°, it is more likely that the landslide is a rockfall which are normally caused by road cuts on mountainous areas.

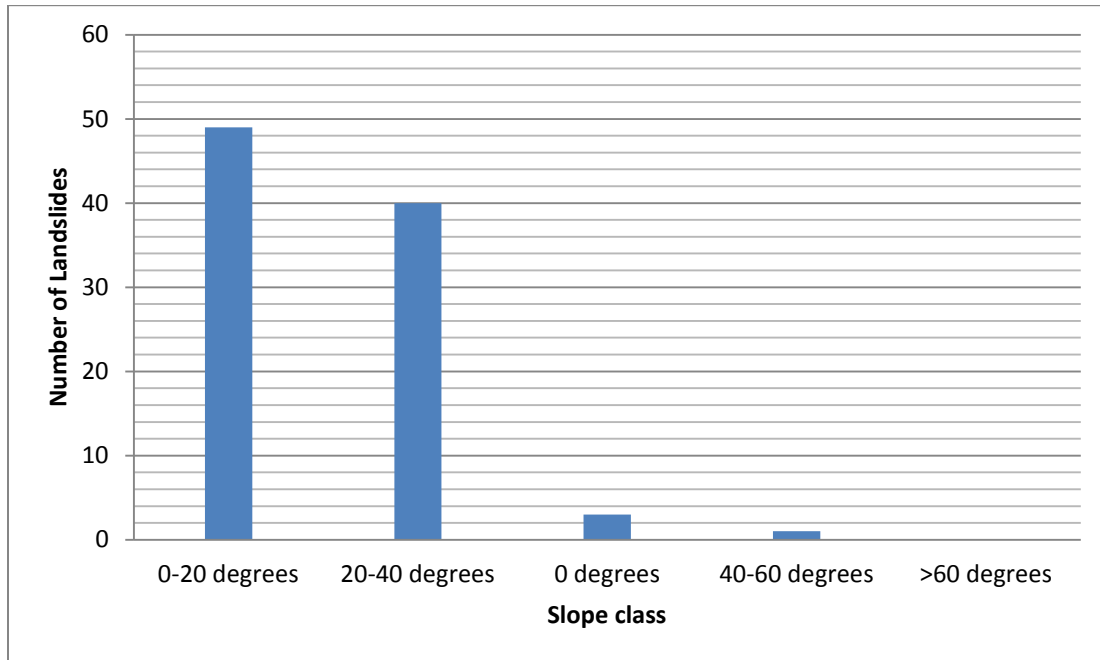


Figure 12: The number of landslides per slope class. Roughly 90 % of the landslides fall on the 0-20° and 20-40° class.

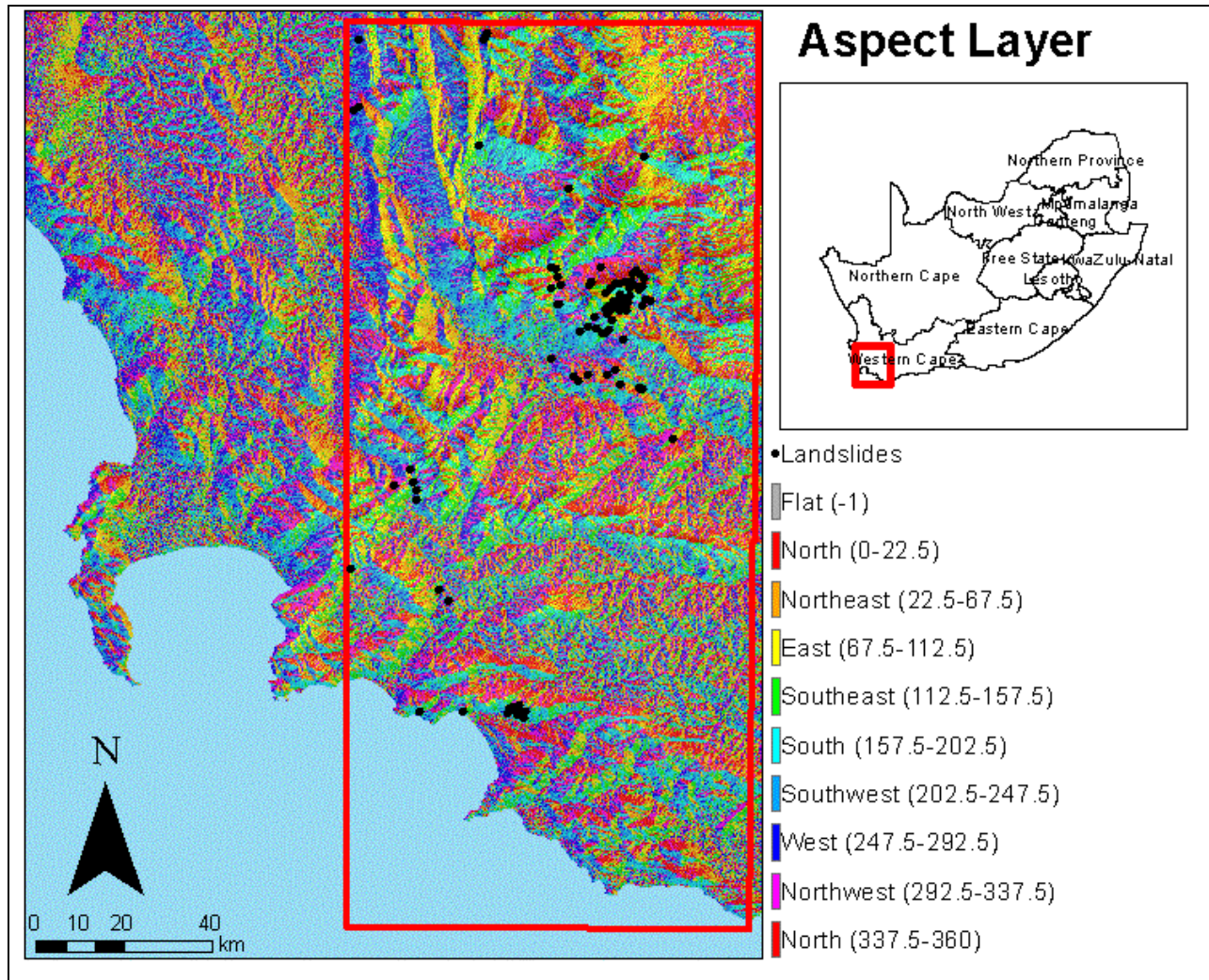


Figure 13: The aspect layer for the study area. The classes are shown in the legend. The aspect thematic layer was one of the causative layers used to model a landslide susceptibility map of the study area, using the weight of evidence method. The black dots on the map are the localities for the known historic landslides within the study area.

The number of landslides per aspect class is presented on Figure 14, interestingly all the aspect classes recorded at least one landslide. A large number of landslides fall on the South and South Western slopes. This can be explained by the fact that south facing slopes are generally wetter as they receive a limited amount of sunlight as compared to the north facing slopes. Moreover the south facing slopes are less vegetated when compared to the north facing slopes. This makes them more susceptible to landslide occurrence. The north facing slopes have a smaller number of landslides, this is no surprise as the north facing slopes receive a large amount of sunlight and therefore generally dry in comparison to the south facing slopes. The east facing slope have only one landslide points.

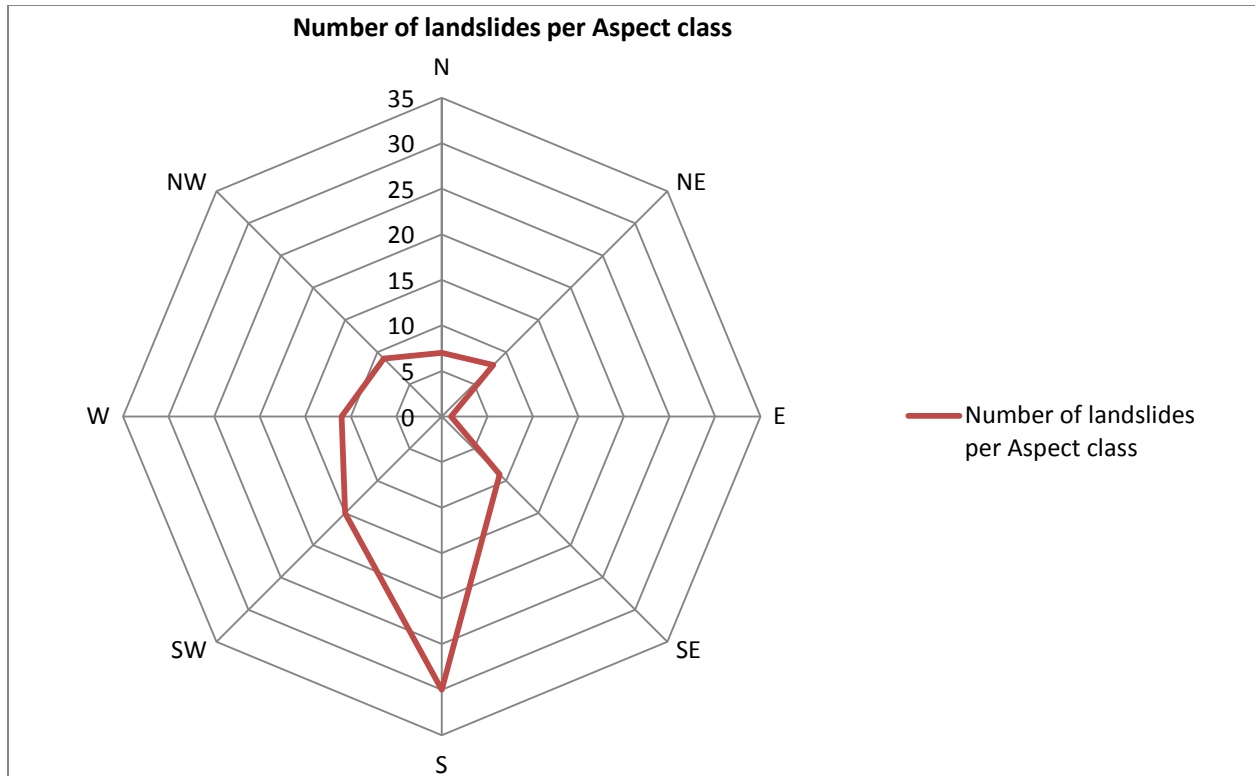


Figure 14: The number of landslides per aspect class. The south facing slope recorded the highest number of landslides and the east facing slopes recorded the least number of landslides.

### 3.1.3 Landcover

Landcover parameters that affect the area's susceptibility to slope instability include (biological and physical landcover, soil depth and soil type). The significance of these parameters on slope instability has been discussed on Section 2.2.1.3 of Chapter 2. The biological and physical landcover layer of the study area was acquired from the CSIR (this is the National Landcover 2000 (NLC2000) product). The soil type and soil depth layer of the study area was acquired from the ARC Institute of Soil Climate and Water (ICSW). The landcover layer (Figure 15), soil depth layer (Figure 17) and the soil type map (Figure 19) were some of the input parameters that were in the weight of evidence method and map combination approaches.

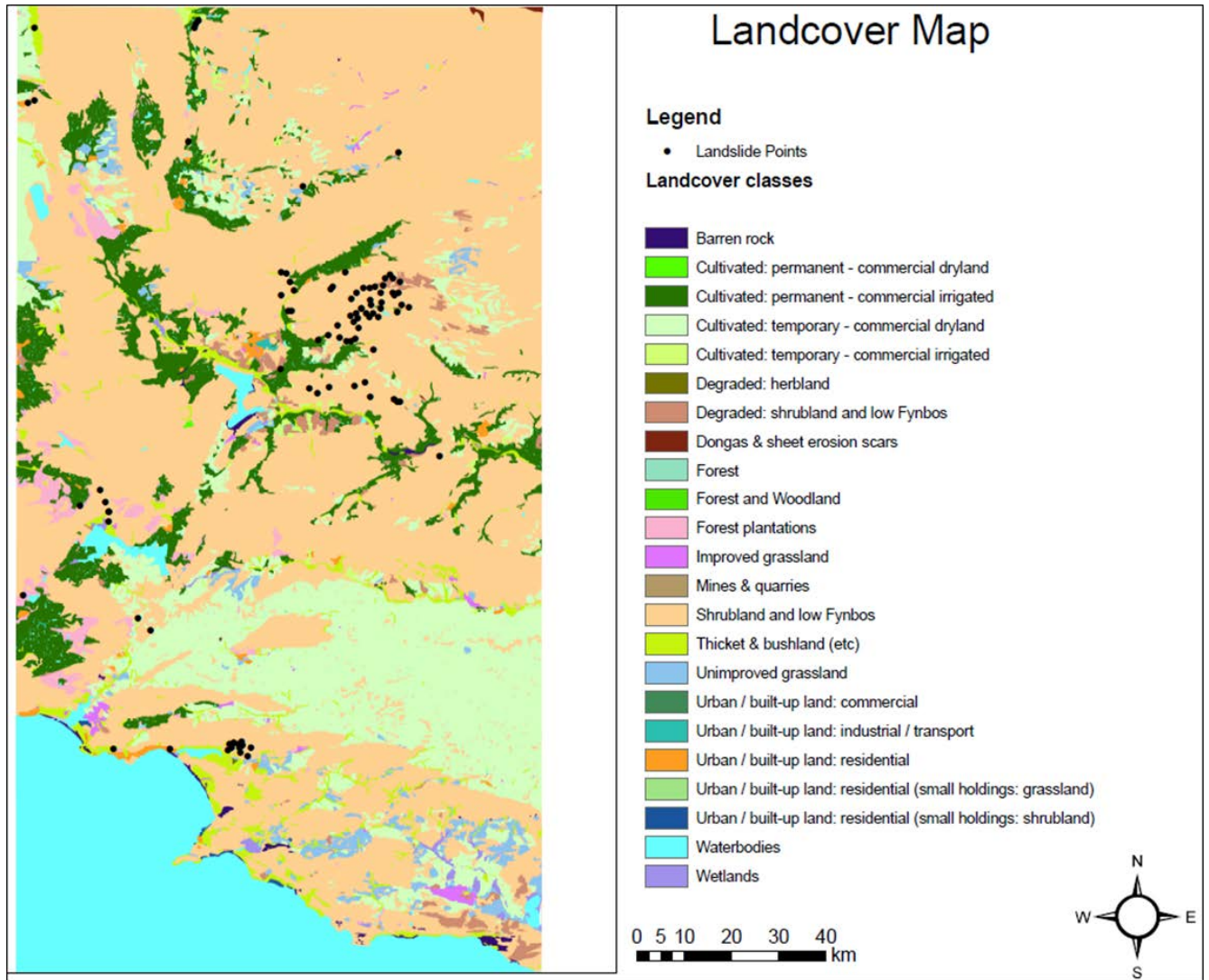


Figure 15: The land cover layer used when modelling the landslide susceptibility map of the study area. The landcover classes are shown in the legend.

The number of landslides per landcover class is shown in Figure 16. It is observed that more than 80% of the landslides fall on the shrubland and low fynbos. The shrubland and low fynbos is the most dominant class (in area), in the study area.

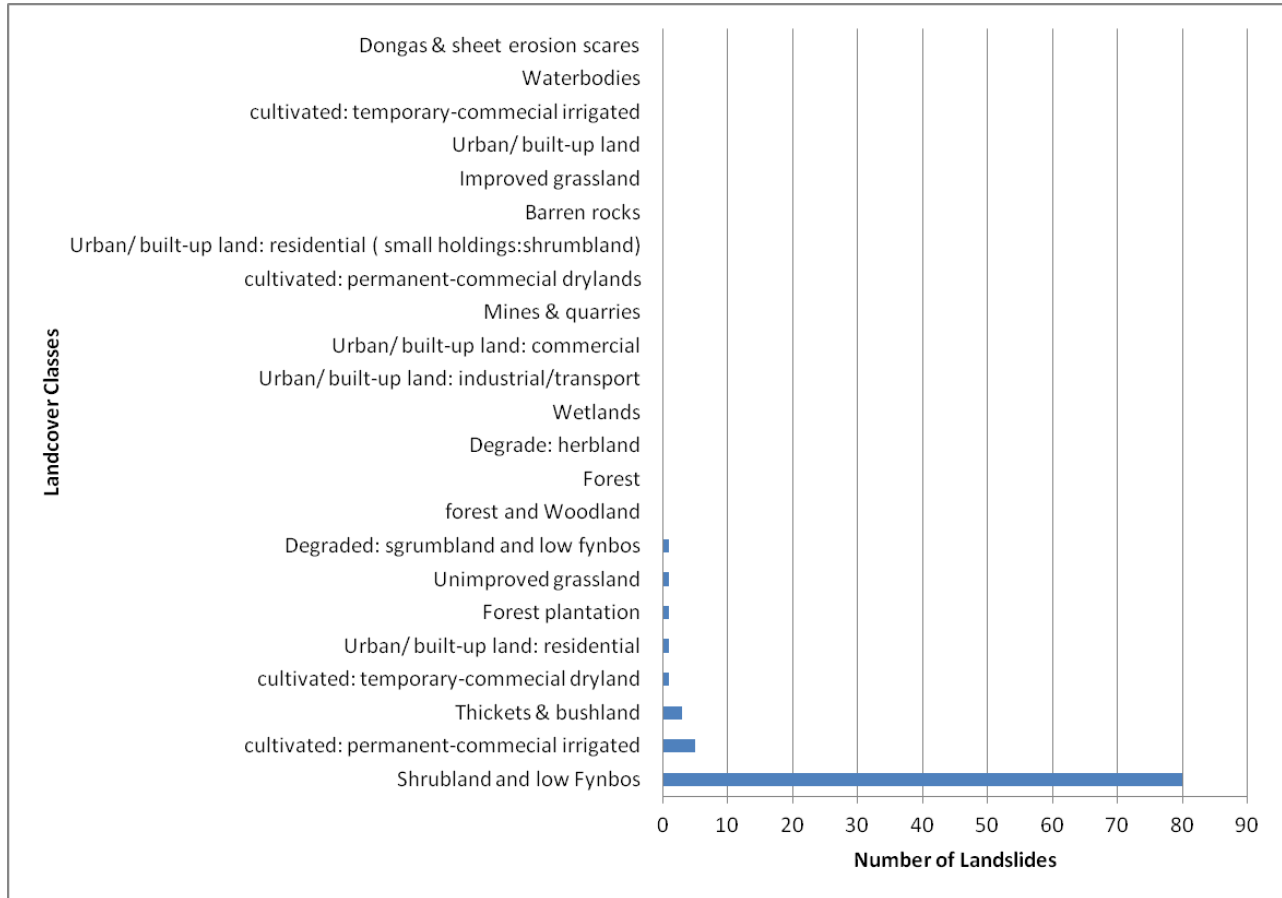


Figure 16: The number of landslides per landcover class. A large number of landslides fall on the Shrubland and low fynbos class. The other landcover classes recorded a very low number of landslides.

Soil depth is considered to be one of the most important causative factors when modelling landslide susceptibility maps. The soil depth map of the study area is shown on Figure 17. The localities for known landslide points are represented by the black dots on the layer.

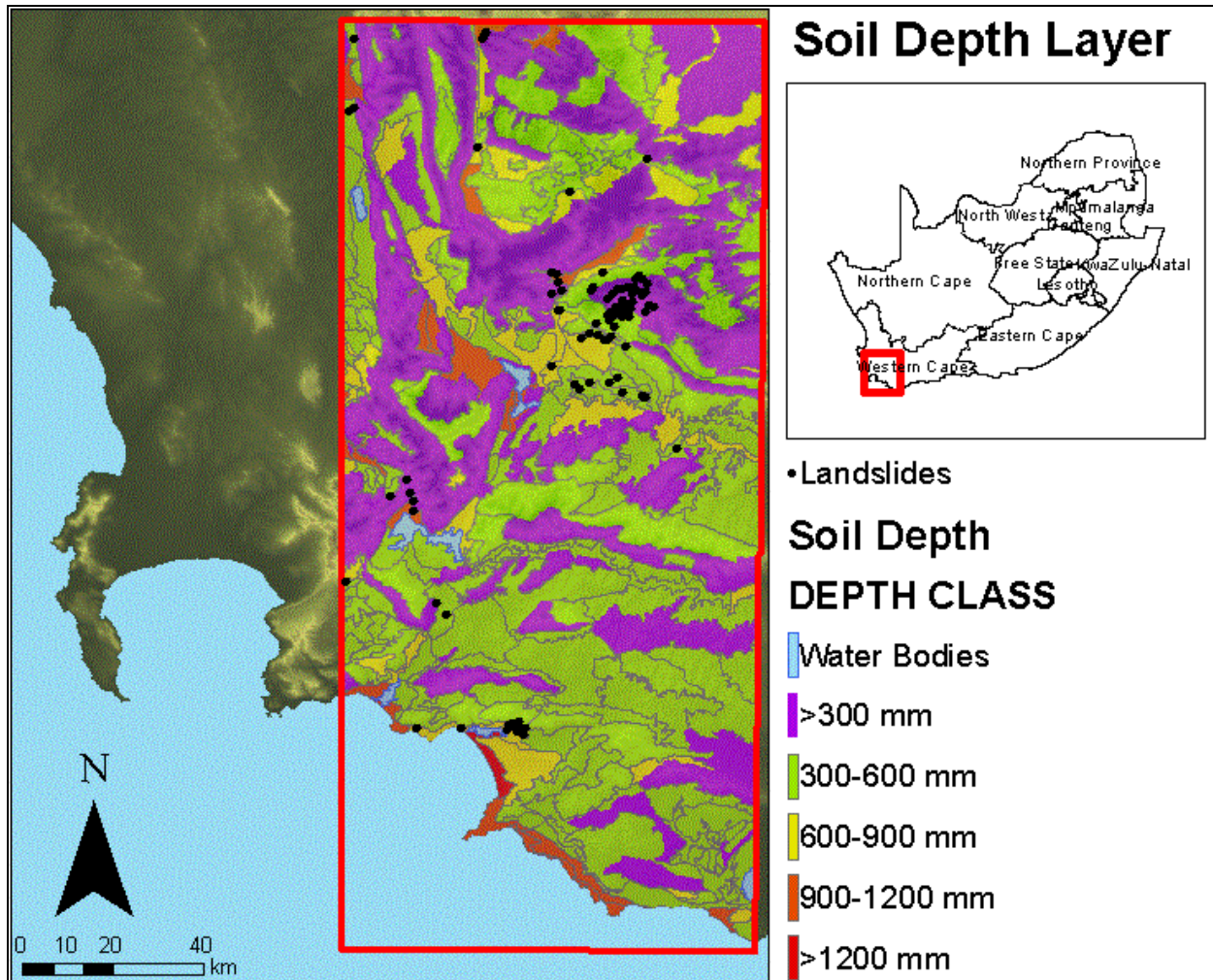
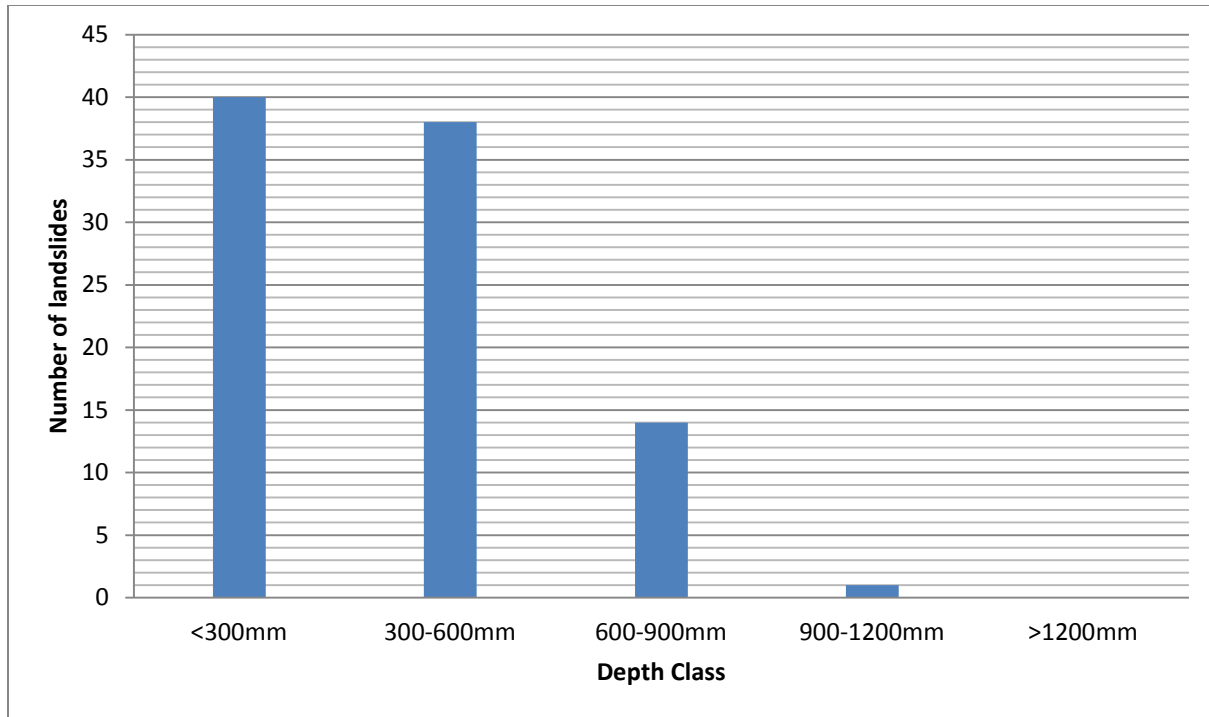


Figure 17: The soil depth layer of the study areas. The depth classes are also shown on the legend. This thematic layer was one of the causative parameters used to model a landslide susceptibility map of the study area.

The number of landslides per soil depth class is presented on Figure 18. A large number of landslide points fall on soil depth less than 300 mm, 300 mm- 900 mm, and 600-900 mm; in decreasing order. Looking at the soil depth map on Figure 17, it is visible that these three classes are the most dominant soil depth classes in the study area. The soil depth greater than 1200 mm makes far less than 1 percent of the study area and the 900-1200mm class makes roughly 1% of the study area.



*Figure 18: The number of landslides per soil depth class. More than 90 % of the landslides fall on the soil depth less 300 mm, 300-600mm and 600-900 mm; in decreasing order. Soil depth less than 300mm recorded the highest number of landslides and the soil depth between 900-1200mm recorded the least number of landslides.*

The soil type thematic map was also used as the input parameter when modelling the landslide susceptibility map using the weight of evidence method. The soil type thematic layer is presented on Figure 19.

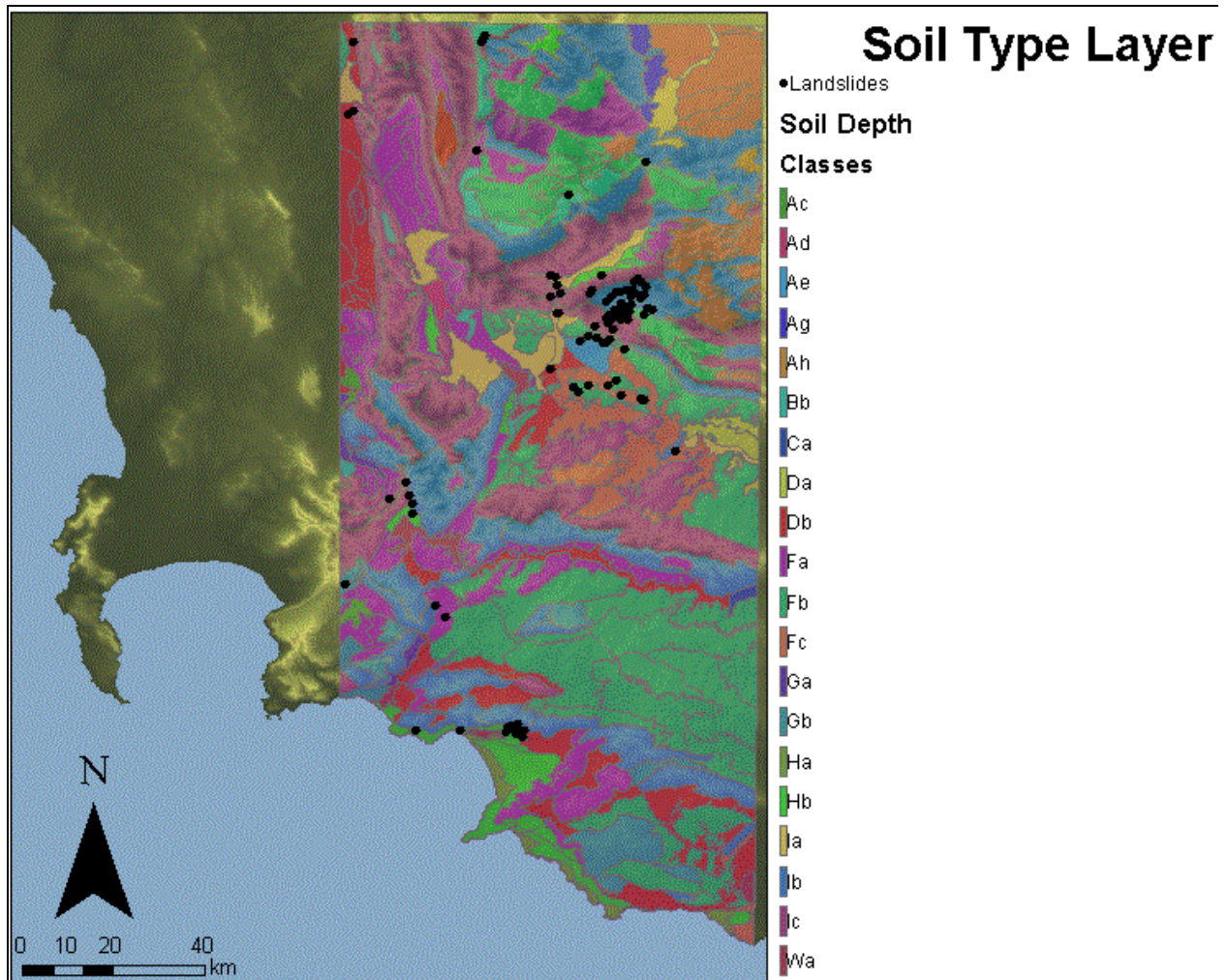


Figure 19: The soil type layer for the study area, which was used to model the landslide susceptibility map using the weight of evidence method. The description for the codes used in the legend is shown on the Table 3.

The numbers of landslides per soil type class are presented on Figure 20, a large number of landslides fall on class Lb, Lc, Fb and Hb in decreasing order. The Lb and Lc classes are dominated by rocky outcrops, as explained on Table 3. Such a high number of landslides on these classes were unexpected. The Fb class is dominated by shallow lime rich soils, and shallow soils are generally low to moderately susceptible to landslide occurrence. The only class that is known to be more susceptible to landslide occurrence is Hb. This class consists of deep grey sands, deep soils are considered to be more susceptible to landslide occurrence according to some landslide researchers.

Table 3: The description for the soil type classes (source: ARC institute for Soil, Climate and Water).

Broad soil pattern code	Description
Aa	Freely drained, red and yellow apedal soils with humic topsoils comprise >40% of the land type
Ab	Freely drained, red and yellow, dystrophic/mesotrophic, apedal soils comprise >40% of the land type (yellow soils <10%)
Ac	Freely drained, red and yellow, dystrophic/mesotrophic, apedal soils comprise >40% of the land type (red and yellow soils each >10%)
Ad	Freely drained, red and yellow, dystrophic/mesotrophic, apedal soils comprise >40% of the land type (red soils comprise <10%)
Ae	Freely drained, red, eutrophic, apedal soils comprise >40% of the land type (yellow soils comprise <10%)
Af	Freely drained, red, eutrophic, apedal soils comprise >40% of the land type (yellow soils comprise <10%); with dunes
Ag	Freely drained, shallow (<300 mm deep), red, eutrophic, apedal soils comprise >40% of the land type (yellow soils comprise <10%)
Ah	Freely drained, red and yellow, eutrophic, apedal soils comprise >40% of the land type (red and yellow soils each comprise >10%)
Ai	Freely drained, yellow, eutrophic, apedal soils comprise >40% of the land type (red soils comprise <10%)
Ba	Red and yellow, dystrophic/mesotrophic, apedal soils with plinthic subsoils (plinthic soils comprise >10% of land type, red soils comprise >33% of land type)
Bb	Red and yellow, dystrophic/mesotrophic, apedal soils with plinthic subsoils (plinthic soils comprise >10% of land type, red soils comprise <33% of land type)
Bc	Red and yellow, eutrophic, apedal soils with plinthic subsoils (plinthic soils comprise >10% of land type, red soils comprise >33% of land type)
Bd	Red and yellow, eutrophic, apedal soils with plinthic subsoils (plinthic soils comprise >10% of land type, red soils comprise <33% of land type)
Ca	Land type qualifies as Ba-Bd, but >10% occupied by upland duplex/margalitic soils
Da	Duplex soils (sandier topsoil abruptly overlying more clayey subsoil) comprise >50% of land type; >50% of duplex soils have red B horizons
Db	Duplex soils (sandier topsoil abruptly overlying more clayey subsoil) comprise >50% of land

	type; <50% of duplex soils have non-red B horizons
Dc	Either red or non-red duplex soils (sandier topsoil abruptly overlying more clayey subsoil) comprise >50% of land type; plus >10% occupied by black or red clays
Ea	Black or red clays comprise >50% of land type
Fa	Shallow soils (Mispah & Glenrosa forms) predominate; little or no lime in landscape
Fb	Shallow soils (Mispah & Glenrosa forms) predominate; usually lime in some of the bottomlands in landscape
Fc	Shallow soils (Mispah & Glenrosa forms) predominate; usually lime throughout much of landscape
Ga	Podzols occur (comprise >10% of land type); dominantly deep
Gb	Podzols occur (comprise >10% of land type); dominantly shallow
Ha	Deep grey sands dominant (comprise >80% of land type)
Hb	Deep grey sands sub dominant (comprise >20% of land type)
Ia	Deep alluvial soils comprise >60% of land type
Lb	Rock outcrops comprise >60% of land type
Ic	Rock outcrops comprise >80% of land type

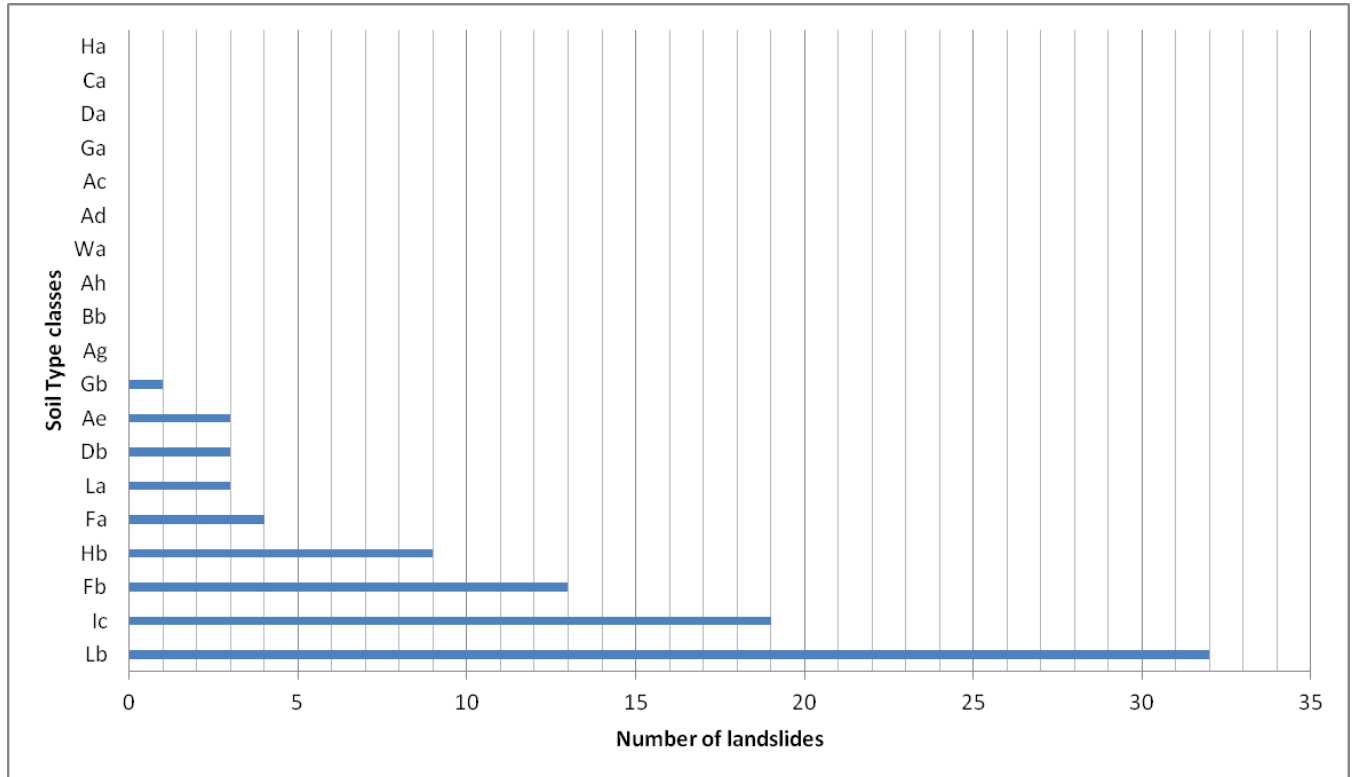


Figure 20: The number of landslides per soil type class. Class Lb (Rock outcrops comprise >60% of land type) recorded the highest number of landslides and class Gb (Podzols occur (comprise >10% of land type); dominantly shallow) recorded the least number of landslides.

### 3.1.4 Anthropogenic influences

Anthropogenic influence on slope instability has been discussed on Section 2.2.1.4 of Chapter 2. The road and rail cut layer of the study area was mapped at 1:50 000 scale, therefore a buffer of 50 metres was used for the roads and rail cuts. The road and rail cuts data was acquired from National Geo-spatial Information (NGI).

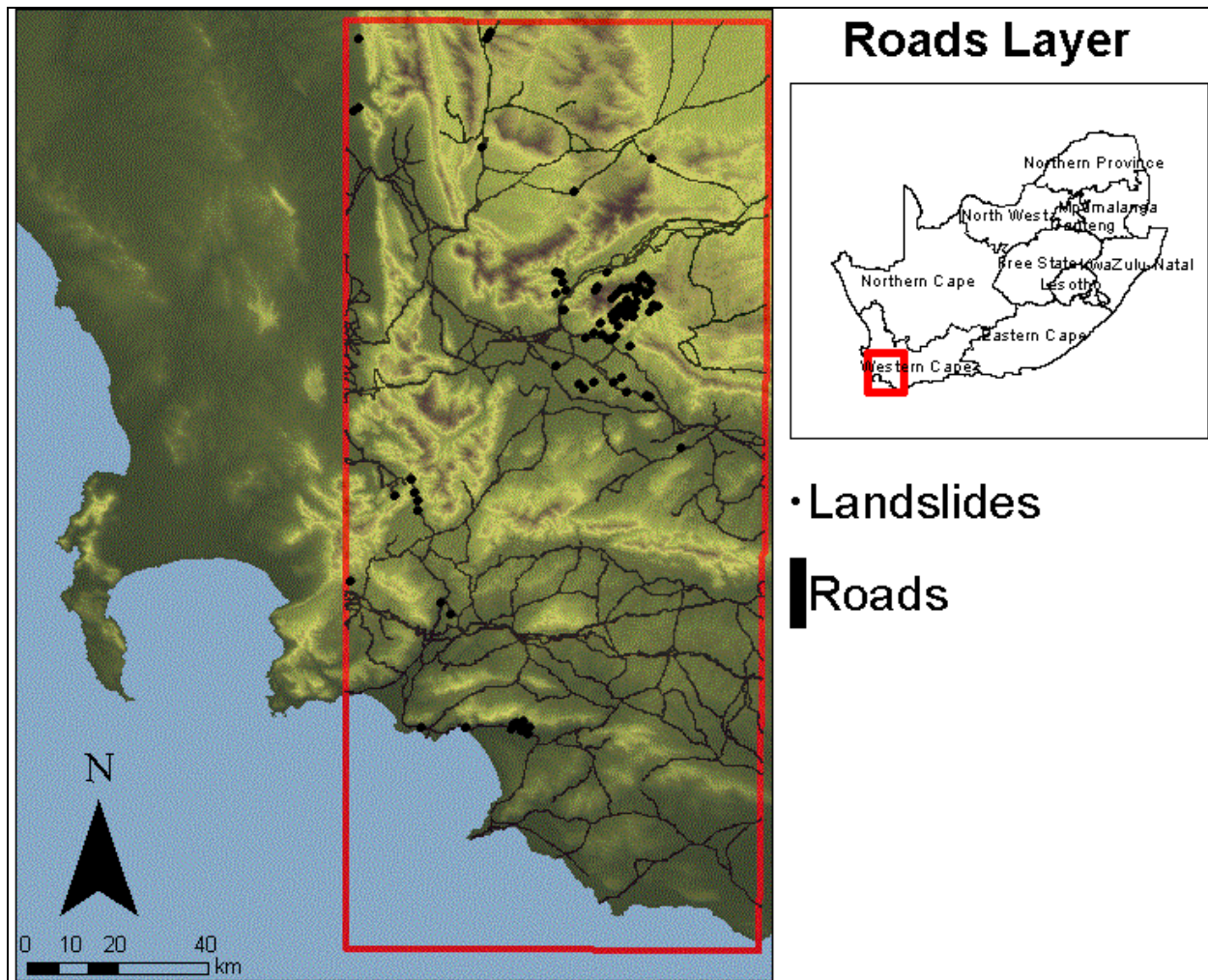


Figure 21: The layer containing the roads and rails within the study area. A buffer of 50 meter was used. The localities of known historic landslides are represented by the black dots on the map.

### 3.2 LANDSLIDE SUSCEPTIBILITY MAPPING – THE WEIGHTS OF EVIDENCE APPROACH

The weight of evidence approach was selected for the creation of a landslide susceptibility map. This method was first described by Bonham-Carter, Agterberg & Wright (1989). It uses the Bayesian probability model and was originally developed for mineral potential assessment (Bonham-Carter, Agterberg & Wright 1988 & 1989). A GIS framework was used to calculate the spatial relationship between landslide occurrence and specific terrain features that are known to have influence on landslide occurrences. These terrain features were selected on the basis that there is a known relationship between the feature and landslide occurrence and that the feature data were available for the entire part of the study

area. Additionally, the location of a selection of known landslides was used as input. The weights of the landslide causative thematic layers (input data) are calculated based on this landslide inventory map. Each feature layer were prepared as, or converted to, raster images and the spatial data modeler was used in order to obtain the statistical relationships between terrain features and landslides, using GIS.

The weight of evidence approach combines the spatial relationships between terrain features from a variety of different thematic layers, each considered to have some relationship to landslide occurrence. For each thematic layer weights are calculated for each individual factor (e.g. slope between 0-20°, 20-40°, 40-60° and greater than 60°) and a weight map is developed from that theme. All thematic weight layers are then added together to develop a landslide susceptibility map. The positive weight (W+) and negative weight (W-) are calculated as the algorithm of the ratio of spatial probabilities, as follows:

$$W^+ = \log_e \frac{P\{B | D\}}{P\{B | D^*\}} \quad \{4\}$$

$$W^- = \log_e \frac{P\{B^* | D\}}{P\{B^* | D^*\}} \quad \{5\}$$

Where P is the probability of having landslide, B is the presence of landslide controlling parameter, B\* is the absence of potential landslide controlling parameter, D is the presence of landslide and D\* is the absence of landslide. A positive (W+) and a negative (W-) indicate a positive and negative correlation between the presence of the predictive variables and the landslide respectively. Positive and negative weights are calculated for each factor in each theme. The positive weight is an indication of the likelihood of encountering a landslide when the specific factor is present. The weight contrast (C) is then calculated and its magnitude reflects the spatial association between the predictable variables and the landslide. Weights and rankings for all parameters are developed based on the analysis of historical landslides.

A positive weight that is greater than zero implies that landslides are more likely than average to occur in the presence of the specific landslide causative factor. A positive weight equal to zero suggests landslides are no more and no less likely than average to be present, and a positive weight less than zero suggests landslides are less likely, than average to be present, given the presence of the specific landslide causative factor. The weights that are strongly negative and strongly positive are therefore more useful in determining landslide susceptibility, as they provide the strongest indication of likely presence or absence of landslides. The weights close to zero give little insights on the likelihood of landslide occurrence.

The algorithm calculates weights for each thematic layer, where each specific factor within that theme is assigned a numeric value equal to its calculated weight. The weights for each weighted layer were then added to yield a combined map.

### **3.2.1 Weight of evidence landslide susceptibility map**

The result of the weight of evidence method is presented on Figure 23. The thematic layer (discussed above) were used to run the weight of evidence method, using spatial data modeler. In addition the verified landslide localities were part of the input layers. The weights were calculated using the known landslide localities. The susceptibility values were between zero and one, with one being the highest susceptibility and zero being the lowest susceptibility. The classified landslide susceptibility map is presented on Figure 24. The classes were created using natural break classification of ArcGIS, as shown in Figure 22. The natural break method was used because it minimizes the variance between the classes. Five classes were selected when applying the natural break classification method. In the map these classes are shown as Very high, High, Moderate, Low and Very Low. The red and orange areas on the map are the Very High and High susceptible areas, respectively, the yellow areas are the moderately susceptible and the light green and green areas are the Low and Very Low susceptible areas, respectively.

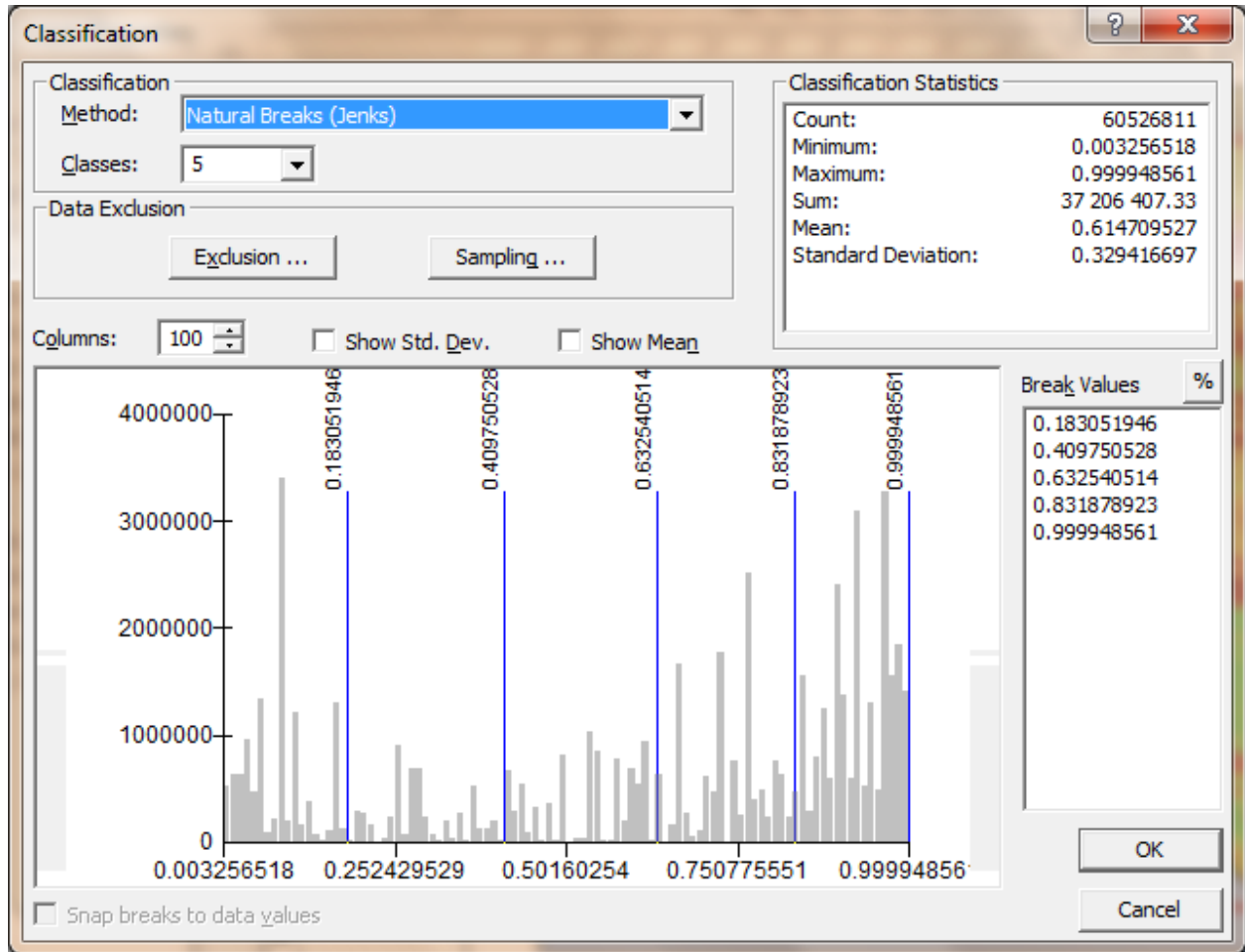


Figure 22: Classification of the landslide susceptibility map using the natural break method.

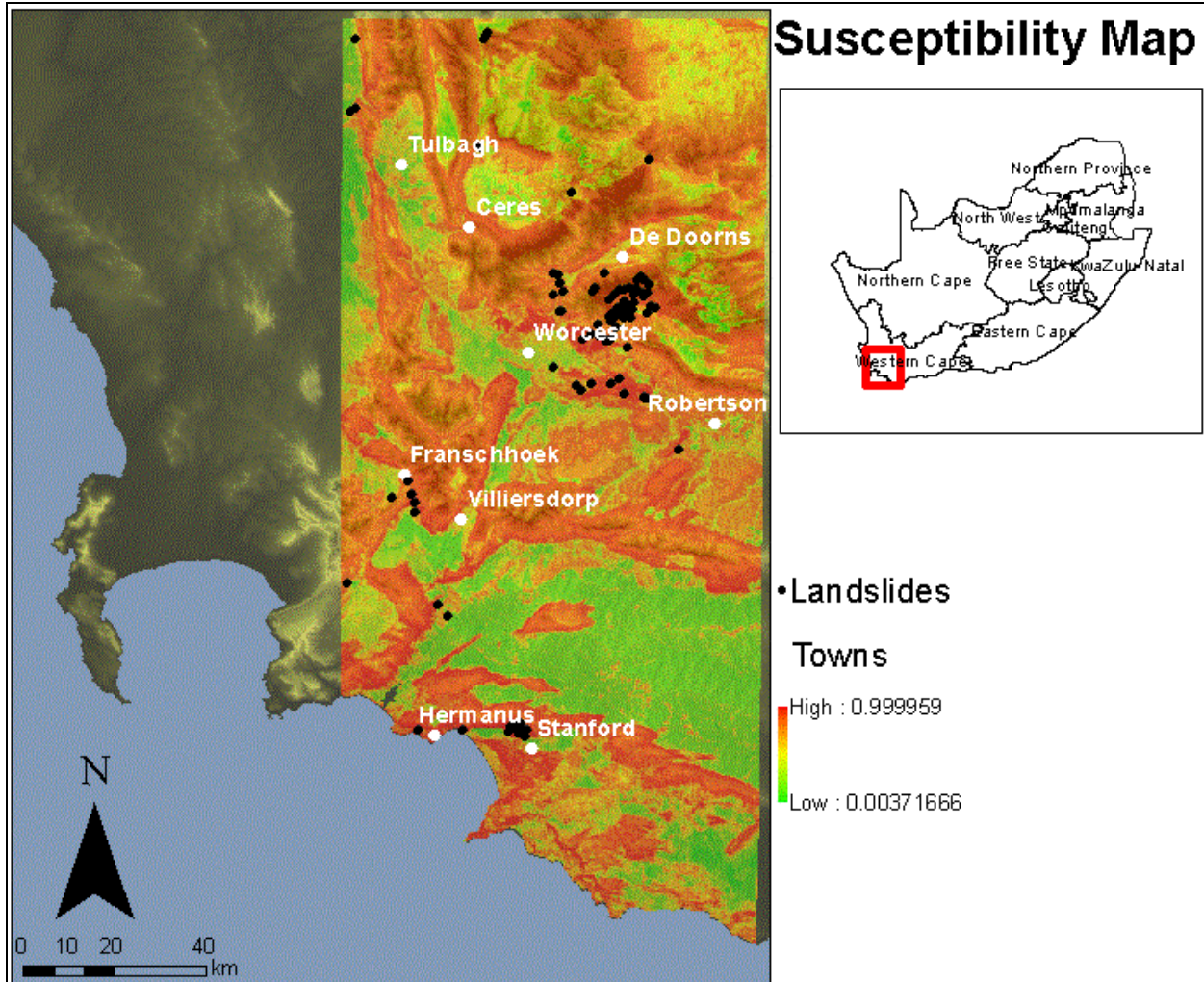


Figure 23: The unclassified weight of evidence landslide susceptibility map. The legend shows the increasing susceptibility of the map, with the higher values representing higher susceptibility and lower values representing lower susceptibility.

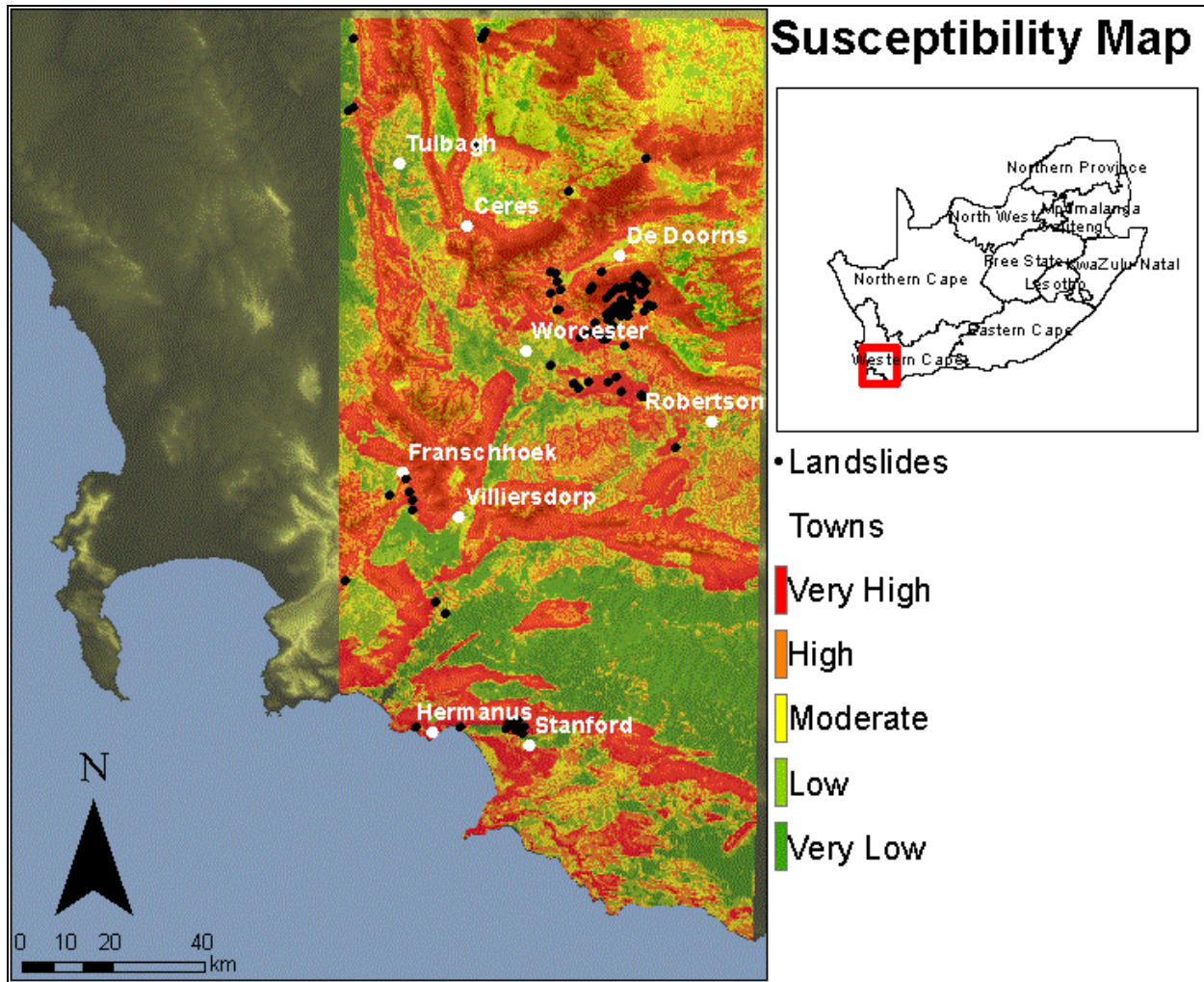


Figure 24: The landslide susceptibility map of the study area based on the weight of evidence model. The classes are shown on the legend. The red and orange areas are very high and high susceptibility, the yellow areas are moderately susceptible areas and the green areas are the very low and low susceptible areas.

Figure 25 shows the number of landslides per susceptibility class. Ideally the Very Low class should not have any landslide point and a large percentage of landslides should fall on the Very High and High Class. Only two landslides plot on the Very Low class, one landslide plots on the Low Class, four on the Moderate Class, 14 on the High class and 72 on the Very High class. Percentage wise, 96.8 % of the landslides plot on the high and very high class and 4%, 2% and 1 % of the landslides plot on the moderate, low and very low class; respectively.

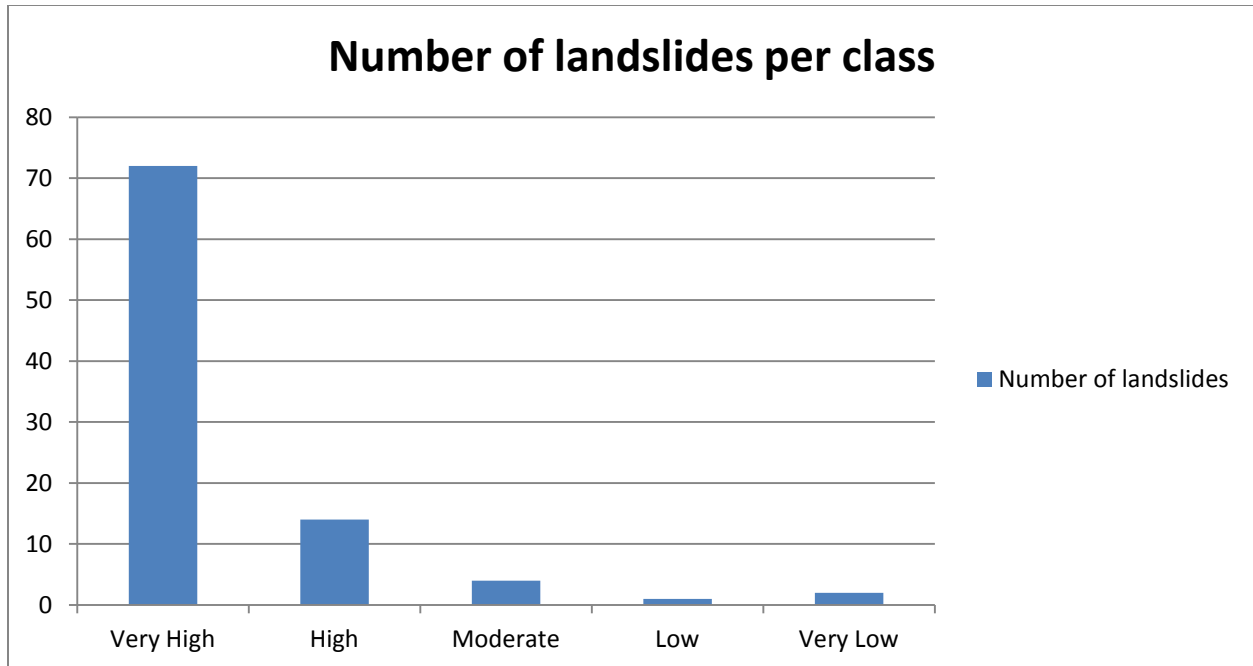


Figure 25: The number of landslides per susceptibility class. These landslides points were used to run the weight of evidence model. A large number of landslides fall on the very high and high class (96.8 %).

Two sets of landslide locality data were obtained from the Council for Geoscience. One set was field verified or confirmed landslides and the other set were not verified. The field verified data set was the only set used to run the weight of evidence method. The values were extracted from the susceptibility map for all the landslides that fall within the study area. Figure 26 shows the number of landslide per susceptibility class, for the unverified data set. Interestingly 730 landslides were on the very high class, 152 on the high class, 68 on the moderate class, 20 on the low class and 2 on the very low class ( as shown in Figure 26). Roughly 90 % of the landslides were on the high and very high class

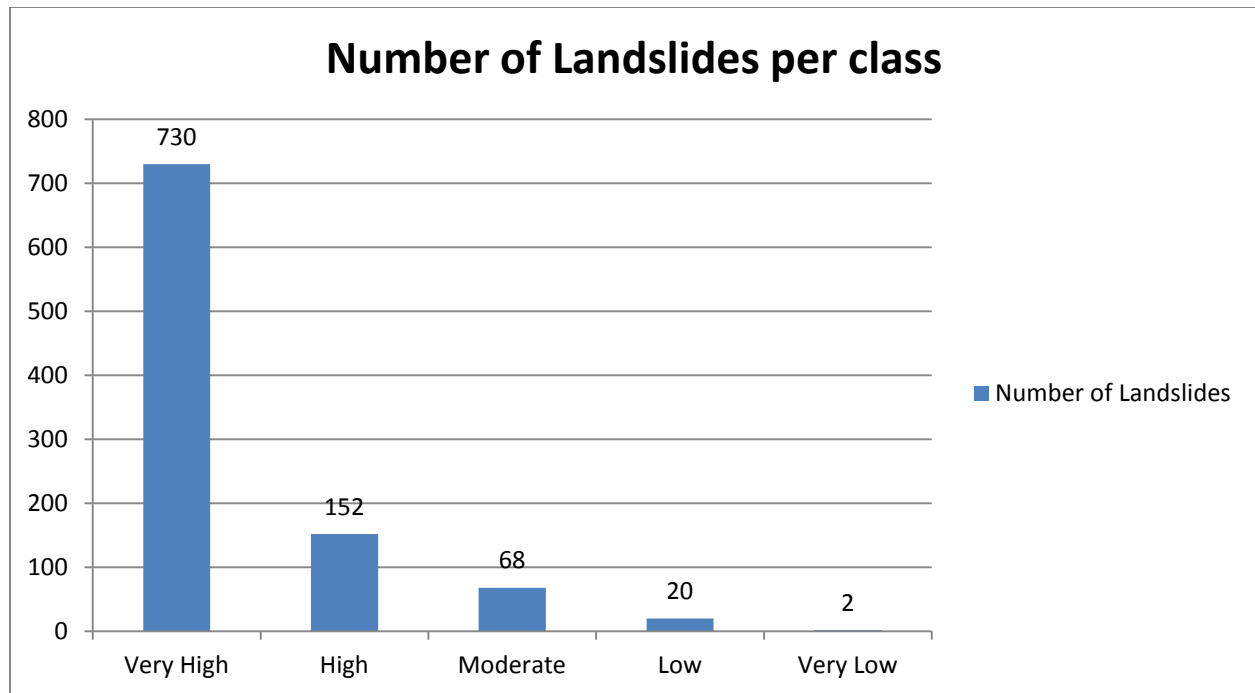


Figure 26: The number of landslides per susceptibility class. These landslide points were not used when the susceptibility map was modelled; they were only used to test the efficiency of the model. A large number of landslides fall on the high and very high class (90 %).

### 3.2.2 Accuracy Assessment for the Weight of Evidence method

A more sensible and holistic evaluation of the weight of evidence model performance can be seen by constructing the success rate curve. The following steps were used to plot the success rate curve:

1. The susceptibility map was classified into 10 classes using equal interval method (Figure 27).

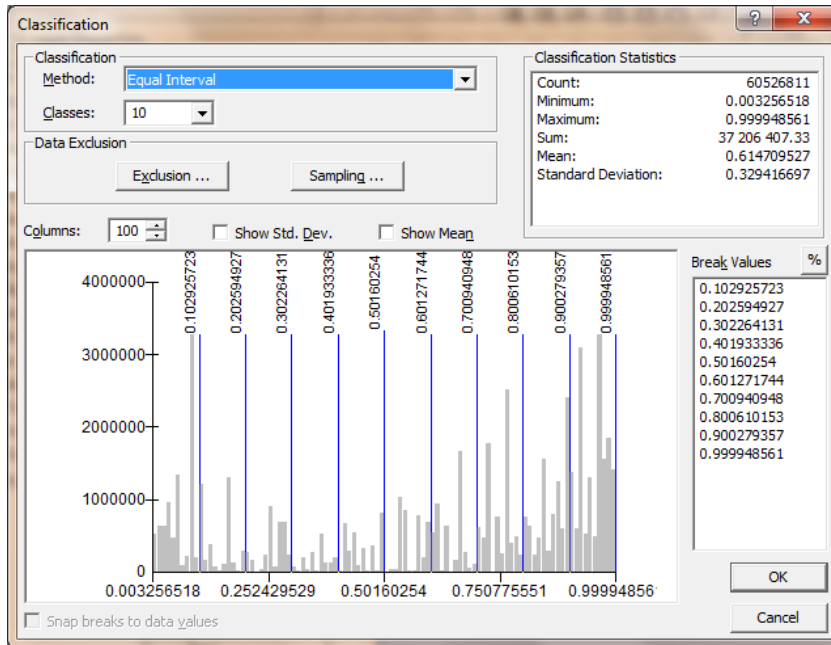


Figure 27: Classification of the landslide susceptibility map using equal interval method.

2. Cumulative percentage susceptibility was then calculated for each class
3. The curve of percentage landslides versus cumulative percentage susceptibility was plotted.
4. The overall accuracy was calculated (basically the area under the curve).

Figure 28 is a curve displaying the cumulative percentage of total landslides, which fall within increasing susceptibility map percentages. The ideal curve on such a plot would be the one that contains 100% of landslides within a small percentage of the susceptibility map, indicating that the model does not over predict. Figure 28 displays both the success rate curve (based on the training data “landslide points that were used to run the model) and the prediction rate curve (based on the reference data “landslide points that were not used to run the model”). The steeper the prediction rate curve, the higher the capacity the model has to predict landslides.

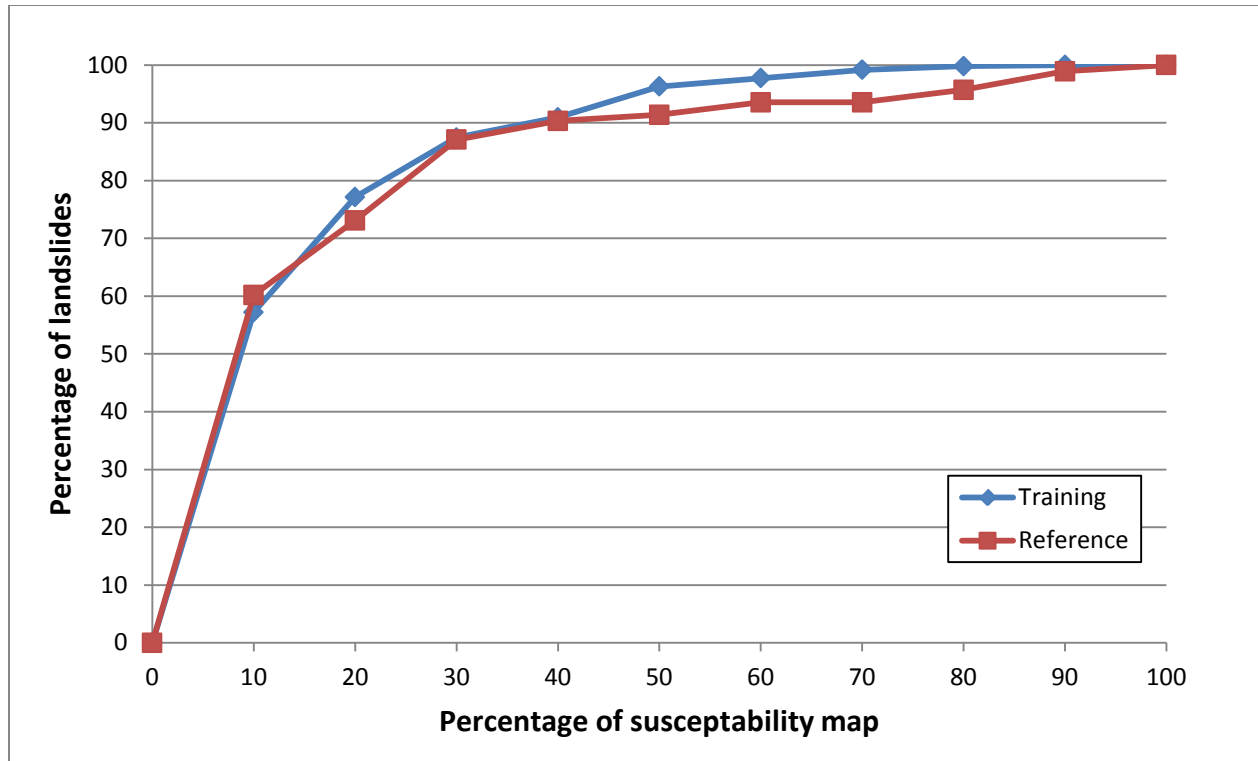


Figure 28: The success (blue) and prediction (red) rate curves for the weight of evidence susceptibility model.

Based on the success rate curve overall accuracy of the weight of evidence susceptibility map is 82.71% for the training data and a prediction rate of 80.37% for the reference data. This can be visualized in Figure 29 and Figure 30 for the training and reference data set; respectively.

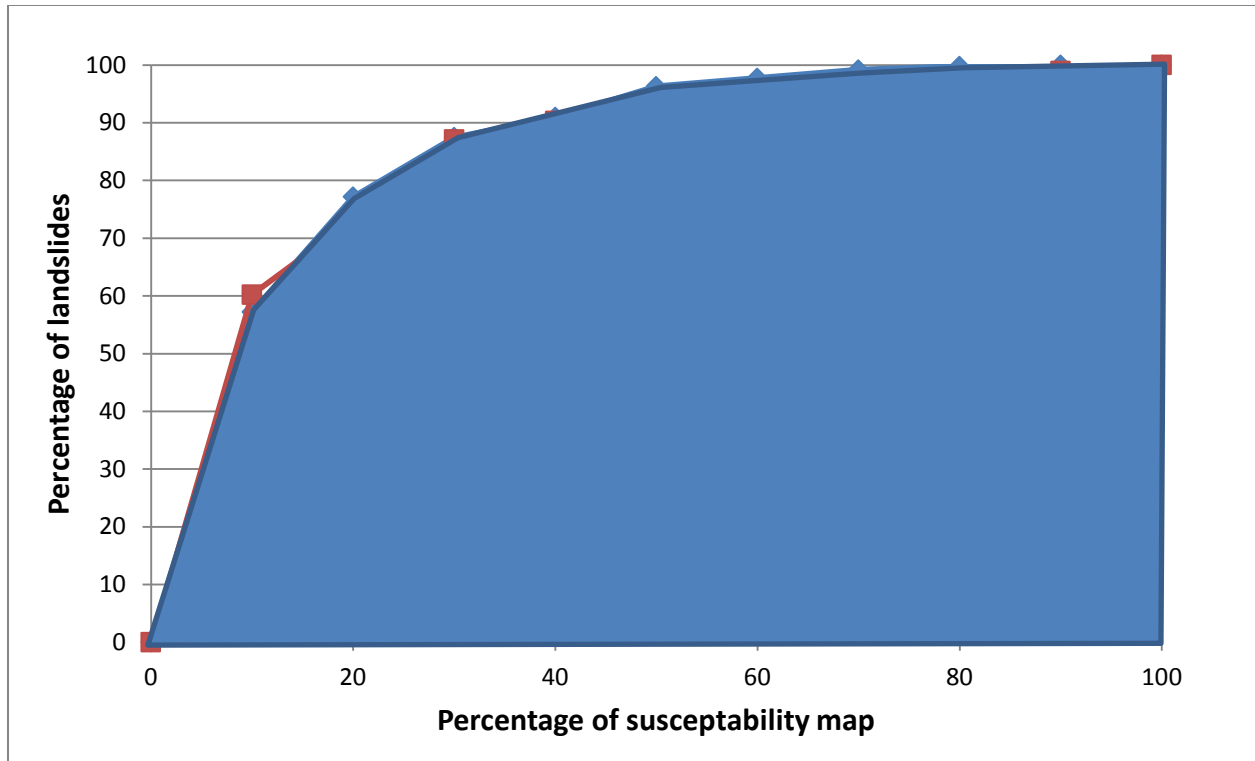


Figure 29: The overall success percentage for the weight of evidence method, the blue highlighted area is the overall percentage for the training data set.

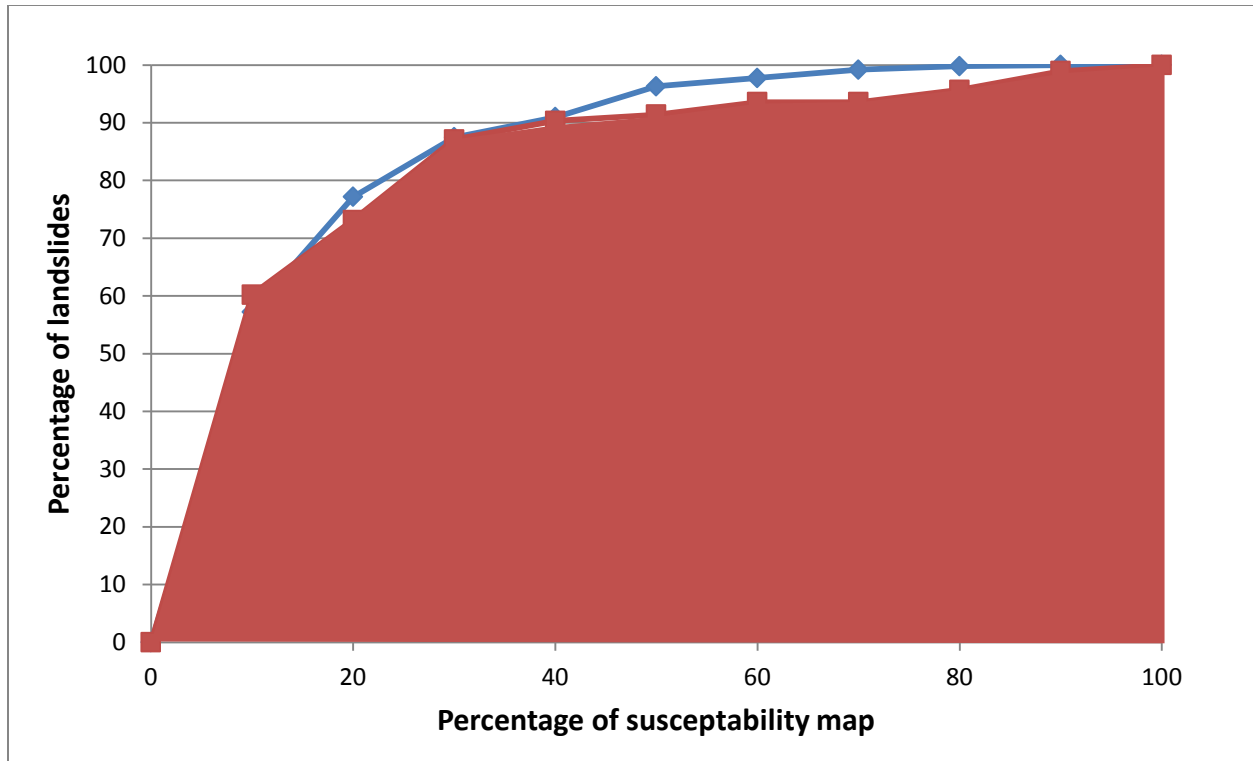


Figure 30: The overall success percentage for the weight of evidence method, the red highlighted area is the overall percentage for the reference data set

### 3.3 LANDSLIDE SUSCEPTIBILITY MAPPING – THE MAP COMBINATION APPROACH

A second landslide susceptibility map was created using the Map Combination Approach. The method involved the weighting and ranking of the causative factors affecting landslide susceptibility. This weighting and ranking was done based on expert knowledge (Stapelberg, pers com 2011). Each thematic layer was given a value based on its significance on landslide occurrence. Those thematic layers that were deemed to be more important were given a higher value e.g. slope was the most important parameter out of the eight thematic layers that were used, and it was given a value/weight of eight. Then each thematic layer was classified based on the expert knowledge e.g. the slope was classed into four classes (0-6°, 6-12°, 12-18°, and greater than 18°). The classes were assigned a value/ranked between one and five, with classes assigned a value of one being the least influential ones and the most influential classes were assigned a value of five. In the case of slope, 0-6° was assigned a value of one, 6-12° was assigned a value of two, 12-18° was assigned a value of 3, and slopes greater than 18° were assigned a value of 5. The weight of the parameters (layers) was then multiplied with the rank of the classes in that parameter, and then summed for all eight the causative parameters (layers) to produce the susceptibility index:

$$\text{LSI} = (\text{SLw} \times \text{SLr}) + (\text{SDw} \times \text{SDr}) + (\text{Rw} \times \text{Rr}) + (\text{LCw} \times \text{LCr}) + (\text{Fw} \times \text{Fr}) + (\text{Gw} \times \text{Gr}) + (\text{STw} \times \text{STr}) + (\text{ASw} \times \text{ASr}) \quad \{6\}$$

Where **LSI** is the landslide susceptibility index, **SL** is slope, **SD** is soil depth, **R** is road and rails, **LC** is landcover, **F** is faults and geological contacts, **G** is geology, **ST** is soil type and **AS** is aspect.

- **W** is the weight of the causative thematic layers
- **R** is the rank for the classes in the causative thematic layers

Table 4 shows the weight and the rank for all the causative thematic maps that were used to model an expert based susceptibility map.

*Table 4: The weights and ranks for the causative thematic layers used to model an expert based landslide susceptibility map.*

Parameter	Classes	Rank	Weight
Slope	0-6°	1	8
	6-12°	2	
	12-18°	3	
	>18°	5	
Soil Depth	<300mm	1	7
	300-600mm	2	
	600-900mm	3	
	900-1200mm	4	
	>1200mm	5	
Roads and Rails	Within 50 meter buffer	5	6
	Outside the buffer	0	
National Landcover	Built up areas	5	5
	Grasslands	2	
	Commercial farmlands	1	
	Dongas	4	
	Forests	1	
Faults and Lithological contacts	Within the 250 meter buffer	5	4
	Outside the buffer	0	
Geology	Sandstone	1	3
	Shales & siltstone	5	
	Conglomerate	2	
	Granites	5	
	Alluvium deposits	5	

Soil type	Clay	5	2
	Sandy	2	
	Deep clay soil	5	
	Deep mixed soil	5	
	Shallow soil	1	
	Rocky	1	
Aspect	Flat	1	1
	North	2	
	North East	2	
	East	1	
	South East	4	
	South	5	
	South West	4	
	West	3	
	North West	2	

The landslide susceptibility map modelled using the expert knowledge approach (Map Combination approach) is presented in Figure 31.

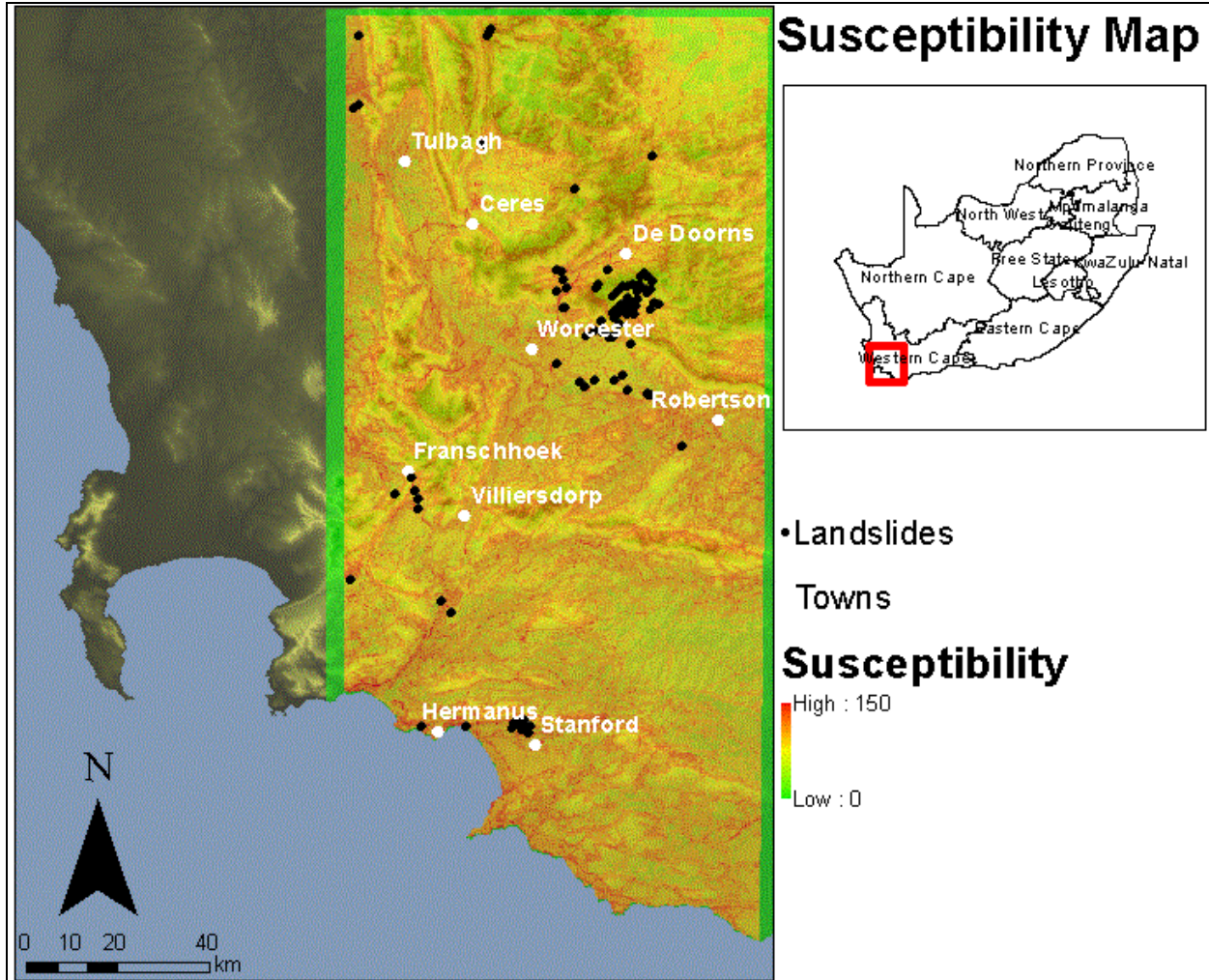


Figure 31: The landslide susceptibility map of the study area. The map was modelled using a map combination approach. The susceptibility values are shown in the legend, the higher the values, the higher the susceptibility and the lower the value the lower the susceptibility.

The classified susceptibility map, modelled using the Map Combination approach is presented on Figure 32. The classes were created using the natural break method, as described in Section 3.2.1

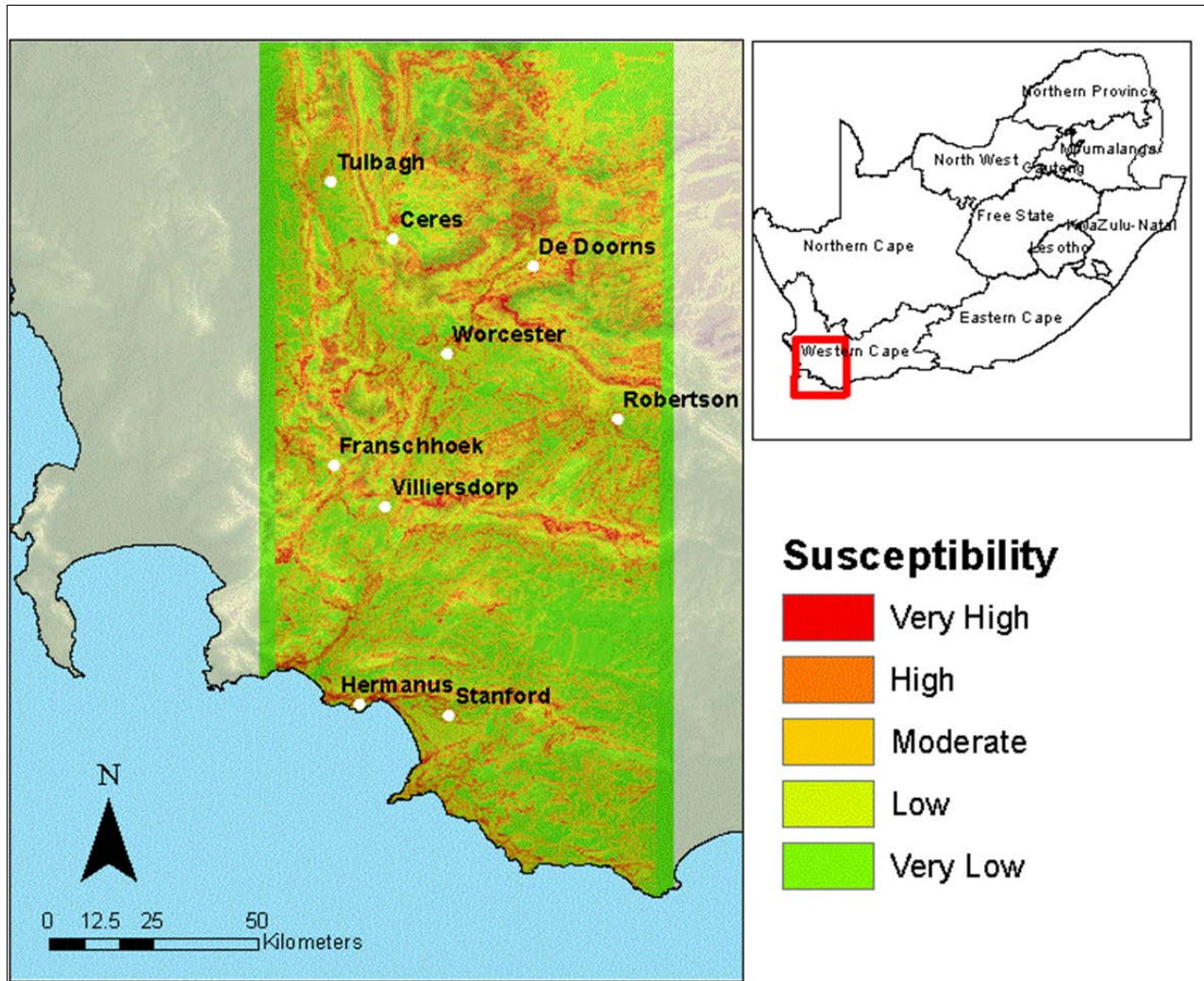


Figure 32: The landslide susceptibility map modelled using the map combination approach. The susceptibility classes are shown on the legend. The red and orange areas represent very high and high susceptibility areas, the yellow areas depict moderate susceptibility areas and the green areas are low susceptible areas.

Figure 33 shows the number of landslides per susceptibility class (only the selected field verified landslide (these landslides were also used to model the weight of evidence based susceptibility map) and Figure 34 shows the number of landslide per susceptibility class for the second data set (unverified landslide localities). The Very High class recorded the least number of landslides, and 42 landslides fall on the Low and Very Low class. Such a large number of landslides on the Very Low and Low class signify the inefficiency of the map combination approach. The Very High and High class recorded 42% of the landslides, while the Very Low and Low class recorded 44 percent of the landslides, slightly higher than the Very High and High class.

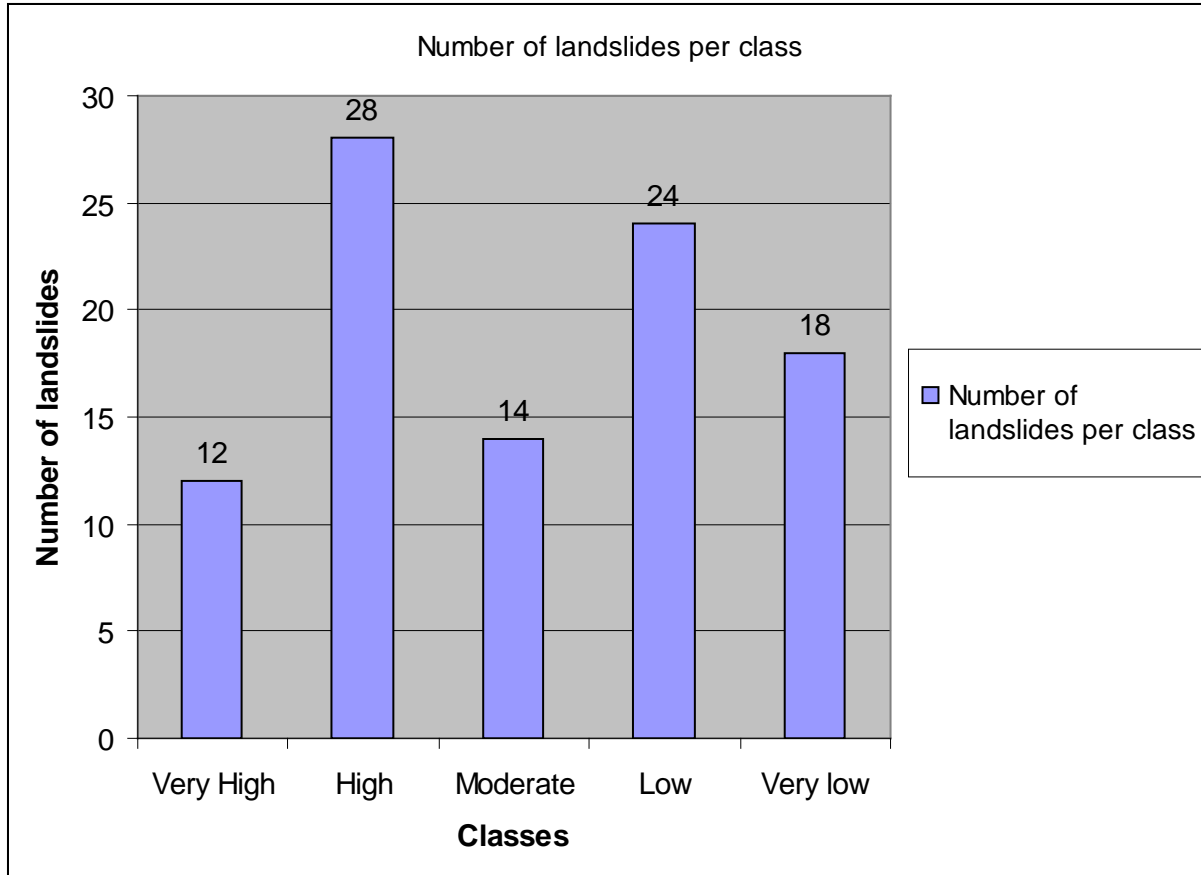


Figure 33: The graph shows the number of landslides per susceptibility class.

The number of landslides per susceptibility class for the unverified landslide points is presented in Figure 34, the Very High class recorded 126 landslides, the High class recorded 512 landslides, moderate class recorded 114 landslides, the Low class recorded 188 landslides and the Very Low class recorded 32 landslides. Percentage wise the Very High and High class recorded 66 percent of the landslides, while the Very Low and Low class recorded 23 percent of the landslides.

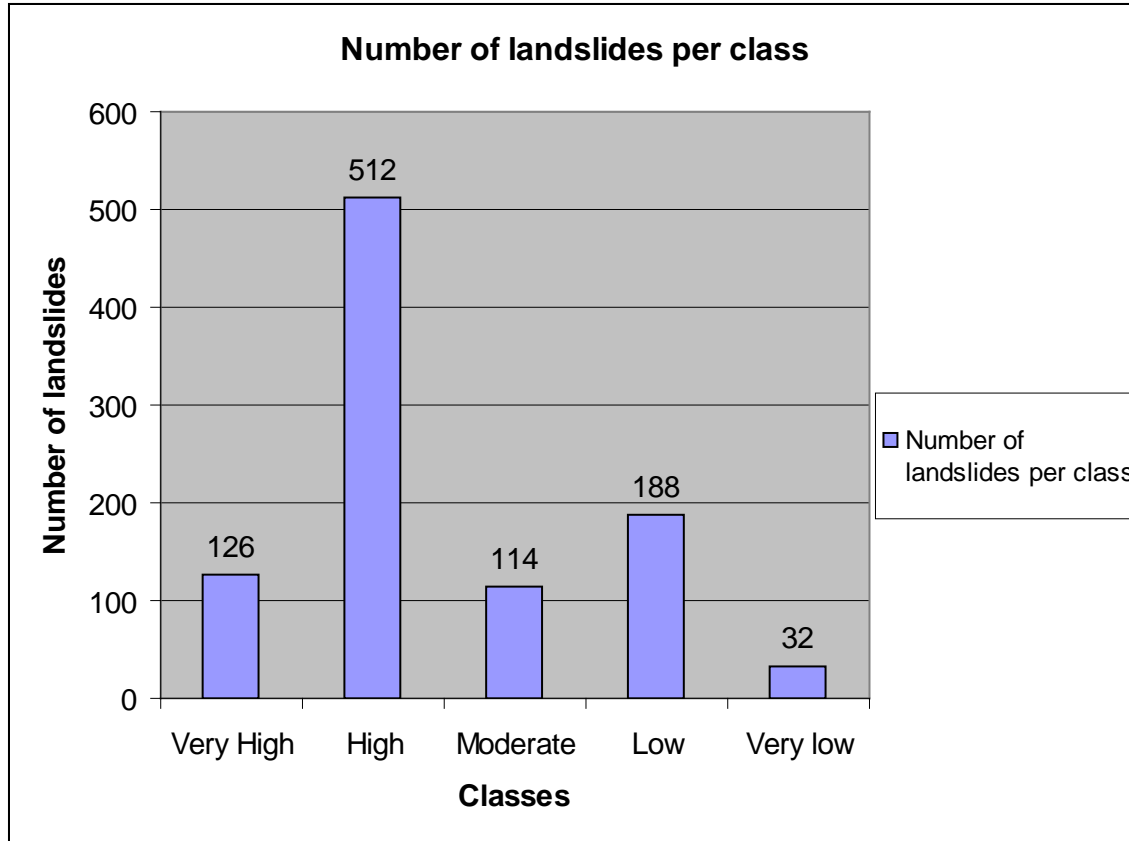


Figure 34: The graph shows the number of landslides per susceptibility class. These landslide localities were attained from the Council for Geosciences.

### 3.3.1 Accuracy Assessment for the Map Combination approach

The success rate curve was plotted using the same procedure that is explained in Section 3.2.2. The success rate curve for the map combination approach is presented on Figure 35. The ideal success rate curve is the one that reaches 100 % within the lowest percentage of susceptibility map.

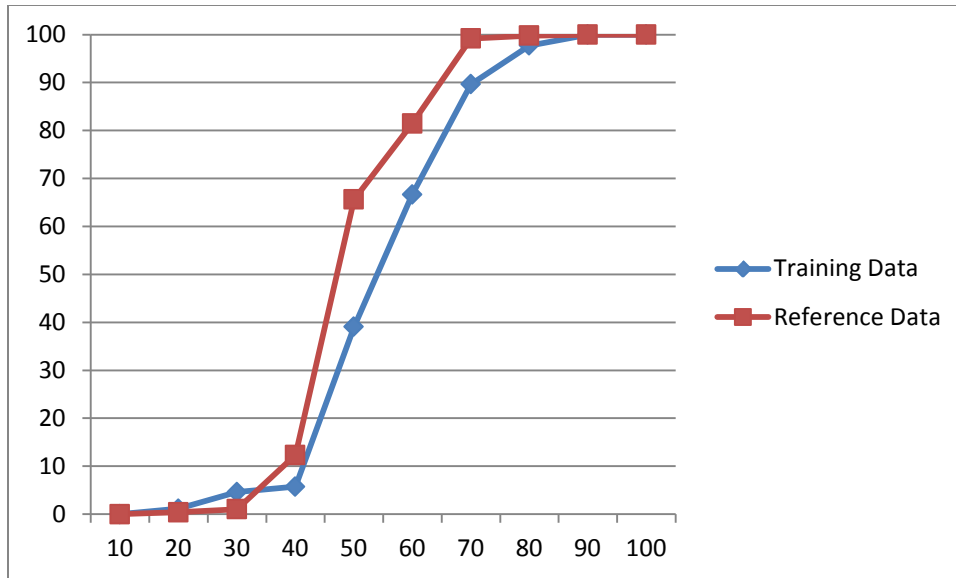


Figure 35: The success rate curve for the map combination approach. The red line is the success rate curve for the reference data set and the blue trend is the success rate curve for the training data set.

The cumulative success percentage for the map combination approach is presented on Figure 36 and Figure 37 for training data and reference data, respectively. A cumulative success percentage of 45.98 % was achieved for the training data set and a cumulative prediction rate percentage of 50.98 % was achieved for the reference data set.

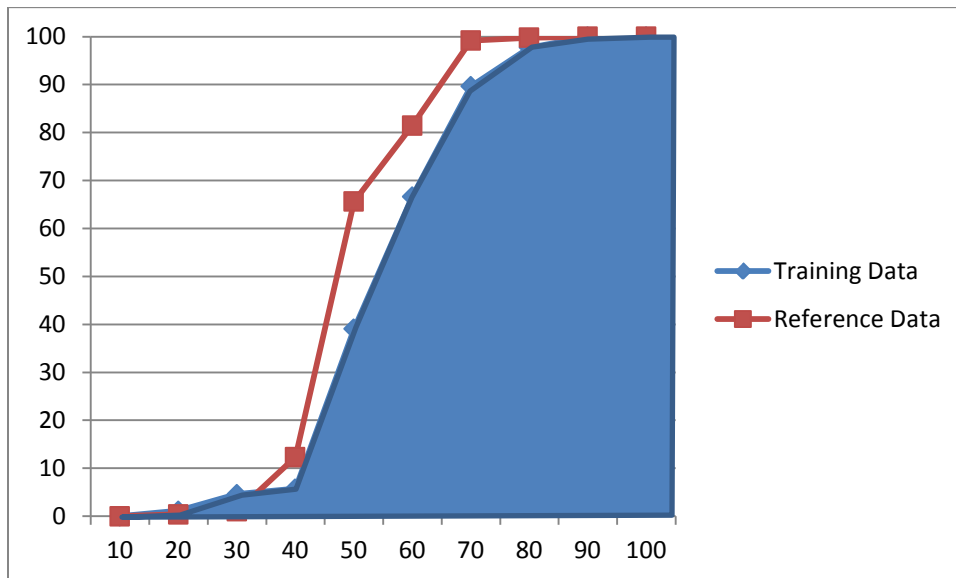


Figure 36: The cumulative success percentage for the map combination approach. The blue highlighted area is the success percentage for the training data.

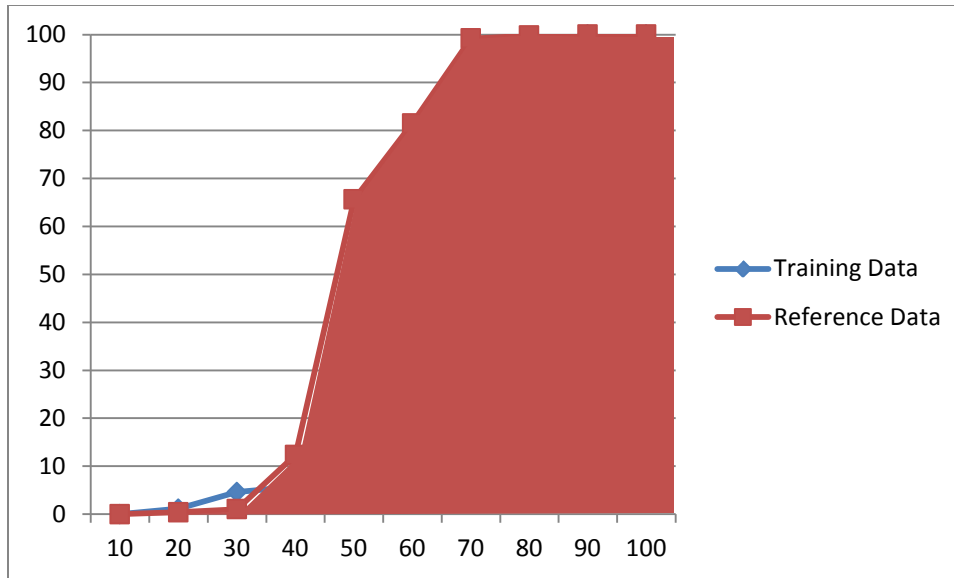


Figure 37: The cumulative success percentage for the map combination approach. The red highlighted area is the success percentage for the reference data.

The following chapter investigates the application of remote sensing techniques in monitoring the changes in variable factors and also attempts to correlate the changes with landslide occurrence, in susceptible areas.

## CHAPTER 4 REMOTE MONITORING OF VARIABLE CONDITIONS AND IDENTIFICATION OF TRIGGERING MECHANISMS

After the generation of the landslide susceptibility map outlined in Chapter 3 considering the static factors affecting landslide susceptibility, the variable factors and triggering mechanisms for landslides can be considered. The variable factors affecting landslide susceptibility include the health and productivity of the vegetation as well as the moisture content of the vegetation and the soils. As described in Chapter 2, satellite remote sensing sensors and analysis approaches are ideal for the monitoring of vegetation through the use of vegetation indexes.

To determine how the health and productivity of vegetation affect landslide susceptibility, several historical landslides were considered. The localities for the different landslides are presented in Figure 38. The period of occurrence and the number of landslides per area are shown in Table 5

*Table 5: Shows the number of landslides and the date of occurrence for each area.*

<b>Area</b>	<b>Number of Landslides</b>	<b>Period of occurrence</b>
<b>1</b>	2	1. Winter of 2005 2. Winter of 2008
<b>2</b>	<b>11</b>	Year 2005
<b>3</b>	<b>1</b>	2007
<b>4</b>	<b>1</b>	2007

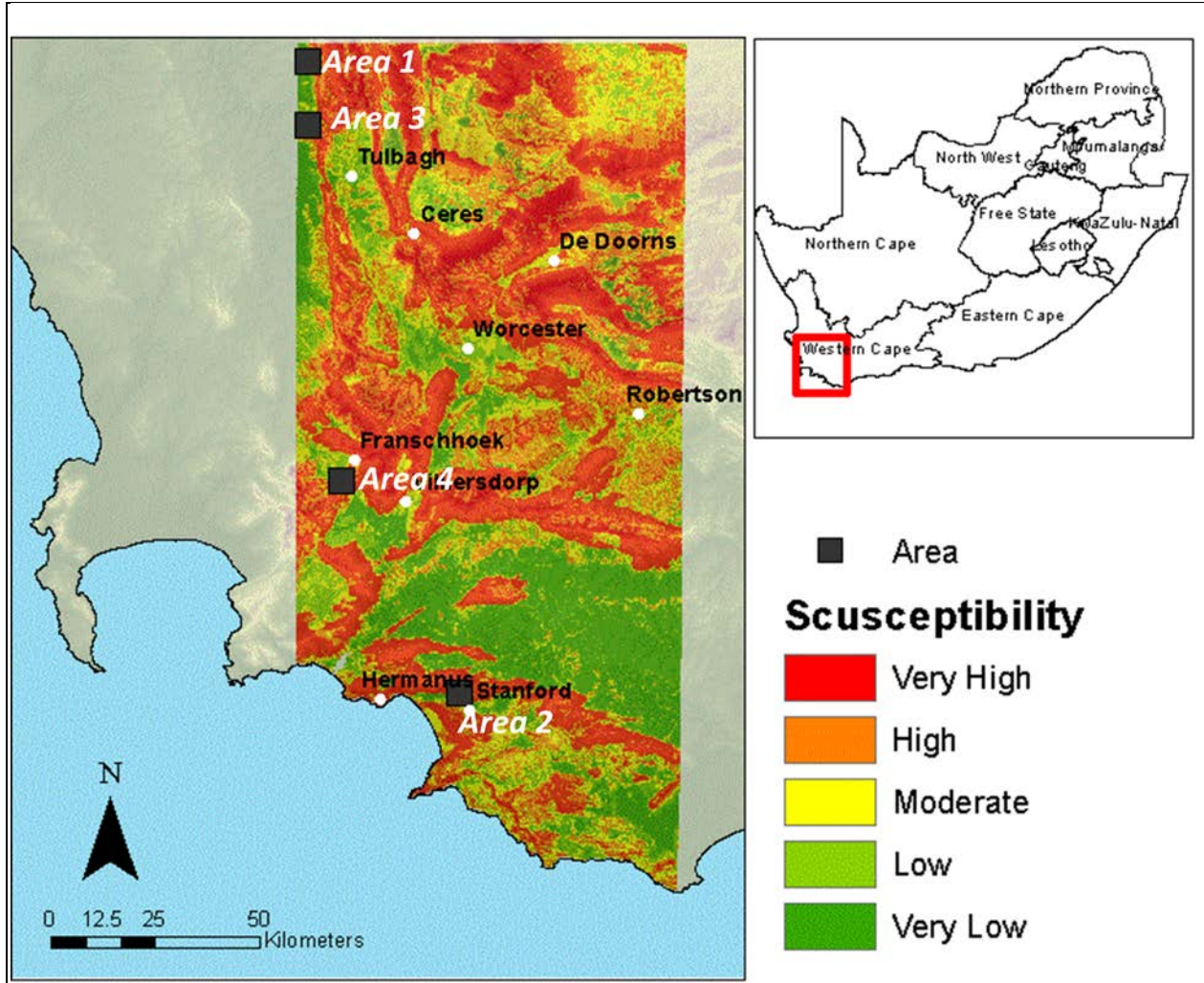


Figure 38: The geographic location of the 2005, 2007 and 2008 landslide events. The landslides are located on the far north western and south western part of the study area.

Area 2, close to the town of Hermanus had landslide scars that are highly visible even in recent images, unlike the other localities whereby the landslide have been cover by vegetation. These landslide fall in the highly susceptible area in the susceptibility map modeled using the weight of evidence method (Figure 39). The Google earth images for this area are presented in Figure 40.

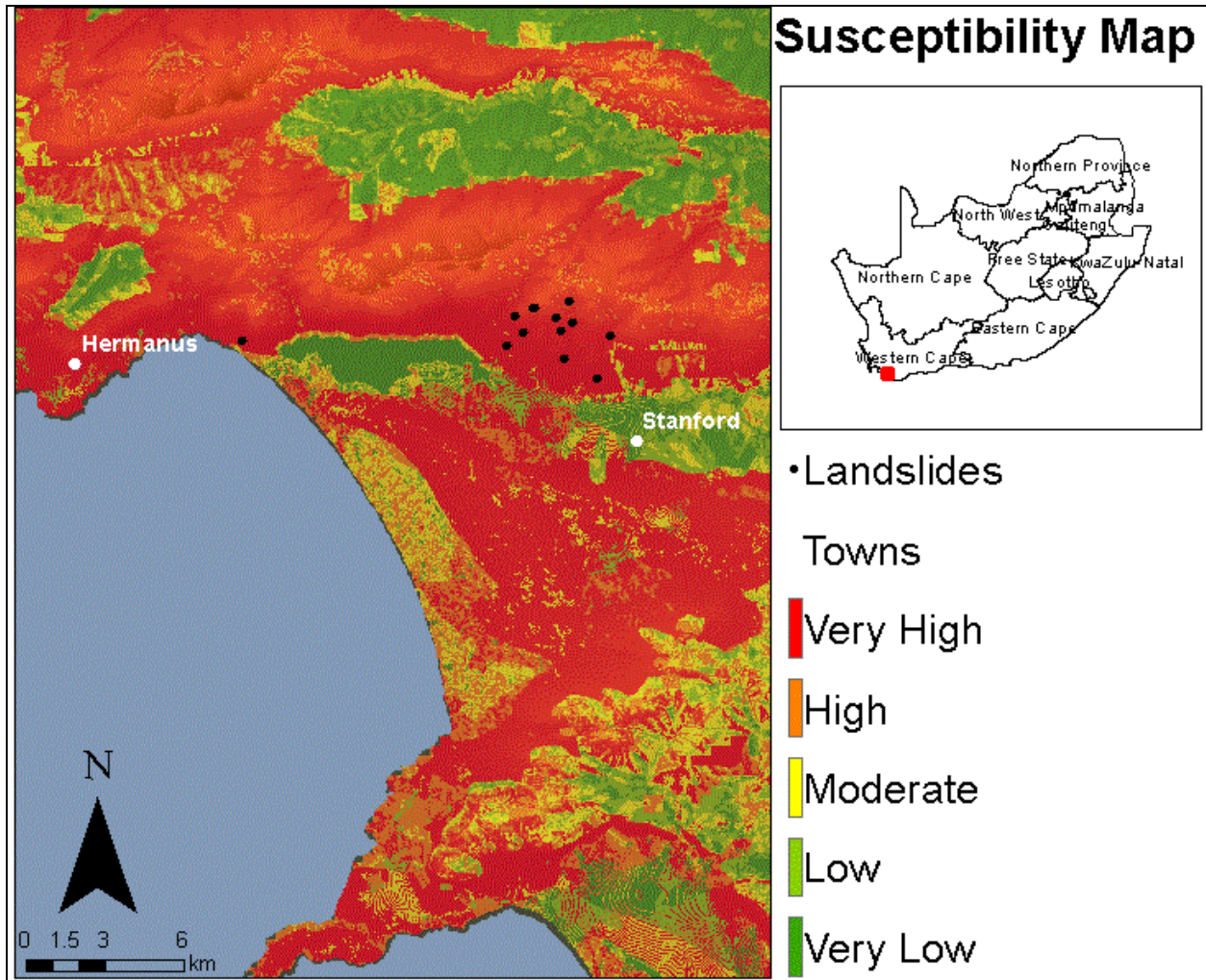


Figure 39: The geographic location of several landslide events. The landslides are located close to the towns of Stanford and Hermanus. The landslide localities are represented by black dots on the map.



Figure 40: Google Earth images indicating the landscape before landslide occurrence (29-09-2004) and the landscape after landslide occurrence (02-11-2006).

The following sections describe the results of the analysis of low spatial resolution – high temporal resolution MODIS data to determine how the vegetative conditions may have influenced the occurrence of these historical landslides. Finally, the triggering mechanisms of these landslides were determined.

#### **4.1 EXTRACTION OF NDVI AND NDWI – MODIS DATA**

The high temporal resolution (daily for the most of the parts of the world) and low spatial resolution (250 m to 1 km) of MODIS data makes it ideal for the study of global change in disciplines including oceanography, biology, and atmospheric science. For the identification and mapping of landslides after they have occurred, the use of MODIS data is not ideal due to its low spatial resolution. However, the high revisit time makes MODIS data a very useful tool to investigate landslide causative factors such as vegetation productivity and soil wetness conditions. The MODIS derived vegetation index (NDVI) is designed to provide improved monitoring and understanding of regional and global dynamics and processes. The temporal trends of the NDVI indices are used for detecting the changes in biophysical and/or biochemical characteristics of the vegetation and the identification of the phenological stage.

In an effort to identify the long-term status of the health and productivity of the vegetation in the area where landslides are known to have occurred, the MODIS time series viewer, (available at <http://afis.meraka.org.za/wamis/time-series-viewer>) were used to extract information on the phenology of vegetation in the study area. The viewer, developed by South Africa's CSIR Meraka Institute, provides access to NDVI data derived from a long time-series of MODIS data. The long term trends of NDVI were investigated in an effort to identify potential changes in landcover conditions that may have affected the occurrence of historical landslides.

For this purpose, areas where landslides are known to have occurred were investigated. The dates of landslide occurrence were not exact. The following sections describe the results of the analysis of the long-term trends in NDVI and their potential effect on landslide susceptibility.

#### **AREA 1**

Area 1 is located on the northern side of the study area, near the town of Tulbagh. In order to investigate the vegetative conditions during the occurrence of the landslide using the MODIS data set, the date at which the landslide occurred must be known. Since the exact date of occurrence is unknown, the exact

NDVI values immediately prior to landslide occurrence could not be pinpointed. However, when the trend of NDVI values is considered for two seasons prior and during 2005 landslide occurrence, some interesting patterns emerge. The NDVI values during this period is presented in Figure 41

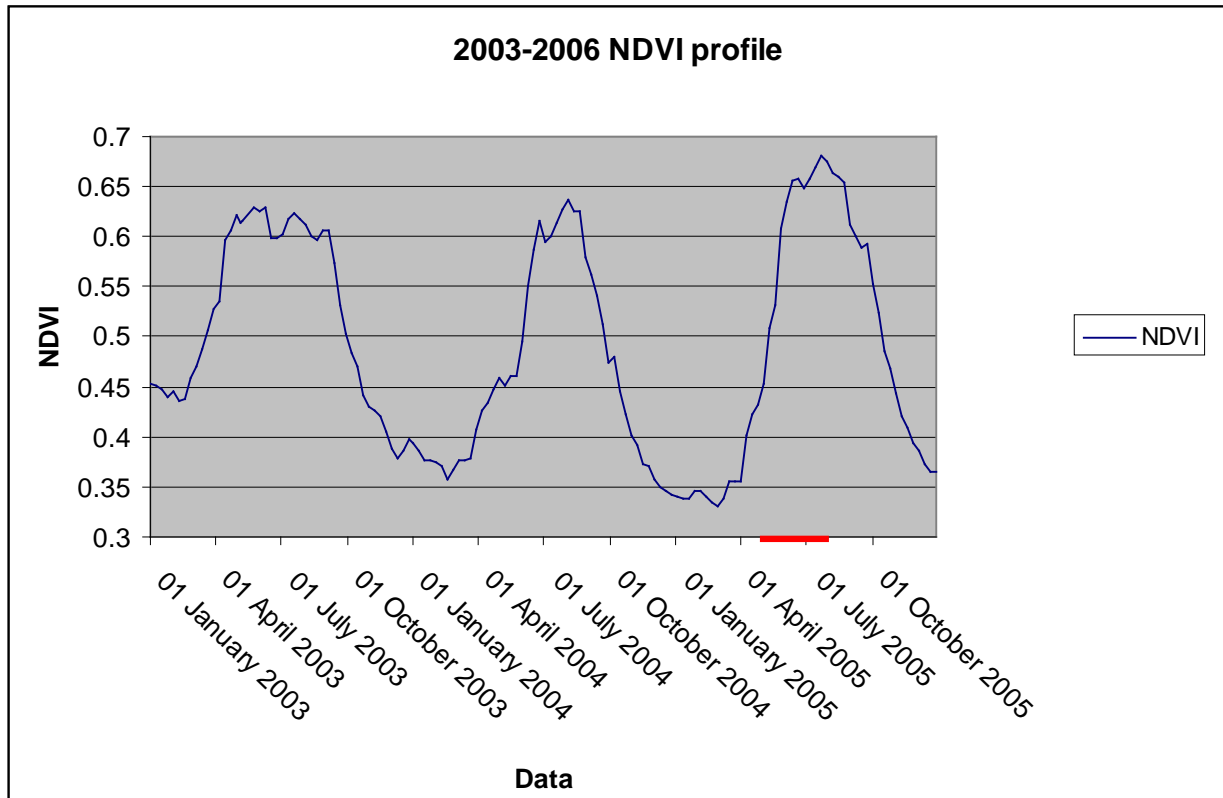


Figure 41: The NDVI time-series profile, of the selected area which is known to have landslide occurrence. The profile is from the year 2003 to the year 2006. The red line indicates the period at which the landslide is thought to have occurred. The plot shows that the minimum NDVI values for the year at which the landslides occurred are lower than the previous years.

The landslide event was known to have occurred in the winter season of 2005 (between the beginning of May and the end of July 2005). The time series of NDVI values during this time suggests that, for the season preceding the landslide occurrence, low NDVI values were recorded. Table 6 indicates the annual average, minimum and maximum NDVI values recorded for the years 2003 to 2008. It is observed that the average NDVI values for the year 2004 (prior to landslide occurrence), was low at 0.461 when compared to later years during which average NDVI values range between 0.485 and 0.510. Additionally, the maximum NDVI value recorded during 2004 was also lower at 0.637 when compared to the years 2005-2007 where a maximum NDVI of between 0.665 and 0.684 were recorded. An exception is observed for the year 2008 for which the lowest maximum NDVI of 0.611 was recorded.

*Table 6: The annual average, minimum and maximum values of NDVI. The values are calculated from the beginning of the year to the end of the year.*

Year	Average NDVI	Minimum NDVI	Maximum NDVI
2003	0.388	0.379	0.629
2004	0.461	0.342	0.637
2005	0.485	0.331	0.680
2006	0.473	0.355	0.665
2007	0.510	0.364	0.684
2008	0.476	0.370	0.611
2009	0.502	0.370	0.664

The 2008 landslide event occurred in the same area as the 2005 landslide, and also in the winter season (between May and July of 2008). It is likely that this landslide was the reactivation of the 2005 landslide event. The NDVI time series profile is presented on Figure 42, the NDVI values for the year preceding landslide occurrence are high. The yearly average, minimum and maximum NDVI values are presented on Table 6. The annual average for the year prior to landslide occurrence (2007) is high at 0.510. The year prior to landslide occurrence also records the maximum NDVI value of 0.684. These high NDVI values for the year preceding landslide occurrence are the opposite of what has been observed for the 2005 landslide event. Nevertheless the lower minimum NDVI values for the year preceding landslide occurrence that has been the prominent feature for the previous NDVI profile, is observed.

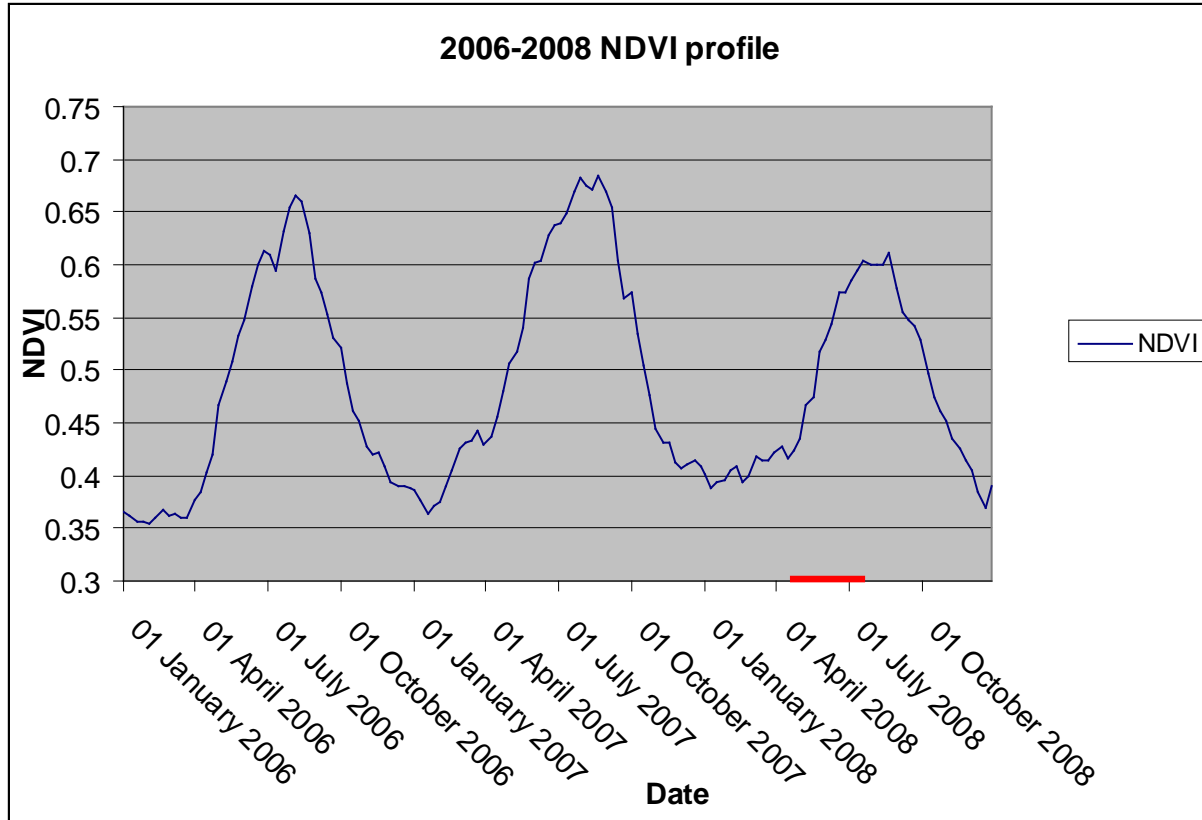


Figure 42: The NDVI time-series profile of the area known to have landslide occurrence. The plot is from the year 2006 to the year 2009. The red line indicates the period at which the landslide is thought to have occurred. The plot shows relatively low minimum NDVI values for the year prior to landslide occurrence.

## **AREA 2**

Figure 43 is the NDVI time-series profile for the area known to have landslide occurrence. The landslide is thought to have occurred in the year 2005. There is no exact date of occurrence for this landslide event. From the graph it is observed that the minimum NDVI values for the year preceding landslide occurrence were slightly lower than normal.

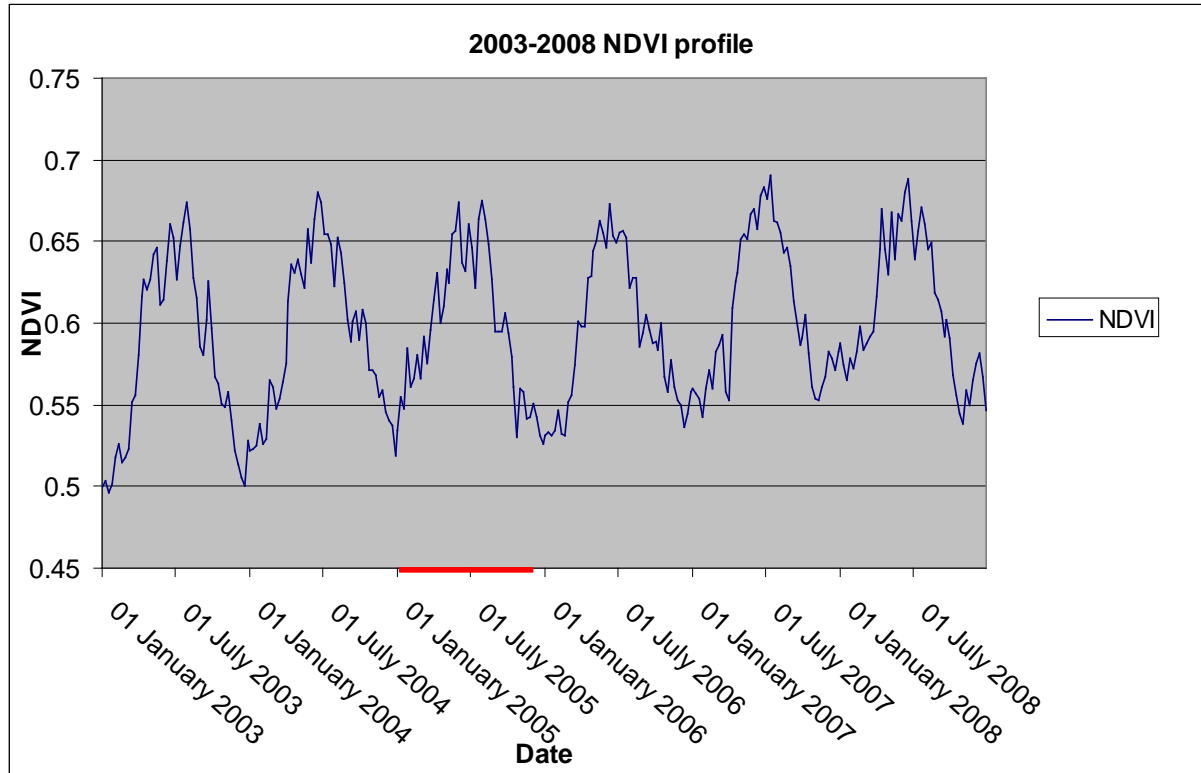


Figure 43: The NDVI time series profile for the year 2003 to 2008. The red line on the graph indicates the period at which the landslide is thought to have occurred. The minimum NDVI values are slightly lower for the year prior to the occurrences of landslide event.

Several landslide scars were observed at the area close to the town of Hermanus and Stanford, in the Western Cape province of South Africa. The exact date of occurrence for these landslides could not be accurately identified, but they are estimated to have occurred between 2004-09-29 and 2006-11-02, based on the interpretation of the Google earth images.

The MODIS NDVI time-series profile is presented in Figure 44. The yearly average, minimum and maximum NDVI values are presented in Table 7. There are no major variations on the yearly average, maximum and minimum NDVI, as from the year 2002 to the year 2006. An exception is the year 2002, which records the highest NDVI value of 0.724. From the previous NDVI time-series profiles, it has been observed that landslide occurrence is associated with lower minimum NDVI values, for the year prior to landslide occurrence.

*Table 7: The yearly average, minimum and maximum values of NDVI. The values are calculated from the beginning of the year, to the end of the year.*

year	Average NDVI	Minimum NDVI	Maximum NDVI
2002	0.646	0.576	0.724
2003	0.631	0.568	0.702
2004	0.642	0.584	0.692
2005	0.639	0.567	0.694
2006	0.631	0.582	0.699

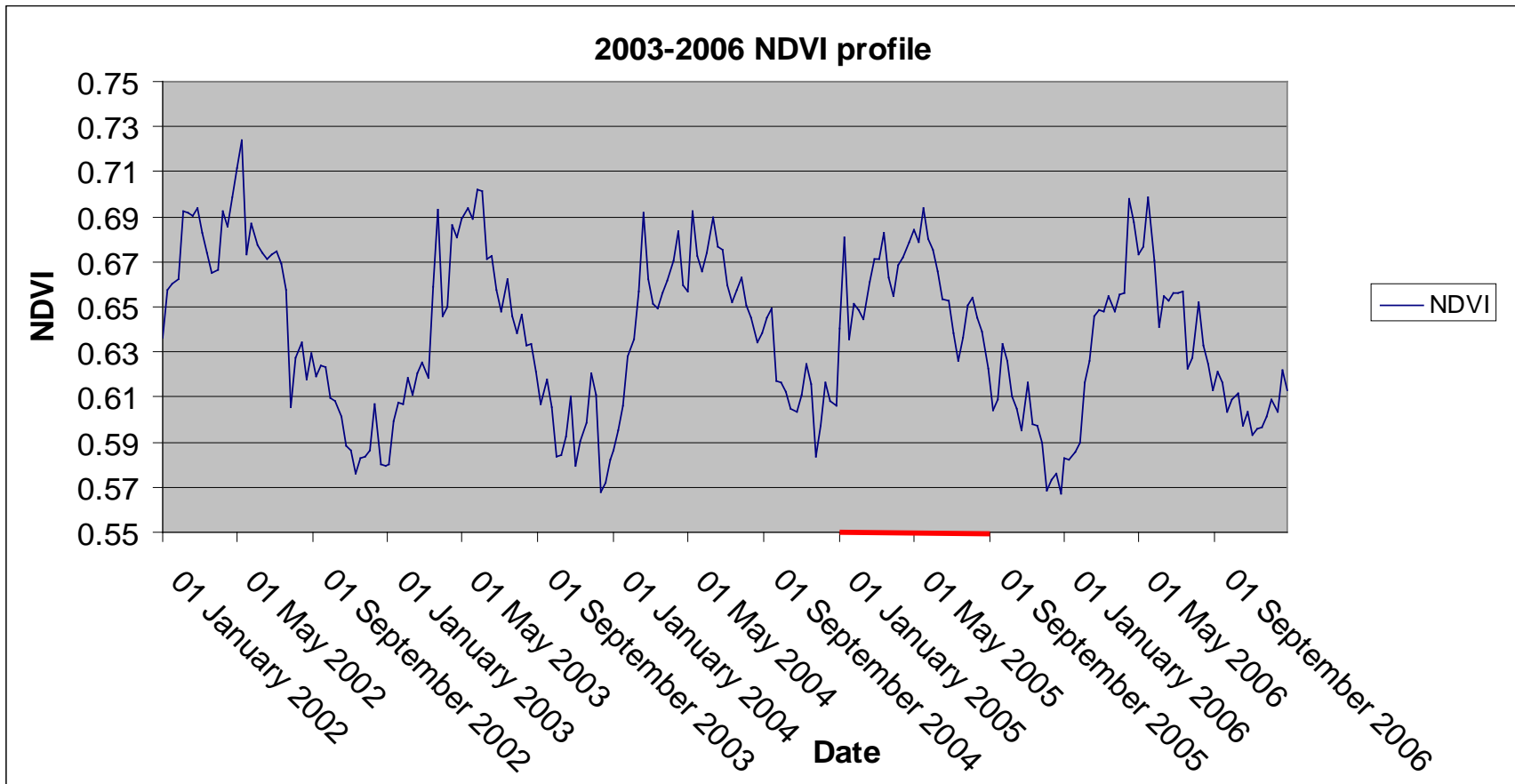


Figure 44: The NDVI time-series profile of an area with numerous landslide scars. The area is close to the town of Hermanus and Stanford. The landslides are estimated to have occurred between the year 2004 and 2006. The red line on the graph indicates the time at which the landslide could have occurred, based on the previous observations that landslide in the study area are associated with low minimum NDVI values for the year prior to landslide occurrence.

### **AREA 3**

The NDVI time series profile for the landslide event that occurred during the heavy rains of the year 2007 is presented on Figure 45. The graph shows lower minimum NDVI values for the year preceding landslide occurrence (2006). These lower than normal minimum NDVI values seems to be the prominent feature for most of the NDVI time series profile, for areas with landslide occurrence, within the study area.

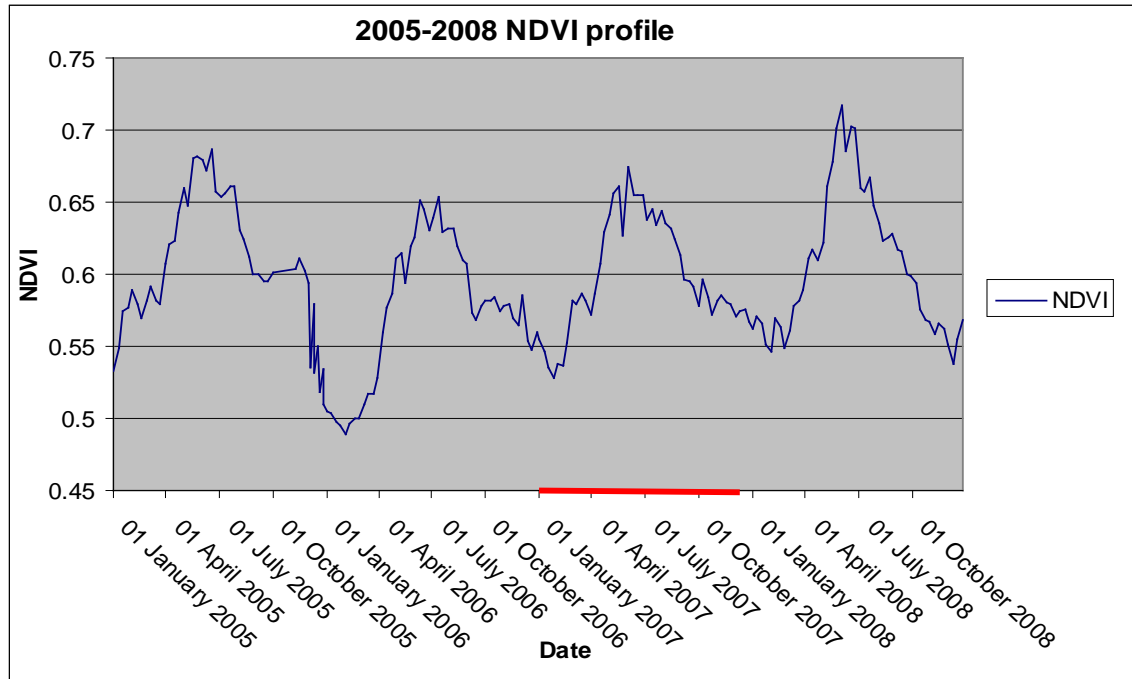


Figure 45: The NDVI time-series profile for the area known to have landslide occurrence. The red line on the graph indicates the period at which the landslide is thought to have occurred. The minimum NDVI values are lower for the year prior to landslide occurrence (2006).

### **AREA 4**

The NDVI time series profile for the landslide event that occurred on the year 2007 is presented on Figure 46. The only trend that is observed on the NDVI profile is the lower minimum NDVI values for the year preceding landslide occurrence.

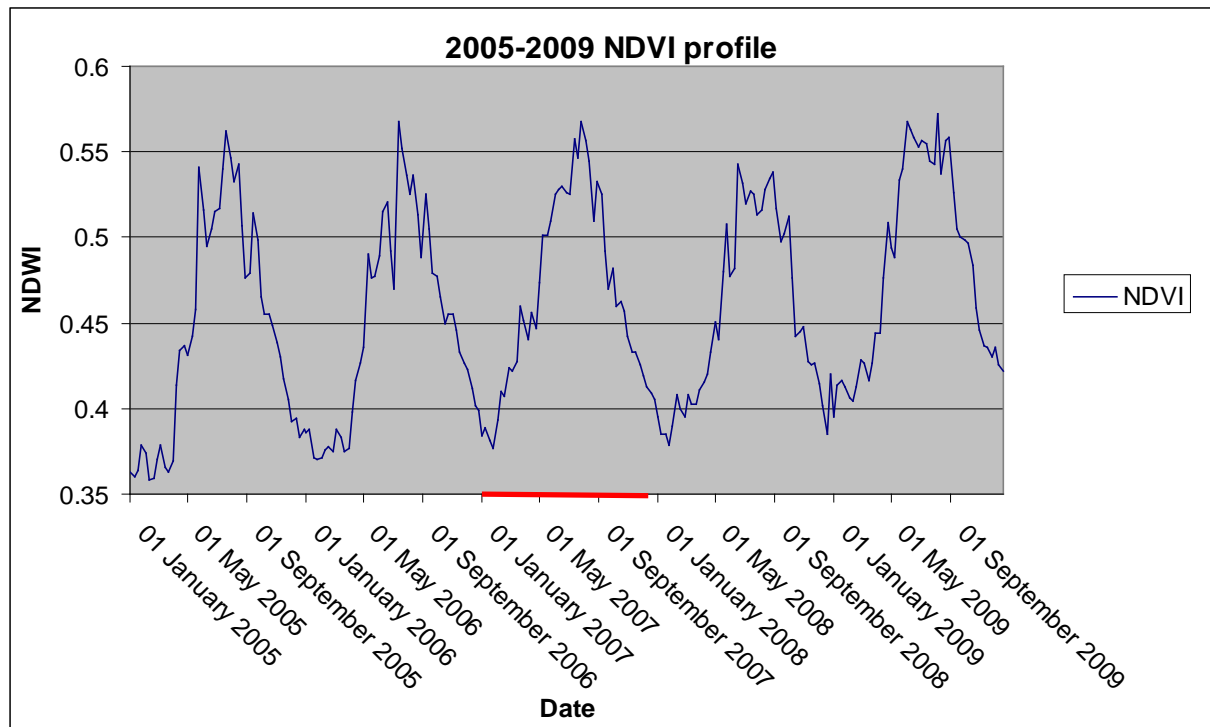


Figure 46: The NDVI time-series profile for the year 2005 to 2009. The red line on the graph indicates the period at which the landslide is thought to have occurred. The minimum NDVI values are slightly lower for the year prior to landslide occurrence.

The interpretation of the NDVI time series profiles for areas with known landslide occurrences, within the study area shows the following:

1. The minimum NDVI values for the year preceding landslide occurrence are relatively low, in most cases.
2. In some cases the maximum, minimum and average NDVI values are relatively low for the year preceding landslide occurrence.

#### 4.2 EXTRACTION OF NDVI AND NDWI AND PHENOLOGY DATA – LANDSAT DATA

The low resolution MODIS data is captured at 250m resolution. The low resolution of the data may imply that localised effects are not accurately observed. For this reason, 30m resolution Landsat data was analysed in an effort to see if localised trends of NDVI can be observed. The problem is that the 30m resolution data is not available at such frequent intervals as the 250 m resolution MODIS data. The Normalized Difference Vegetation Index (NDVI) is very important when estimating vegetation health. The information about the NDVI was computed from the 30m resolution Landsat 5 TM and Landsat 7 ETM+ images. For the purpose of this study, six Landsat 5 and two Landsat 7 images were requested from South African National Space Agency (SANSA), in order to investigate the possible dates of occurrence for the landslide events close to the town of Stanford and Hermanus, and also investigate the vegetation conditions associated with landslide occurrences.

*Table 8: Landsat scenes that will be used in this study.*

<b>Scene No.</b>	<b>Satellite Sensor</b>	<b>Path/Row</b>	<b>Image Date</b>
1	Landsat 7 ETM+	175/84	2002/03/15
2	Landsat 7 ETM+	175/84	2002/07/21
3	Landsat 5 TM	175/84	2004/09/20
4	Landsat 5 TM	175/84	2006/02/14
5	Landsat 5 TM	175/84	2006/08/09
6	Landsat 5 TM	175/84	2007/02/17

### **4.2.1 Image pre-processing**

The use of satellite image data for a spatial database requires several pre-processing procedures. These procedures include geometric correction and image enhancement. The purpose of digital image processing is to increase both accuracy and the interpretability of the digital data during the image processing phase. The normalization of satellite imagery takes into account the following: the combined measurable reflectances of the atmosphere, aerosol scattering and absorption, and the earth's surface (Kim & Elman 1990). The goal of atmospheric correction as stated by Hall, Stebel, Nickesen & Goetz (1991) should be that after image pre-processing, all images should appear as if they were acquired from the same sensor. Geometric errors are caused by factors such as the earth's curvature and rotation as well as variations in the velocity, altitude and attitude of the sensor platform. Geometric rectification of the imagery changes the pixel grid to fit that of a map projection or another reference image. This becomes important when scene to scene comparisons of individual pixels in applications such as change detection are being sought (ERDAS 1999).

#### *4.2.1.1 Geometric correction*

The major purpose of geometric corrections is to correct the inaccuracy between the location coordinates of the picture elements in the image data, and the actual location coordinates on the ground. Geometric correction of the imagery changes the pixel grid to fit that of a map projection or another reference image.

The ERDAS IMAGINE 2011 image geometric correction module was used for the geometric correction of the images. The Landsat geometric model was chosen, which allows for the orthorectification of Landsat data. A 20 meter resolution digital elevation model (DEM) of the study area was used as the elevation file. Twenty five ground control points were collected and the maximum root mean square error (RMSE) of 1.6 was achieved (refer to Table 9). The nearest neighbour re-sampling method was

applied. This method uses the value of the closest pixel to assign to the output pixel value and thus transfers original data values without averaging them as other methods do, therefore, the extremes and subtleties of the data values are not lost (ERDAS 1999). Nearest neighbour re-sampling was selected because it preserves pixel values perfectly during resampling. Table 9 shows the RMSE and the number of ground control points (GCP) for each Landsat scene that was geometrically corrected.

Table 9: Table representing the scene date RMS error and the number of GCP's collected when geometric correction was performed.

SCENE DATE	RMS error	NUMBER GCP
2004-09-20	0.5526	25
2005-02-27	1.2596	25
2005-09-07	0.9788	25
2006-08-09	1.1970	25
2006-04-19	1.5570	25
2007-02-17	1.5262	25

#### 4.2.1.2 Radiometric calibration

In order to standardize the impact of illumination geometry on the 8-bit digital number (DN) imagery, it first had to be converted to at-satellite radiance, and then to at satellite reflectance, using information extracted from the image header files.

Calculation of at-sensor spectral radiance is the fundamental step in converting image data from multiple sensors and platforms into a physically meaningful common radiometric scale. The following equation is used to perform the digital number to spectral radiance conversion for Level 1 products:

$$L_{\lambda} = ((LMAX_{\lambda} - LMIN_{\lambda}) / (QCALMAX - QCALMIN)) * (QCAL - QCALMIN) + LMIN_{\lambda} \quad \{7\}$$

Where

$L_{\lambda}$  = Spectral radiance at the sensor's aperture [W/ (m<sup>2</sup> sr $\mu$ m)]

Qcal = Quantized calibrated pixel value [DN]

Qcalmin = Minimum quantized calibrated pixel value corresponding to LMIN $\lambda$  [DN]

Qcalmax = Maximum quantized calibrated pixel value corresponding to LMAX $\lambda$  [DN]

LMIN $\lambda$  = Spectral at-sensor radiance that is scaled to Qcalmin [W/ (m<sup>2</sup> sr $\mu$ m)]

LMAX $\lambda$  = Spectral at-sensor radiance that is scaled to Qcalmax [W/ (m<sup>2</sup> sr $\mu$ m)]

Grescale = Band-specific rescaling gain factor [(W/ (m<sup>2</sup> sr $\mu$ m))/ DN]

Brescale = Band-specific rescaling bias factor [W/ (msr $\mu$ m)]

**Conversion to TOA reflectance (L<sub>λ</sub>-to- ρ<sub>P</sub>)**

A reduction in scene-to-scene variability can be achieved by converting the at-sensor spectral radiance to exoatmospheric TOA reflectance, also known as in-band planetary albedo. When comparing images from different sensors, there are three advantages to using TOA reflectance instead of at-sensor spectral radiance. First, it removes the cosine effect of different solar zenith angles due to the time difference between data acquisitions. Second, TOA reflectance compensates for different values of the exoatmospheric solar irradiance arising from spectral band differences. Third, the TOA reflectance corrects for the variation in the Earth-Sun distance between different data acquisition dates. These variations can be significant geographically and temporally. The TOA reflectance of the Earth is computed according to the equation:

$$\rho_{\lambda} = \frac{\pi \cdot L_{\lambda} \cdot d^2}{ESUN_{\lambda} \cdot \cos \theta_s} \quad \{8\}$$

$\rho_{\lambda}$  = Planetary TOA reflectance [unitless]

$\pi$  = Mathematical constant approximately equal to 3.14159 [unitless]

$L_{\lambda}$  = Spectral radiance at the sensor's aperture [W/ (m<sup>2</sup> sr $\mu$ m)]

$d$  = Earth-Sun distance [astronomical units]

$ESUN_{\lambda}$  = Mean exoatmospheric solar irradiance [W/ (m<sup>2</sup>  $\mu$ m)]

$\Theta$  = solar elevation angle (from imagery header files)

**4.2.1.3 Atmospheric correction**

The objective of a radiometric atmospheric correction is to convert satellite generated digital counts to ground reflectance (absolute reflectance). Various complex models have been developed to correct atmospheric effect (Chavez 1996). However, these models need some data, about atmospheric conditions for the date and time that remote sensing data was acquired, which are not usually available. The ENVI's fast line-of-sight atmospheric analysis of spectral hypercubes (FLAASH) was used. FLAASH is the MODTRAN-4 based atmospheric correction software package, which consist of term to account for the adjacency effect and also performs spectral polishing.

FLAASH is a first-principles atmospheric correction tool that corrects wavelengths in the visible through near- infrared and shortwave infrared regions, up to 3  $\mu$ m. Unlike many other atmospheric correction programs that interpolate radiation transfer properties from a pre-calculated database of modelling results, FLAASH incorporates the MODTRAN-4 radiation transfer code. You can choose any of the standard MODTRAN model atmospheres and aerosol types to represent the scene; a unique MODTRAN solution is computed for each image.

**FLAASH also includes the following features:**

- Correction for the adjacency effect (pixel mixing due to scattering of surface-reflected radiance).
- An option to compute a scene-average visibility (aerosol/haze amount). FLAASH uses the most advanced techniques for handling particularly stressing atmospheric conditions, such as the presence of clouds.

The steps shown on Figure 47 were used when performing atmospheric correction using ERDAS 2011.

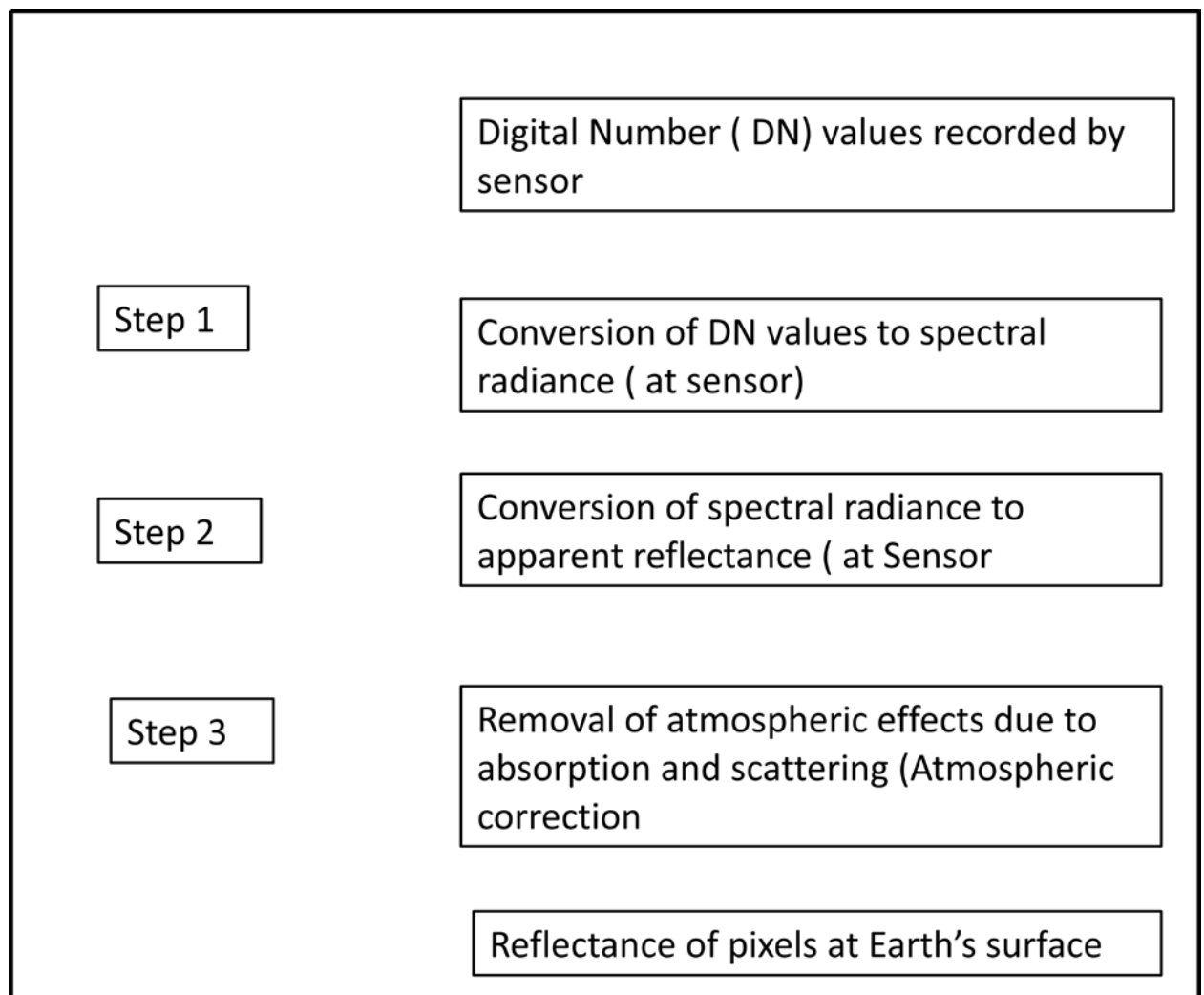


*Figure 47: Steps followed when performing atmospheric corrections.*

**4.2.2 Derivation of information on vegetation health and productivity and moisture conditions**

The Landsat series of satellites provide the longest continuous record of satellite-based observations. As such, Landsat is an invaluable resource of monitoring regional and global changes. The 30 meter resolution Landsat data is a useful tool on the identification of small and large landslides. The 2005-02-27

Landsat scene (see Figure 48); shows no landslide scars in the Hermanus area; while the 2005-09-07 scene shows several landslides scars (see Figure 49). Therefore the landslide events in the area occurred between the 27th February and the 7th September 2005.



*Figure 48: The 2005-02-27 scene for the area close to the town of Stanford and Hermanus. There are no visible landslide scars on this image, except one feature close the small round water body.*



Figure 49: The 2005-09-27 scene for the area close to the town of Stanford and Hermanus. The image shows several landslide scars (the bright feature on the south facing slope on the mountain).

### **NDVI change detection**

The primary goal of using the high spectral and spatial resolution images is to investigate the vegetation conditions associated with landslide occurrences. For this purpose, the Landsat image scenes were analysed for the NDVI, using ERDAS IMAGINE 2011. Change detection is an important application of remote sensing technology. It is a technology ascertaining the changes of specific features within a certain time interval. Remote sensing change detection technique can be classified as either pre or post-classification change method. The computerized NDVI change detection (pre-classification) was used to analyse the amount of change in NDVI. The NDVI change detection between two dates can be summarised by the following equation:

$$\text{NDVI change detection} = ((\text{NIR-Red}) / (\text{NIR+Red}))_{t_2} - ((\text{NIR-Red}) / (\text{NIR+Red}))_{t_1} \quad \{9\}$$

Where  $t_1$  and  $t_2$  represent the two dates of images captured. The changes in NDVI values from 2004-09-20 to 2005-02-27 are presented on Figure 50, the light red and bright red colours on the map depicts areas that have experienced less than 15% decrease in NDVI and more than 15% decrease in NDVI, respectively. The light green and the bright green colours on the map depict areas that have less than 15% NDVI increase and more than 15% increase, respectively. The exact localities for the landslide scars that

have been observed close to the town of Stanford and Hermanus are represented by the black stars on the map. It is observed from the NDVI change detection map that all the landslide points plot on the areas that have experience some decrease and a 15 % decrease in NDVI values, from the 20th of September 2004 to the 7th of February 2005. This means that the landslide occurrences in this area coincide with a decrease in vegetation conditions for the season prior to landslide occurrence. This does not necessarily mean that a decrease in NDVI values will cause landslide occurrences, but it simply means that the decrease in NDVI values makes the area more likely to have landslide when the triggering mechanism befalls.

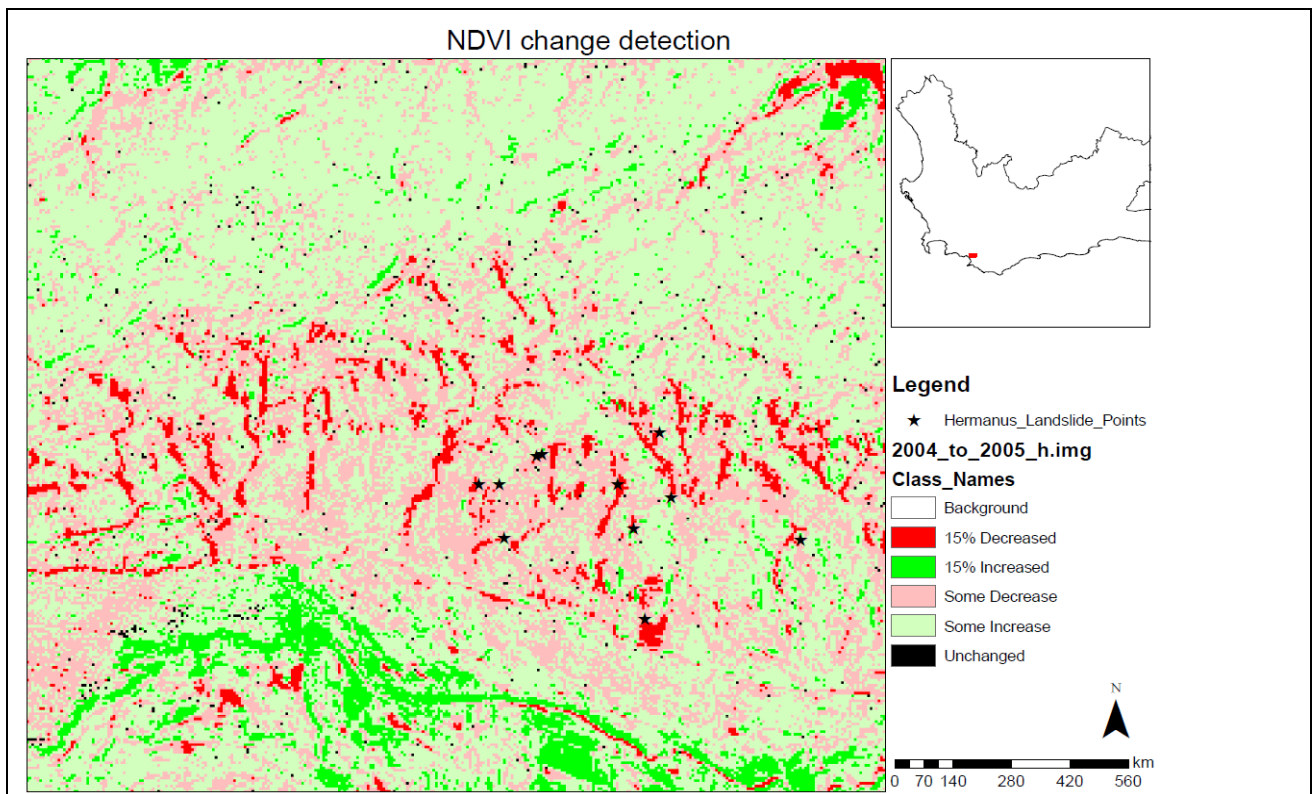


Figure 50: NDVI change detection computed from the landsat scenes between 2004-09-20 and 2005-02-27. The light red areas on the map are areas where there has been a decrease in NDVI and the strong red areas are those that had more than 15 % NDVI decrease. The light green and bright green areas depict those areas that experienced some NDVI increase and greater than 15 % NDVI increase, respectively. The localities of the landslides are represented by the black stars on the map.

Figure 51 shows the changes in NDVI as from 2005-09-07 to 2006-04-19. The light green and green areas depict areas that have experienced less than 15% increase and more than 15% increase in NDVI, respectively. The light red to red areas represent areas that have experienced less than 15% decrease and more than 15% increase in NDVI values, respectively. The large parts of the area shows a decrease in NDVI values, but there were no new landslide scares or expansion of the existing landslides, which has been observed from the Landsat images. This does not rule out the influence of the decrease in NDVI on landslide susceptibility, but it could simply mean that there were no heavy rainfalls to trigger landslide

occurrence in the area, during the time when the vegetation conditions were more suitable for landslide occurrence.

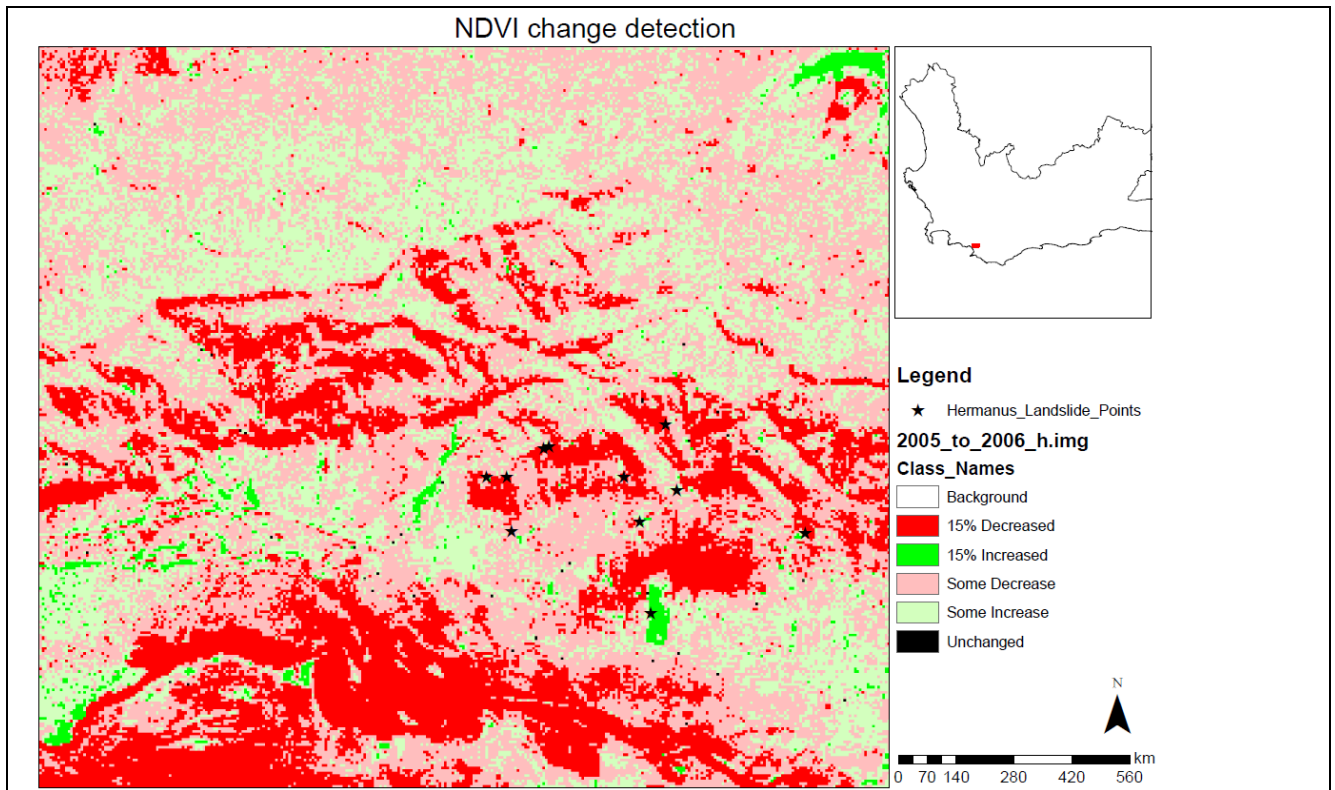


Figure 51: NDVI change detection computed from the images taken from 2005-09-07 and 2006-04-19. The light red areas on the map are areas where there has been a decrease in NDVI and the strong red areas are those that had more than 15 % NDVI decrease. The light green and strong green areas depict those areas that experienced some NDVI increase and greater than 15 % NDVI increase, respectively. The exact localities of the landslides are represented by the black stars on the map.

The changes in NDVI values 2006-08-09 to 2007-02-17 are presented on Figure 52. The light green and bright green areas on the map depict areas that have experienced less than 15% increase in NDVI and more than 15% increase in NDVI values, respectively. The light red and red areas depict those areas that have experienced less than 15% decrease in NDVI values and more than 15% increase in NDVI, respectively. It can be seen that large parts of the area shows an increase in NDVI values, therefore based on the previous observations the vegetation conditions do not favour landslide occurrence. Nevertheless that does not mean that the landslide will not occur in the area when the triggering mechanism crops up, as vegetation is not the sole parameter that controls landslide occurrence.

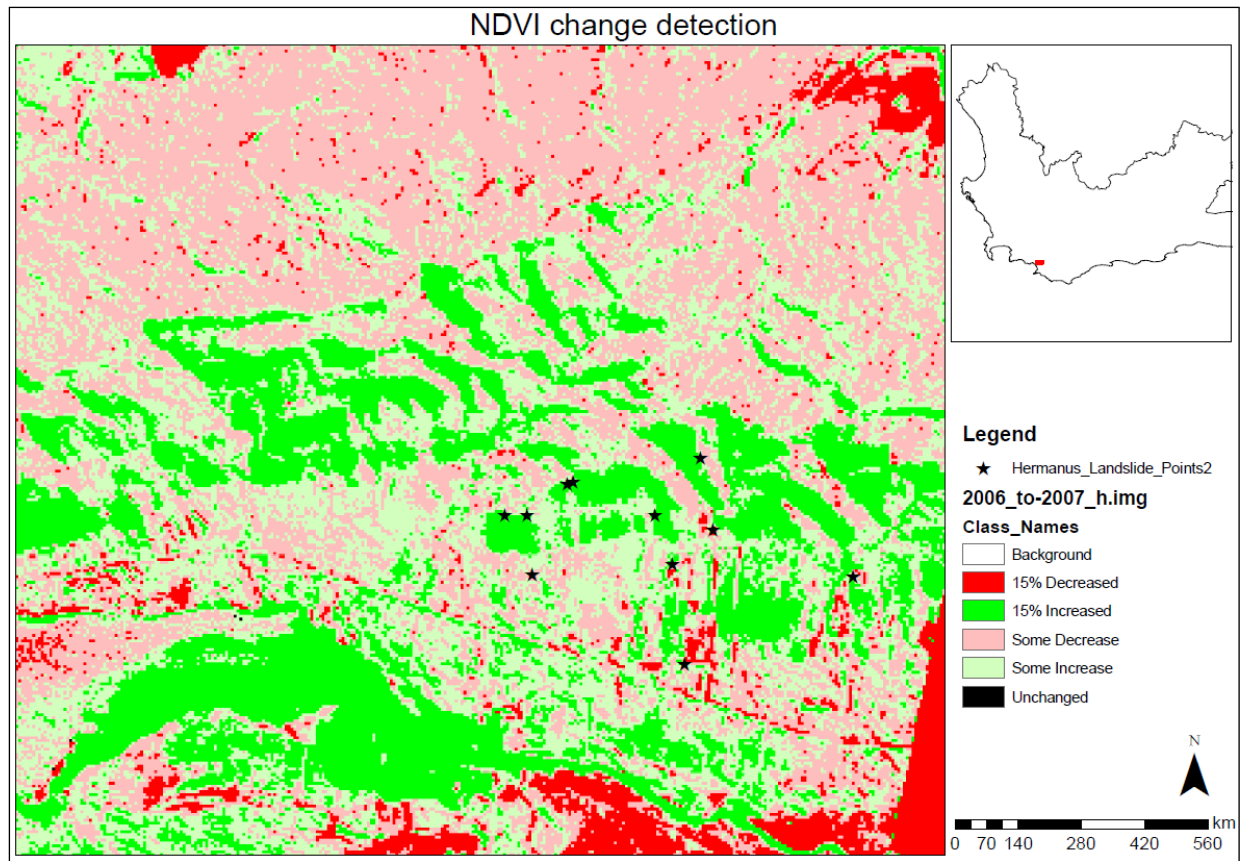


Figure 52: NDVI change detection computed from the images taken from 2006-08-09 to 2007-02-17. The light red areas on the map are areas where there has been a decrease in NDVI and the strong red areas are those that had more 15 % NDVI decrease. The light green and strong green areas depict those areas the experienced some NDVI increase and greater than 15 % NDVI increase, respectively. The exact localities of the landslides scars are represented by the black stars on the map.

### 4.3 TRIGGERING MECHANISMS

Rainfall data from the South African Weather Services was used to investigate if rainfall was the triggering mechanism. For those landslides that have known dates of occurrences, the intensity of rainfall during the occurrence of those landslides was investigated. It is crucial to know the rainfall conditions during the occurrence of landslides in order to know if the rainfall was the triggering mechanism, and also to have an insight of the rainfall threshold that triggers landslides.

In order to investigate the triggering mechanism for the landslide events close to the town of Stanford and Hermanus the seismic and the rainfall record of the area was investigated. Investigation of the seismic data that was obtained from the seismology unit of the Council for Geosciences, showed no seismic activity for the year 2005, which is the year at which the landslides occurred. Nevertheless the rainfall record acquired from the South African Weather Services (SAWS) for the weather station located in the town of Hermanus showed some interesting results. The three year annual rainfall record in this area

showed that the year of 2005 had the highest rainfall at 822.5mm as compared to 619.5 mm of the year 2004 and 641 mm of the year 2006. The monthly average for the year 2005 was also at the highest at 68.54 mm as compared to 51.63mm and 53.42 mm, for the year 2004 and 2006, respectively. Based on Landsat image interpretation, the landslides were discovered to have occurred on the year 2005 (after the 27th of February 2005), the high rainfall for the year 2005 supports the longstanding idea that most landslides in mountainous areas of South Africa are triggered by heavy rainfalls, but nothing much has been done to identify the rainfall threshold that triggers landslides.

*Table 10: The annual rainfall for the weather station in Hermanus (-34.417: 19.237). The monthly average and the total annual rainfall are also indicated. The rainfall is in millimetres (mm).*

<b>Month</b>	<b>2004 Monthly rainfall</b>	<b>2005 Monthly Rainfall</b>	<b>2006 Monthly rainfall</b>
January	15.5	52.5	14.5
February	32	31.5	33
March	33	12.5	16
April	33	246.5	56
May	14.5	101.5	93.5
June	67	178	33
July	86	13	156.5
August	48.5	88.5	60
September	52	38.5	30.5
October	161	24	81.5
November	32.5	26	39.5
December	44.5	10	27
Monthly Average	51.63	68.54	53.42
<b>TOTAL</b>	<b>619.5</b>	<b>822.5</b>	<b>641</b>

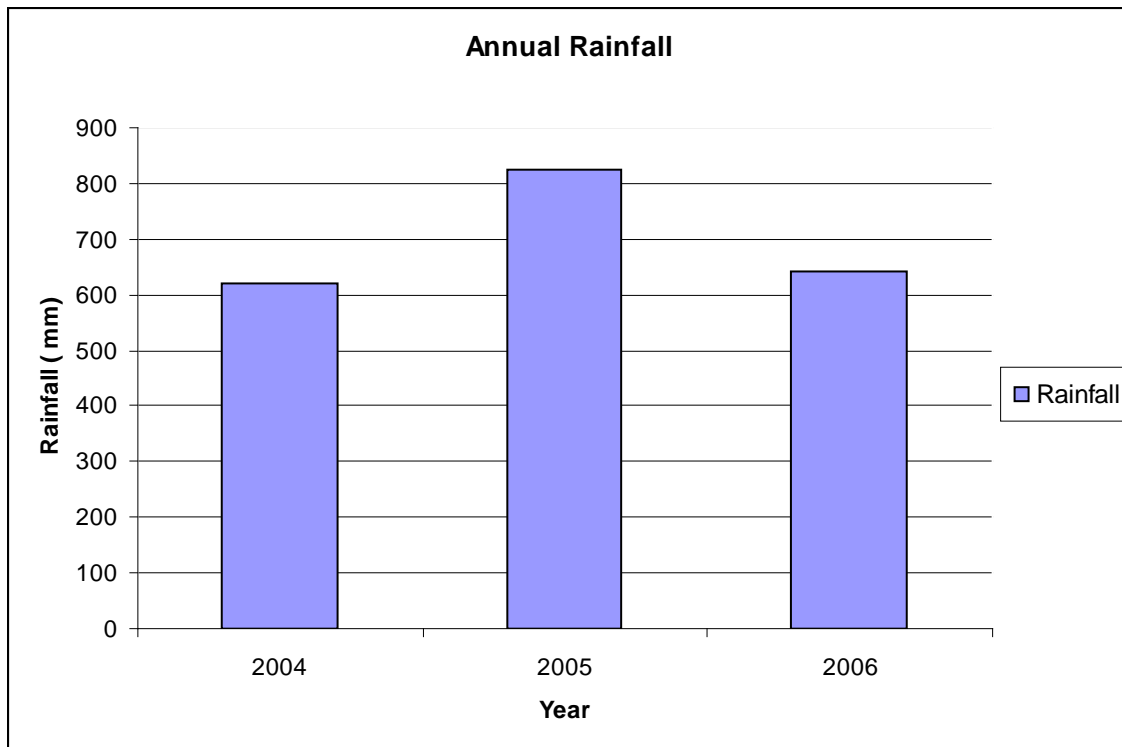


Figure 53: Annual rainfall for the year 2004, 2005 and 2006. The year of 2005 recorded the highest annual rainfall, slightly higher than 800 mm.

Rainfall is the major triggering mechanisms for landslides in many parts of the world, and also in South Africa. Heavy rainfall for a number of days can trigger landslides in areas that are susceptible to landslide occurrence. Landsat interpretation indicates that the landslides occurred between the 27th of February 2005 and 7th of September 2005, this also gives insight that the winter rainfalls are likely to have triggered the landslides in the area. The month of April and June recorded the highest and the second highest monthly rainfall for the year 2005, respectively (referrer to Figure 54). The daily rainfall record for the Month of April in the year of 2005 shows significant rainfall in the space of three days. It is worth mentioning that 82% of the rainfall in the month of April occurred between the 9th and 11th of April 2005 (see Table 11), based on these observations the landslides are more likely to have occurred between the 9th and the 11th of April 2005.

Table 11: The annual rainfall data (in millimeters) for the weather station close to the town of Hermanus. The blank areas in the table indicate that no rain fell on that day, \*\*\* indicates that the data is missing or not yet available in the current month, C next to the value indicates that the rainfall was accumulated over a number of days, = indicates that the total for the month is unreliable due to missing daily values, and A or B indicates that any rainfall that did occur is included in the accumulation.

Hermanus Station: Latitude and longitude: -34.417:19.237 Year: 2005												
Day	JAN	FEB	MAR	APR	MAY	JUN	JUL	AUG	SEP	OCT	NOV	DEC
1					1.0 C				5			0.5
2						18.5			2			2.5
3	0.5					A			A	7		4
4					3.5	32.0 C			16.0 C		2.5	
5					0.5					6	3.5	
6												2.5
7	3.5		3.5			36		A		A		
8						30		6.0 C		A		
9			9	A						A		
10				164.0 C						A		
11	1.5				42			A		9.0 C	A	
12					18.5	7.5		A			15.5 C	
13	16				6	6		A				
14	9.5					16.5		18.0 C				
15												
16												2
17					22.5		1	18.5				
18		1.5		3.5	1.5		1					
19	3.5	19		14		3	7.5			1		8
20	1			9.5		6.5	1.5			3		
21		3.5										
22	3.5			A	11			3	0.5			
23				13.5 C	9							
24	0.5	7.5							A	2		
25						A		24	7.5 C			
26					2	22.0 C	2	7	4.5			
27	4.5				A							
28	8.5				8.5 C							
29		***										
30		***		A				4.5				1
31		***		***	17.5	***		0.5	***		***	
TOTAL	52.5	31.5	12.5	246.5=	101.5=	178.0=	13	88.5=	38.5=	24.0=	26.0=	10

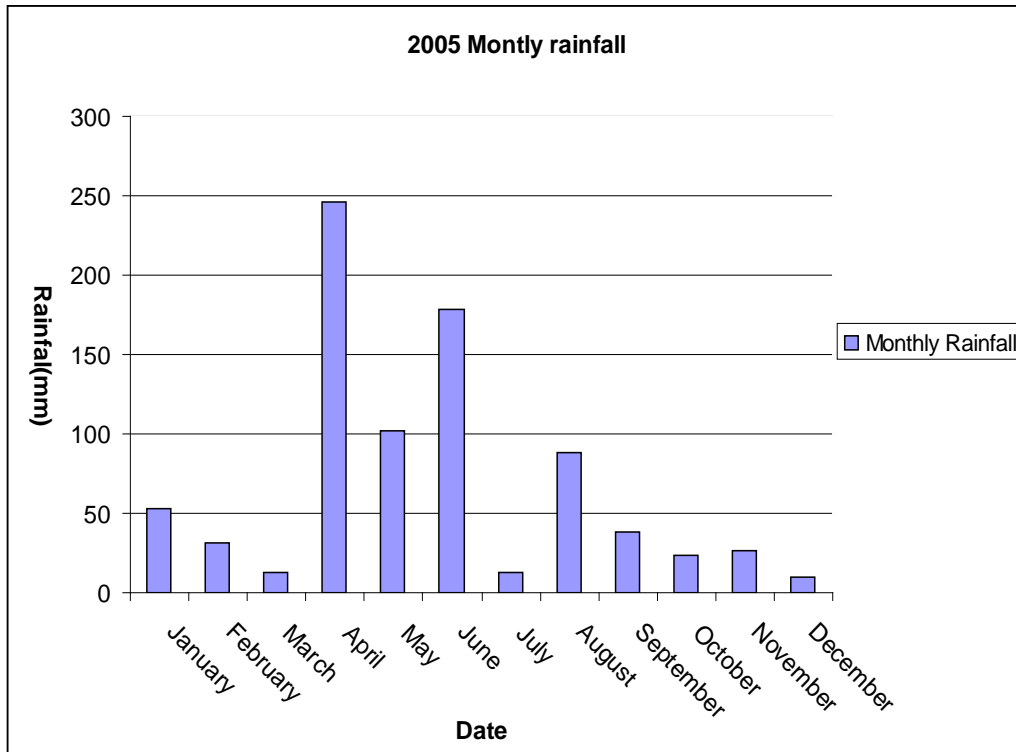


Figure 54: The plot for the monthly rainfall for the year 2005. The months of April and June show monthly rainfall greater than 100 mm, with the month of April recording close to 250mm.

## CHAPTER 5 DISCUSSION, RECOMMENDATIONS AND CONCLUSIONS

### 5.1 DISCUSSION

The aims of the study was to investigate landslide causative factors, synthesize a landslide susceptibility map using geographic information system and also monitor changes that affect the areas susceptibility using remote sensing techniques. Selecting the landslide causative parameters is the primary and the most critical step when modeling a landslide susceptibility map. The static factors are the only causative factors that are typically used when modeling a landslide susceptibility map, mainly because they do not change over a short space of time. Different static factors were investigated in this study and their influence on slope instability was investigated.

It has been observed that slope is the most important parameter on landslide susceptibility and the high and very high susceptibility classes on the weight of evidence modeled susceptibility map coincide with steeply sloped areas. About 90 % of field verified landslides fell on slopes between 0-40°, with slopes between 0 and 20° recording slightly more than 50 % of those landslides. This is no surprise in South Africa, as slopes greater than 18° are considered to be susceptible to landslides, and therefore not suitable for construction. South facing slopes have long been known to be more susceptible to landslides, Boelhouwers et al (1998) was one of the authors to make this findings. This was further confirmed in this study when the South facing slopes recorded the highest number of landslides (see Figure 14). The south facing slopes in South Africa, receive less sunlight as compared to the north facing slopes. The increase water content in the soil decreases the cohesive strength of clay minerals and also pore fluid pressure can have negative impact on slope stability. Sunlight plays a significant role in decreasing the water content in the soil, in two ways (1) releasing of water from the ground through evaporation, and (2) releasing of water from the ground through the process of transpiration. The south facing slopes are generally wetter than the north facing slope, resulting in an increased susceptibility to landslides (Stapelberg pers com, 2011). It was also discovered by Boelhouwers et al. (1998) that 78 % of the landslides fell on the South facing slopes, in an area within the Western Cape Province of South Africa. The north facing slopes recorded a very small number of landslides (see Figure 14), this can be explained by the fact that the north facing slope receive a significant amount of sunlight, in South Africa. Therefore the negative impact of increased water content is eliminated, as water is released from the ground through the process of evapotranspiration. The high sunlight content can have negative impact on landslide susceptibility, if the dominant soil type in the area in question is expansive clay i.e montmorillonite. The clay would expand during rainy days and contract during sunny days, resulting in the weakening of the bonds between clay particles. Expansive clays are known not to be suitable for building construction. Stapelberg (pers com, 2011) also highlighted increased susceptibility in clayey rich soil.

Vegetation has been proven by Varnes (1985) to have positive effects on slope stability i.e. the natural anchorage that limits the effects of rainfall on erosion, and the release of water from the ground, as a vapour during evapotranspiration. In general the north facing slopes are normally dry and therefore less vegetated and the south facing slopes are generally much more wetter and therefore more vegetated, in South Africa. It would be expected that the South facing slopes would be less susceptible to landslides, as they are more vegetated. This is not the case, as this study has shown that there was a large number of landslides in the south facing slopes than the north facing slopes, which also supports Boelhouwers et al. (1998) observations. Although vegetation plays a positive role on decreasing the negative effect of water on slope stability, its impact can be inconsequential if there is a limited amount of sunlight, as the rate of transpiration will be much lower and also the leaves can cover the ground counteracting the process of evaporation.

The soil type is also a major parameter on slope instability as different soils have different hydrological properties. Clay rich soils are more susceptible to landslide occurrence, but surprisingly a large number of landslides occurred on the rocky outcrops. But also a considerable number of landslides occurred on deep soils. Soil depth has been found to be the most important parameter when modeling landslide susceptibility maps. Soil depth less than 300 mm and between 600 and 900 mm recorded the highest and second highest number of landslides, respectively. Deepest soil class had the least number of landslides but this was mainly because this class covered merely less than 1% of the study areas. It has been noted by Dahal et al. (2007) that deep soils are more susceptible to landslides, but this was not the case in the study area, mainly because the deeper soils comprised less than 1 percent of the study areas.

The geology of the area plays a significant role on landslide susceptibility, as different rock types have different hydrological properties and different strength. Geological structures can have weakening effects on rocks. A large number of landslides plotted on unconsolidated alluvium deposits. These deposits have a higher hydraulic transmissivity and less cohesive strength, the effect of increased water content on cohesive strength of clayey minerals is shown on Figure 4. Moreover, pore fluid pressure would have negative impact on slope stability. Most of the landslides in the study area could be proven that they were triggered by rainfall event, hence the hydrological properties of rocks is of importance when investigating landslide susceptibility. The sandstone and quartzite units also recorded a significant number of landslides. Sandstone has a very high hydraulic transmissivity and quartzites have slightly lower hydraulic conductivity. Higher transmissivity means easy passage of water deep into the ground; increasing negative effects of water (i.e. decrease of cohesive strength of clay minerals and increased pore fluid pressure (Warric, Mullen & Nielsen 1977, Wilson 1980). If the top rock unit is composed of highly transmissive sandstone units and the lower unit is made of less permeable and expansive clay units; such an area would be highly susceptible. However this needs to be specifically

investigated in future studies. Slightly more than 50 % of landslides fell within the 250 m buffer of faults and geological contacts. This also shows that the faulted areas are much more susceptible to landslides. Faults and lithological contacts are known to be zones of weakness; hence they are much more likely to be susceptible to landslides than unfaulted areas.

Understanding and selecting the landslide causative factors is important, if the causative parameters are properly understood, higher level of accuracy can be achieved on landslide susceptibility modelling. The accuracy of the landslide susceptibility map strongly depends on the weighting of the causative parameters in accordance to their influence to slope instability; therefore the selection of a suitable weighting system was critical in this study. In this study the weight of evidence and the map combination approach were used. The weight of evidence method produced exceptional results in comparison with the map combination approach. This can be seen from the success rate curve and the cumulative percentage of these models, presented in Chapter 3. It is worth mentioning that similar approach, as the map combination approach (DRASTIC) have been applied successfully to model a ground water vulnerability maps, by the Council for Geosciences. The unsatisfactory results of the map combination approach on landslide susceptibility mapping are largely attributed by the fact that there are several causative parameters that govern slope instability. The map combination approach can be more useful when modelling a certain type of mass movement i.e. rock falls, debris flow etc. The very high susceptibility class on the susceptibility map modelled using the map combination approach coincides with the road cuts, even in low lying areas. This is mainly because the expert classified road cuts as the major parameter when weighting the causative factors. If the focus of the study was to model a rock fall susceptibility map, it is likely that the map combination approach could have yielded acceptable results.

One of the primary goals of this study was to investigate if remote sensing techniques can be used to monitor the variable parameters that influence landslide susceptibility, and use them as a warning system for potential slope failure. The remote sensing techniques are ideal for monitoring changes that can increase the area's susceptibility to landslides, mainly for variable factors i.e. vegetation health. Lower than normal minimum NDVI values were observed on the MODIS derived NDVI time series profile, and in some cases the minimum, maximum and average NDVI values were low for the year prior to landslide occurrence. The Landsat derived NDVI change detection also showed a decrease in NDVI for the season prior to landslide occurrence. These findings imply that the vegetation health was poor for the season prior to landslide occurrences. Based on these findings, a decrease in NDVI values (vegetation health) increases the area's susceptibility to landslides and therefore remote sensing can be used to monitor changes in variable factors, which favours landslide occurrence. There might be a seasonal component to the variations, and the conclusions drawn from this data might not be entirely conclusive.

The triggering mechanism for the landslides within the study area was rainfall. Heavy rainfall for a number of days is a major trigger for landslides in mountainous areas of the Western Cape. Due to the uncertainty in the timing of landslide occurrences, the rainfall threshold that triggers landslide could not be properly investigated in this study. The rainfall threshold that triggers landslide has not been properly investigated in this study. However a 200 mm rainfall in the space of three days, in April 2005 triggered several shallow landslides (debris flow) in the mountainous areas within the study area. This indicates that heavy rainfalls in a short space of time can trigger landslides, in susceptible areas.

## **5.2 INTERGRATION OF LANDSLIDE SUSCEPTIBILITY MAPPING AND DEVELOPMENT PLANNING**

The susceptibility of the area to landslide occurrence is crucial for development planning. Landslide activities can adversely affect human activities and also have socio-economic disturbances. In this regard, information about the susceptibility of the area to landslides is crucial. Although landslide susceptibility maps are only capable of depicting areas that are likely to have landslides, not the period at which the landslide can occur. The planner can use these estimates to certain decisions regarding the site suitability, the type of development, and appropriate mitigation measures. By so doing the planner has determined the acceptable or unacceptable risk for development programs. Decisions can then be made regarding avoidance, prevention or mitigation of existing and future landslide hazard in the development program.

Determining whether there is a need for landslide susceptibility information is the first step in ensuring that landslide risk does not exceed an acceptable level in planning for future land use. Landslide risk can be defined as the degree of loss due to a particular landslide. The objectives of landslide information are to determine which landslide susceptible areas are best suited for what type of development activities. For example, assessing landslide susceptibility would not be crucial when determining areas that could be national parks or game reserves; on the other hand, landslide susceptibility would be important in development of building infrastructure in mountainous, tropical terrain. The type of development in an area is deterministic for the amount of landslide information needed for the area in question. The failure to consider the potential effect of landslides on a project can bring an increased risk; and some other projects like road cuts can affect the susceptibility of an area to landslide, therefore landslide information is crucial for development planning (<http://www.oas.org/dsd/publications/unit/oea66e/ch10.htm>).

### 5.3 RECOMMENDATIONS

1. Detailed landslide inventory and classification of the landslides prior to the modeling of landslide susceptibility map needs to be done. This would allow the researcher to develop a rock fall susceptibility map, debris flow susceptibility map and a deep seated landslide susceptibility map. This is crucial as these class of landslides are influence by different causative factors e.g. roads and rail cuts are more influential on rockfalls,
2. Accurate dating (i.e. dendrochronological dating) of landslides would allow the correlation of landslides with rainfall events and help on investigating the rainfall threshold that triggers landslide in the study area and Western Cape as a whole. A lot of work still needs to be done on the investigation of the rainfall threshold that triggers landslides.
3. Future studies should put more focus on performing sensitivity analysis, as this can help in understanding the influence of different landslide causative parameters, which govern landslide susceptibility.
4. Although very high accuracies of landslide susceptibility was obtained using the weight of evidence method, in theory, for landslide susceptibility even higher accuracies would be ideal. Additional expert-based information and additional parameters affecting landslide susceptibility should be investigated.
5. It would be interesting if future studies investigate the performance of the map combination approach, on a specific class of mass movement, and see if it yields acceptable results.

### 5.4 CONCLUSIONS

- The weight of evidence method is ideal when modelling landslide susceptibility maps. The results attained when modelling a landslide susceptibility map using this method where highly acceptable.
- The map combination approach is not the best method to use when modelling landslide susceptibility maps.
- Remote monitoring of variable factors i.e. vegetation can be achieved using remote sensing techniques and this can be used as the warning system.

## REFERENCES

Aleotti P. & Chowdhury R 1999. *Landslide Hazard Assessment: Summary, Review and New Perspectives*, Bulletin of Engineering Geology & Environment, vol. 58, pp.21-44.

Anderson GL, Hanson JD & Haas RH 1993. *Evaluating landsat thematic mapper derived vegetation indices for estimating above-ground biomass on semiarid rangelands*. Remote Sensing of the Environment. vol. 45(2), pp.165-175.

Athanasopoulos GA., Pelekis, PC.& Leonidou E A 1995. *Effects of surface topography on seismic ground response in the Egion (Greece) 15 June 1995 earthquake*, Soil Dyn. Earthqu. Eng., vol. 18, pp.135–149.

Atkinson PM & Massari R 1998. *Generalized linear modelling of landslide susceptibility in the Central Apennines, Italy*. Computer Geoscience, vol.24 (4), pp. 373–385.

Boelhouwers J, Duiker JMC & van Duffelen EA 1998. *Spatial, morphological and sedimentological aspects of recent debris flows in Du Toit's Kloof, Western Cape*. South African Journal of Geology. vol. 101, pp.73–89.

Bonham-Carter GF, Agterberg FP & Wright DF 1988. *Integration of geological datasets for gold exploration in Nova Scotia*. Photogram. Remote Sens., vol. 54, no. 11, pp. 1585–1592.

Bonham-Carter GF, Agterberg, FP & Wright DF 1989. *Weights of evidence modelling: a new approach to mapping mineral potential*, in Agterberg. *Statistical Applications in the Earth Sciences: Geological Survey Canada paper 9-9*, pp. 171–183.

Borcherdt RD 1970. *Effects of local geology on ground motion near San Francisco Bay*, *Bull. Seis. Soc. Am.* vol.60, pp. 29–61.

Brunetti MT, Peruccacci S, Rossi M., Luciani S, Valigi D & Guzzetti F 2010. *Rainfall thresholds for the possible occurrence of landslide in Italy*. *Natural Hazards and Earth System Sciences*, vol.10, pp. 447-458.

Campbell RH 1975. *Soil slips, debris flows, and rainstorms in the Santa Monica Mountains and vicinity, southern California*. In: *US Geological Survey Professional Paper 851*. Washington DC: U.S. Government Printing Office, pp. 51.

Cardinali M, Galli M, Guzzetti F, Ardizzone F., Reichenbach P & Bartoccini P 2005. *Rainfall induced landslides in December 2004 in South-Western Umbria, Central Italy*. *Nat Hazard Earth Sys Sci* 6. pp. 237–260.

Carson MA & Kirkby MJ 1972. *Hillslope form and process*. Cambridge University Press, Cambridge University Press, Cambridge, pp. 475.

Chauhan S, Sharma M, Arora MK & Gupta NK 2010. *Landslide susceptibility zonation through ratings derived from artificial neural network*. International journal of applied earth observation and geoinformation, vol. 12, pp. 340-350.

Chung CJF & Shaw JM 2000. *Quantitative Prediction Models for Landslide Hazard Mapping*. [http://www.nrcan.gc.ca/gsc/mrd/sdalweb/sdi\\_cd/index.html](http://www.nrcan.gc.ca/gsc/mrd/sdalweb/sdi_cd/index.html)

Clark RN 1999. *Spectroscopy of Rocks and Minerals, and Principles of Spectroscopy*. In A. N. Rencz (Ed.). *Manual of Remote Sensing. Remote Sensing for the Earth Sciences*, New York: John Willey and Sons, vol. 3, pp. 3-58.

Clerici A, Perego S, Tellini C & Vescovi P 2002. *A procedure for landslide susceptibility zonation by the conditional analysis method*. *Geomorphology*, vol. 48 (4), pp. 349-364.

Corominas J 2000. *Landslides and climate*. Keynote lecture- In *Proceedings 8th International Symposium on Landslides*, (Bromhead E, Dixon N, Ibsen ML, eds). Cardiff: A.A. Balkema, vol. 4, pp.1-33.

Corominas J & Moya J, 1999. *Reconstructing recent landslide activity in relation to rainfall in the Llobregat River basin, Eastern Pyrenees, Spain*. *Geomorphology*. vol. 30, pp. 79-93.

Crozier & Michael J 1986. *Landslide, consequences & environment*.

Cruden DM & Varnes DJ 1996. *Landslide types and Processes*. In *Landslides investigation and Mitigation*. Transportation Research Board, US National Research Council. Special Report, vol. 247, pp. 36-75.

Chavez PS, Jr 1996. Image-based atmospheric corrections-revised and improved. *Photogrammetric Engineering and Remote Sensing*, vol. 62 (9), pp.1025-1036.

Dahal RK, Hasegawa S, Nonomura A, Yamanaka M, Masuda T & Nishino K 2007. *GIS-based weight of evidence modelling of rainfall-induced landslides in small catchments for landslide susceptibility mapping*. *Environ Geol*.

Dai FC, Lee CF, Li J & Xu ZW 2001. *Assessment of landslide susceptibility on the natural terrain of Lantau Island, Hong Kong*. *Environ Geol*. vol.40, pp.381–391.

Dai FC & Lee CF 2002. *Landslide characteristics and slope instability modelling using GIS, Lantau Island, Hong Kong*. *Geomorphology*, vol.42: pp. 213-228.

Elias PB & Bandis SC 2000. *Neurofuzzy Systems in Landslide Hazard Assessment*, In: *Proceedings of 4<sup>th</sup> International Symposium on Spatial Accuracy Assessment in Natural Resources and Environmental Sciences*, pp. 199-202.

Gao B 1996. *NDWI – A normalized difference water index for remote sensing of vegetation liquid water from space*, *Remote Sensing of Environment*, vol. 58(3), pp.257–266.

Garland G & Olivier MJ 1993. *Predicting landslides from rainfall in a humid, sub-tropical region*, *Geomorphology*, vol. 8, pp. 165-173.

Glade T & Crozier M 2005b. *A review of scale dependency in landslide hazard and risk analysis*.

Glade T 2005. *Linking debris-flow hazard assessments with geomorphology*, *Geomorphology*, vol 66, pp. 189-213.

Gomez H & Kavzoglu T 2005. *Assessment of Shallow Landslide Susceptibility using Artificial Neural Networks in Jabonosa River Basin, Venezuela*, *Engineering Geology*, vol 78(1-2), pp.11-27.

Gray DH & Leiser, AT 1982. *Biotechnical slope protection and erosion control*. Van Nostrand Reinhold, New York.

Greenway DR 1987. *Vegetation and slope stability*. In: Anderson MG, Richards KS (eds) *Slope stability*. Wiley, New York, pp.187–230.

Griggs GB & Plant N 1998. *Coastal-bluff failures in northern Monterey Bay induced by the earthquake, in: The Loma Prieta, California, earthquake of 17 October 1989*. Landslides, (Ed) Keefer, D., USGS Prof. Paper 1551-C, C33–C50.

Hall FG, Strebel DE, Nickeson JE & Goetz SJ 1991. *Radiometric rectification. Toward a common radiometric response among multirate, multisensor images*, Remote Sensing of Environment, vol 35, pp.11–27.

Hanvey PM., Lewis CA. & Lewis GE 1986. *Periglacial slope deposits in Carlisle's Hoek, near Rhodes, Eastern Cape Province*. South African Geographical Journal, vol. 68, pp. 164–174.

Harp EL, Wilson RC & Wieczorec GF 1981. *Landslides from the 4 February 1976, Guatemala earthquake, The Guatemala earthquake of 4 February 1976*, Geology. Survey. Prof. Paper 1204-A, pp.1–35.

Hung LQ, Batelaan O, San DN & Van TT 2005. *GIS –Remote sensing application of landslide hazard mapping-Case study Thua-Thien-Hue Province, Vietnam*. New Strategies for European remote sensing.

Iverson MR 2000. *Landslide triggering by rain infiltration*. Water resource research, vol.36 (7), pp.1897-1910.

Janisch EP 1931. *Notes on the central part of the Soutspanberge Range and on the origin of Lake Funduzi*. Transactions of the Geological Society of South Africa, vol. 34, pp. 151–162.

Johnson MR, Annhauser CR & Thomas RJ 2006. *The geology of South Africa. Johannesburg/Pretoria*. Geological Society of South Africa/Council for Geoscience. pp 691.

Joyce KE, Samsonov S & Levick SR 2011. *The current status of remote sensing for mapping and monitoring geological hazards.*

Kanungo DP, Arora MK., Sarkar S & Gupta RP 2009. *Landslide susceptibility zonation (LSZ) mapping-A review.* Journal of South Asia Disaster Studies, vol.2.

Kim HH & Elman GC 1990. *Normalization of satellite imagery.* International Journal of Remote Sensing, 11(8), pp.1331-1347.

Lee S, Choi J & Min K 2004b. *Probabilistic Landslide Hazard Mapping using GIS and Remote Sensing Data at Boun, Korea.* International Journal of Remote Sensing. vol. 25, pp. 2037-2052.

Lewis CA. & Illgner PM 1998. *Fluvial conditions during the Holocene as evidenced by alluvial sediments from above Howison's Poort, near Grahamstown, South Africa.* Transactions of the Royal Society of South Africa, vol.53, pp. 53–67.

Lewis CA 1996. *Periglacial features.* In The Geomorphology of the Eastern Cape, South Africa, Grocott & Sherry, Grahamstown. pp. 103–119.

Mantovani F, Soeters F & Van Western CJ 2000. *Remote sensing techniques for landslide studies and hazard zonation in Europe.* Geomorphology, vol. 15, pp. 213-225.

Mc Cloy KR 2010. *Development and evaluation of phenology changes indices derived from time series of image data.* Remote Sensing, vol. 12, pp.2442-2473.

Mc Feeter SK 1996. *The normalised difference water index (NDWI) in the delineation of open water features*. International Journal of Remote Sensing, vol. 17, pp. 1425-1432.

Morton M, Alvarez, RM & Campbell RH 2003. *Preliminary soil-slip susceptibility maps, south western California*. USGS Open-File Report OF 03-17.

Paige-Green P 1989. *Landslides: extent and economic significance in southern Africa*. In: Brabb, Paruelo JM, Epstein HE, Lauenroth WK & Burke IC., 1997. *ANPP estimates from NDVI for the central grassland region of United State of America*. Ecology, vol. 78(3), pp.953-958.

Pats S & Chavez JR 1996. *Image-Based atmospheric corrections-Revised and improved*. Photogrammetric Engineering and Remote Sensing, vol. 62 (9), pp.1025-1036.

Perry CR & Lautenschlager LF 1984. *Functional equivalence of spectral vegetation indices*. Remote Sensing of Environment, vol. 14, pp.169-182.

Prandini L, Guidicini G, Buttura JA, Pancano WL & Santos AR 1977. *Behaviour of the vegetation in slope stability: A critical review*. Int.Ass. Engineering Geology, vol.16, pp.5-51.

Rahman KM 2011. *Remote sensing-based determination of deciduous and understory phenology over boreal forest*. PhD thesis. University of Gagary Department of geoinformatics Engineering.

Ray RL, Jacobs JM & de Alba P 2009. *Impact of vadose zone soil moisture and groundwater on slope instability*, Journal of Geotechnical and Geoenvironmental Engineering.

Roering J & McKean J 2004. *Objective landslide detection and surface morphology mapping using high resolution airborne laser altimetry*. Geomorphology, vol 57, pp. 331-351.

Sarkar S & Kanungo DP 2004. *An integrated approach for landslide susceptibility mapping using remote sensing and GIS*. Photogrammetric Engineering & Remote Sensing, vol. 70 (5), pp. 617-625.

Siddle HJ, Jones DB & Payne HR 1991. *Development of a methodology for landslip potential mapping in the Rhondda Valley In: Chandler RJ (ed) Slope stability engineering*. Thomas Telford, London, pp.137–142.

Sidle RC, Pearce AJ & O'Loughlin, CL 1985. *Hillslope Stability and Land Use*, Water Resources Monograph (Washington, D.C.: American Geophysical Union, 1985), Series No. 11.

Singh R, Forbes C, Diop S, Musekiwa C & Claasen D 2011. *Report on landslide geohazards, their socio-economic impacts, mitigation and remediation measures as well as landslide susceptibility mapping of South Africa*. Earth Observation & Geological Hazard Assessment: Towards creation of the Geological Atlas of South Africa.

Singh RG 2009. *Landslide classification, characterization and susceptibility modelling in KwaZulu-Natal*. Master of Science Thesis, Witwatersrand University.

Soeters R & van Westen CJ 1996. *Slope Instability Recognition, Analysis and Zonation*. In: Turner. A. K.& Schuster R. L. (eds.) *Landslides, Investigation and Mitigation*, Transportation Research Board, National Research Council, National Academy Press, Washington, DC, U.S.A., Special Report 247, pp. 129-177.

Spudich P, Hellweg M, & Lee WHK 1996. *Directional topographic site response at Tarzana observed in aftershocks of the Northridge, California, earthquake: implications for mainshock motions*, Bull. Seis. Soc. Am, vol.86, pp.193–208.

Stoner ER & Baumgardner MF 1980. *Physiochemical site, and bidirectional reflectance factor characteristics of uniformly moist soils*. Tech Report 11679, LARS/Purdue University of West Lafayette.

Styczen ME & Morgan RPC 1995. *Engineering properties of vegetation*. In: Morgan RPC, Rickson RJ (eds) *Slope stabilisation and erosion control: a bioengineering approach*, London, pp 5–58.

Swanson FJ & Dyrness CT 1975. *Impact of Clearcutting and Road Construction on Soil Erosion by Landslides in the Western Cascade Range, Oregon*, Geology, vol. 3, pp. 393-396.

Temesgen B, Mohammed MU & Korme T 2001. *Natural hazard assessment using GIS and remote sensing methods, with particular reference to the landslide in the wondogenet area, Ethiopia.* Phys.Chem.Earth ©, vol.26 (9), pp. 665-675.

Terzaghi K 1950. *Mechanism of landslides, in Application of Geology to Engineering Practice.*

Van Schalkwyk A & Thomas MA 1991. *Slope failures associated with the floods of September 1987 and February 1988 in Natal and Kwa-Zulu, Republic of South Africa.* Geotechnics in the African Environment, Blight et al. (Eds), pp. 57-63.

Varnes DJ 1978. *Slope movement types and processes.* In: Schuster R.L and Krizek R. J., ED., *Landslides, analysis and control.* Transportation Research Board Special report, vol. 176, pp 11-33.

Varnes DJ 1984. *Landslide hazard zonation: a review of principles and practice.* IAEG Publication. Paris, Unesco.

Warrick AW, Mullen GJ & Nielsen DR 1977. *Scaling field measured soil hydraulic properties using a similar media concept.* Water Resource. Res. vol. 13 (2), pp. 355-362.

Wagner H & Pathe C 2008. *Has SAR failed in soil moisture retrieval?* ENVISAT & ERS Symposium, Salzburg, Austria, 6-10 September 2004, ESA SP-572, pp. 1745-1751.

Wieczorek GF 1984. *Preparing a Detailed landslide-Inventory map for Hazard Evaluation and Reduction*, Bulletin of International Association of Engineering Geologists, vol. 21, pp.337-342.

Wieczorek GF 1987. *Effect of rainfall intensity and duration on debris flows in central Santa Cruz Mountains*. In: Debris flow/avalanches: process, recognition, and mitigation (Costa JE, Wieczorek GF, eds), Geological Society of America, Reviews in Engineering Geology, vol.7: pp. 93–104.

Wilson RC 1989. *Rainstorms, pore pressures, and debris flows: a theoretical framework*. In: Landslides in a semi-arid environment (Morton DM, Sadler PM, eds). California: Publications of the Inland Geological Society, vol.2, pp. 101–117.

Wu W & Siddle RC 1995. *A distributed slope stability model for steep forested basins*. Water Resource Res, vol. 31:pp.2097–2110.

Xiao X., Zhang J., Yan H., Wu W & Biradar C 2009. *Land surface phenology: Convergence of Satellite and Co2 Eddy Flux observations*. A. Noormets (Ed.), Phenology of ecosystem processes, New York: Springer Sciences & Business Media, pp. 247-270.

Zhou Y 2006. *Slope stability*. Geotechnical Engineering. Publication No. FHWA NHI-06-088.

## **SPECIAL REFERENCES**

Stapelberg 2011. Engineering geologist at Council for Geosciences. Bellville. Interviewed on the 9 June 2011 about the parameters that affect the area's susceptibility to landslide.

Landslide hazard zonation (Online). Available from  
<http://www.oas.org/dsd/publications/unit/oea66e/ch10.htm> (Accessed 30 October 2012).